Electronic Theses and Dissertations   Theses, Dissertations, and Major Papers

2005

Experimental and numerical investigations of chemical grouting in heterogeneous porous media.

Tirupati Bolisetti
University of Windsor

Follow this and additional works at: https://scholar.uwindsor.ca/etd

EXPERIMENTAL AND NUMERICAL INVESTIGATIONS OF CHEMICAL GROUTING IN HETEROGENEOUS POROUS MEDIA

by
Tirupati Bolisetti

A Dissertation
Submitted to the Faculty of Graduate Studies and Research
through Civil and Environmental Engineering
in Partial Fulfillment of the Requirements for
the Degree of Doctor of Philosophy at the
University of Windsor
Windsor, Ontario, Canada
2005

© 2005 Tirupati Bolisetti

Library and
Archives Canada

Bibliothèque et
Archives Canada

Published Heritage
Branch

Direction du
Patrimoine de l'édition

395 Wellington Street
Ottawa ON K1A 0N4
Canada

395, rue Wellington
Ottawa ON K1A 0N4
Canada

NOTICE:
The author has granted a non-exclusive license allowing Library and Archives Canada to reproduce, publish, archive, preserve, conserve, communicate to the public by telecommunication or on the Internet, loan, distribute and sell theses worldwide, for commercial or non-commercial purposes, in microform, paper, electronic and/or any other formats.

The author retains copyright ownership and moral rights in this thesis. Neither the thesis nor substantial extracts from it may be printed or otherwise reproduced without the author's permission.

AVIS:
L'auteur a accordé une licence non exclusive permettant à la Bibliothèque et Archives Canada de reproduire, publier, archiver, sauvegarder, conserver, transmettre au public par télécommunication ou par l'Internet, prêter, distribuer et vendre des thèses partout dans le monde, à des fins commerciales ou autres, sur support microforme, papier, électronique et/ou autres formats.

L'auteur conserve la propriété du droit d'auteur et des droits moraux qui protège cette thèse. Ni la thèse ni des extraits substantiels de celle-ci ne doivent être imprimés ou autrement reproduits sans son autorisation.

In compliance with the Canadian Privacy Act some supporting forms may have been removed from this thesis.

While these forms may be included in the document page count, their removal does not represent any loss of content from the thesis.

Conformément à la loi canadienne sur la protection de la vie privée, quelques formulaires secondaires ont été enlevés de cette thèse.

Bien que ces formulaires aient inclus dans la pagination, il n'y aura aucun contenu manquant.

Canada

ABSTRACT

The objective of the present study is to understand the processes influencing the colloidal silica grout injection into porous media through experimental and numerical investigations. Experimental studies include viscosity measurements, grout injection into columns and grouted sand testing. The grout viscosities are measured during gelation under shear. Colloidal silica grout injection experiments are performed on two different sizes of columns to understand the grouting processes as well as to generate data for numerical simulations. The larger diameter column experiments are performed by varying colloidal silica solution and the type of water. The smaller diameter column (slim tube) experiment was conducted to obtain the data in the absence of fingers. The use of dyes aided in visualizing the grout flow patterns and understanding the processes.

A numerical model is developed by non-iteratively coupling a groundwater flow simulation model (MODFLOW) and a 3-D multi-species reactive transport model (RT3D) and adding modules for the gelling process to simulate the chemical grouting in porous media. A grout gelation model is developed to estimate gel viscosity as a function of reaction time, grout concentration and shear rate. The flow field is periodically updated by taking into account the changing effective hydraulic conductivity in each cell as a result of non-uniform gel viscosity.

The numerical model is verified and validated against (i) an analytical solution developed in this study, and (ii) the available numerical model results from literature, respectively. The grout model is used to analyse the experimental data of sodium silicate grout injection into the sand column as reported in literature. The grout model is also used to analyse the observations made in the colloidal silica grout injection experiment performed as part of this study.

Simulation of grout injection has shown that the shear is an important parameter not incorporated in previous grouting models. The model captured the viscous fingers observed in the column experiments. The model has been able to predict the

iii

experimentally observed injection pressures in the mild slope region. The difference between experimental observations and numerical results increased towards the end of the simulation when the pressures increased steeply. It is hypothesized that this is due to the absence of filtration component in the model. The macromolecules filtered out at the pore throats contribute to the need for higher grout injection pressures. The model provides valuable insights in identifying the complex processes such as viscosification, shear, viscous finger formation and filtration, occurring during grouting.

iv

Dedicated

to

My beloved parents

and

Teachers —

who educated me from the alphabets
to
what I am today.

v

ACKNOWLEDGEMENTS

An effort like Ph.D. needs the direct and/or indirect help of several people. This is an opportunity to remember their help and acknowledge their contribution to enlighten, educate and enable me bring out this piece of work.

My sincere thanks go to my supervisors, Dr. Stanley Reitsma and Dr. Ram Balachandar, for introducing me to this topic and helping me sail through the exercise.

I am grateful to my dissertation committee members, Prof. Ron Barron, Prof. Nihar Biswas, Dr. Fauzi Ghrib and Dr. Rupp Carriveau for sitting through the presentations, reviewing my thesis and making invaluable suggestions. I am benefited a lot through the critical reviews and stimulating discussions with Prof. Barron.

I would like to thank Prof. Biswas, and Prof. Balachandar, the former and present heads of the Civil and Environmental Engineering Dept., for all the help during this program. I acknowledge the facilities provided by the University of Windsor, financial aid provided in terms of Graduate Assistantships and tuition scholarships. I would like to thank the Ontario Graduate Scholarship system for granting me the scholarship. Technical support provided by Chitra Gowda, Richard Clark and Lucien Pop has been great help in performing some of these experiments.

I sincerely acknowledge the stimulating discussions and email exchanges with numerous researchers. I thank Prof. Dan De Kee for getting viscosity measurements made for colloidal silica gelation under shear. My thanks are due to Ms. Inger Jansson, M/s Eka Chemicals, particularly for providing me with the sample of Bindzil for my experiments, viscosity data and, patient and narrative email replies on the subject.

Its time to say thank you to my friends Dr. R. Mantha for motivating and pursuing all the required paper work, for the interesting discussions and reviews by Dr. Nagaraju Kumar, Dr. Ramesh and Robin have been a great help. The inspiration and moral boost extended by adnan, ananth, Dr. Gopi and Dr. Dai Qunli had been a great experience. The help extended by my friends during the experimental work and dissertation reviews is thankfully acknowledged.

Coming to home, the constant and inspiring support and never ending love from my parents, brothers Mouli, Baba and Kapil, and sister Anu have been instrumental in surviving the pressures of this degree. I wished that my father was alive today to see me reaching this stage. The most important person, my son Arvind whose love has been the motivating factor in this endeavour. I thank my wife Lakshmi for adjusting to live with the student income and for all her help.

CONTENTS

x

LIST OF TABLES

LIST OF FIGURES

LIST OF SYMBOLS

a,b,c Fitting parameters for soil moisture equation (Eq. 3.1)

a_1, a_2 and a_3 Fitting parameters of Berkeley gelation model (Eq. 2.2)

C Proportionality constant in shear rate expression (Eq. 2.13)

c_b Boundary conditions for grout concentration (Eq. 4.10)

C_c Shear rate coefficient (Eq. 2.15)

C_{cg} Concentration of colloidal silica in gel phase (Eq. 2.3)

C_{co} Colloidal silica concentration (Eq. 2.3)

$C_{cs,}$ Concentration of colloidal silica in sol phase (Eq. 2.3)

c_o Initial conditions for grout concentration (Eq. 4.8)

C^k Dissolved concentration of species k, $[ML^{-3}]$ (Eq. 4.1)

C_s^k Concentration of the source or sink flux for species k, $[ML^{-3}]$ (Eq. 4.1)

d Dimensionless parameter that describes transition from zero shear rate region to power law region (Eq. 2.9)

D_{ij} Hydrodynamic dispersion coefficient tensor, $[L^2T^{-1}]$ (Eq. 4.1)

F_g Volumetric fraction of gel phase (Eq. 2.3)

$F_{s,}$ Volumetric fraction of sol phase (Eq. 2.3)

h Hydraulic head, $[L]$ (Eq. 4.2)

h_b Boundary conditions for head, L (Eq. 4.9)

h_o Initial conditions for head, L (Eq. 4.7)

k Intrinsic permeability (Eq. 2.13)

$K(x)$ Variable hydraulic conductivity along the length (Eq. 4.14)

k_g Permeability of the grouted porous medium (Eq. 3.5)

$K_{grouted}$ Hydraulic conductivity of the grouted soil media (Eq. 4.4)

K_i Principal component of the hydraulic conductivity tensor, LT^{-1} (Eq. 4.2)

K_o Initial hydraulic conductivity

k_o Initial permeability of the porous medium (Eq. 3.5)

m_{ch} Exponent of Chauveteau shear gelation equation (Eq. 2.11)

n Exponent in power law viscosity relation (describes $\mu(\gamma)$ curve slope)(Eq. 2.9, 2.14)

n_c Cross model exponent (Eq. 2.7)

n_{ch} Exponent of Chauveteau shear gelation equation (Eq. 2.11)

p Empirical parameter (Eq. 2.8)

Q Grout injection rate

q Specific discharge or Darcy flux through the relationship, $v_i = q_i / \phi$ (Eq. 4.1)

q_s Volumetric flow rate per unit volume of aquifer representing fluid $i.e.,$ fluid sink/source term [LT^{-1}] (Eq. 4.1, 4.2)

R Retardation factor (Eq. 4.13)

r_1 Gelation reaction rate coefficient (Eq. 2.3)

s_1, s_2 and s_3 fitting parameters for empirical shear viscosity equation (Eq. 3.2)

S_s Specific storage of the aquifer, L^{-1} (Eq. 4.2)

t Time, [T] (Eq. 4.1)

t^* Normalised time $(= t/t_{0.5})$ (Eq. 2.5)

$t_{0.5}$ Time it takes from the initiation of the reaction to the time when gel phase occupies half the volume of the solution (Eq. 2.4)

v_i Seepage or linear pore water velocity, [LT^{-1}] (Eq. 4.1)

v_x, v_y, v_z Velocity along x, y and z directions respectively

X Colloidal silica concentration (Eq. 3.5, 3.6)

X_{gel} Fraction of grout concentration (Eq. 2.16, 2.17)

$x_{i,j}$ Distance along the respective Cartesian coordinate axis, [L] (Eq. 4.1)

X_l Fraction of grout concentration (Eq. 2.16, 2.17)

X_{min} Minimum grout concentration required for reaction to take place (Eq. 4.14)

α A constant associated with the rupture of linkages (Eq. 2.7)

α_l Longitudinal dispersivity

α_T Transverse dispersivity

γ Shear Rate

$\gamma_{1/2}$ Shear rate at which viscosity is $\mu_0 /2$ (Eq. 2.8)

$\Delta x, \Delta y, \Delta z$ Grid sizes along x, y and z directions respectively

ζ Fitting parameter corresponding to gel time t in Honma gelation model

θ Moisture content at any instant (Eq. 3.1)

θ_r Residual moisture content (Eq. 3.1)

θ_s Moisture content at saturation (Eq. 3.1)

λ Time constant in Carreau and Carreau-Yasuda gelation models (Eq. 2.9, 2.10)

μ_o Viscosity of solution at zero shear rate (Eq. 2.7, 2.12)

μ_∞ Viscosity of solution at infinite shear rate (Eq. 2.7, 2.12)

μ Viscosity of the grout according to gel time relation Equation 2.1 or 2.6 (Eq. 2.17)

μ_{gel} Viscosity at a given time t after gel reaction is initiated (Eq. 2.2, 2.5, 2.6)

$\mu_{l\,or\,p}$ Viscosity of the grout after mixing with water due to dilution –subscripts l and p refer to linear and power law mixing rules (Eq. 2.17)

μ_{max} Maximum achievable viscosity for a given shear rate (Eq. 3.2)

μ_{min} Minimum or initial viscosity of the grout (Eq. 3.2)

μ_r Ratio of viscosity of grout to the viscosity of water

μ_{ro} Ratio of viscosity of initial viscosity of the grout to the viscosity of water

μ_w Viscosity of water present in the porous media (Eq. 2.17)

μ_s Viscosity of sol phase (Eq. 2.5)

ρ_{bulk} Bulk density of the colloidal silica solution (Eq. 3.5, 3.6)

ρ_{solids} Density of the colloidal silica solids (Eq. 3.5, 3.6)

σ Fitting parameter corresponding to gel time t in Honma gelation model

ΣR_n Chemical reaction term, $[L^{-3}T^{-1}]$ (Eq. 4.1)

ϕ Porosity (Eq. 2.13, 4.1)

ϕ_{cs} Volume fraction occupied by the colloidal silica (Eq. 3.6)

ϕ_g New porosity after grout is injected (Eq. 3.5, 3.6)

ϕ_o Initial porosity of the porous medium (Eq. 3.5 and 3.6)

ψ Soil water pressure head (Eq. 3.1)

CHAPTER 1

INTRODUCTION

1.1 GENERAL

Grouting is a process by which a material is injected into a soil or rock formation to change the physical characteristics of the formation (American Society of Civil Engineers, 1997). Grouting is one of the ground modification and soil stabilization techniques that is commonly used to increase strength. Application of grouting may also be found in the areas of sewer and tunnel restoration. More recently, grouting has been used for environmental containment (Moridis *et al.*, 1999; MSE Technology Applications, 2001; Kim and Corapcioglu, 2002a,b). Various grouting techniques in practice include jet grouting, compaction grouting, permeation grouting, soil fracture grouting and slurry grouting (Welsh, 1997).

Grouts are classified into particulate and chemical grouts. Particulate grouts, also called suspension grouts, form suspension when mixed with water. The particles in particulate grouts, when injected into soil, travel along with water until they are dropped out of suspension (Karol, 1990). Bentonite, cement, lime and fly ash are examples of this type. Particulate grouts cannot be injected into soils finer than medium sands with hydraulic conductivities less than 10^{-5} m/sec (Spooner *et al.*, 1984). Chemical grout is defined as any grouting material characterized by being a pure solution, *i.e.*, no particles in suspension (Committee on Grouting 1980). The popular chemical grouts are sodium silicate, acrylamide and acrylate (U.S. Army Corps of Engineers, 1995). Penetrability of particulate grouts is a function of their particle size, whereas penetrability of chemical grouts is a function of viscosity (Karol, 1990).

1.2 CHEMICAL GROUTING

Chemical grouting is defined as the process of injecting a chemically reactive solution into soil. This reactive solution behaves as a fluid but reacts after a predetermined time to form a solid, semi-solid or gel (US Army Corps of Engineers, 1995; American Society of

Civil Engineers, 1997). Chemical grouts are low viscosity solutions comprised of water-soluble polymers (such as sodium silicate, colloidal silica, polyacrylamide) and cross-linkers (brine solution such as NaCl, $CaCl_2$). Once the polymers and cross-linkers are mixed, the viscosity of the solution increases as the reaction progresses and eventually a solid, semi-solid or gel is produced at the end of a predetermined reaction time referred to as the gel time. When such grout solutions are injected into soil formations, the water is displaced by the grout solution, which eventually form chemically and biologically inert, impermeable, in situ barriers as a result of greatly increased viscosity (Durmusoglu and Corapcioglu, 2000). This solid or gel reduces the hydraulic conductivity without significantly changing the structure or volume of the soil.

The chemical grouting process depends on the principle of permeation. The grout permeation depends on the initial viscosity of the grout as well as the viscosity during gelation. The penetrability of various chemical grouts in different formations is shown in Figure 1.1. Sodium silicate (SS) is the most predominantly used chemical grout in geotechnical applications such as soil stabilization and ground improvement (Karol, 1990). Sometimes sodium silicate is grouted in conjunction with cement and/or microfine cement (American Society of Civil Engineers, 1997). Permeation grouting can be achieved with silicate based grouts in soils having hydraulic conductivity of 10^{-4} m/s, whereas soils with hydraulic conductivity of 10^{-5} m/s or less require expensive resin based grout (Karol, 1990; Gallavresi, 1992; Bruce, 1994). Sodium silicate grouts are considered to be the safest and the most environmentally compatible and hence they are extensively used in the field (US Army Corps of Engineers, 1995; American Society of Civil Engineers, 1997). Acrylamides are less viscous (and hence have better penetrability) compared to sodium silicates and have better gelation control. However, they are surrounded by controversy about their adverse environmental and health affects. Acrylates have similar or better penetrability than that of acrylamides (Karol, 1990). Though sodium silicates are safer, they have higher initial viscosity. They also exhibit syneresis, which is the process of exudation of liquid (generally water) from set gel, which is not stressed, due to the tightening of the grout material structure (Yonekura and Kaga, 1992). Hence researchers in the recent past have focused on the environmentally benign colloidal silica (CS) applications (Noll *et al.*, 1992; Finsterle *et al.*, 1994; Moridis

2

et al., 1999; Kim and Corapcioglu, 2002a,b) due to its low viscosity on the order of 2-5 cP, absence of syneresis and better gel time control.
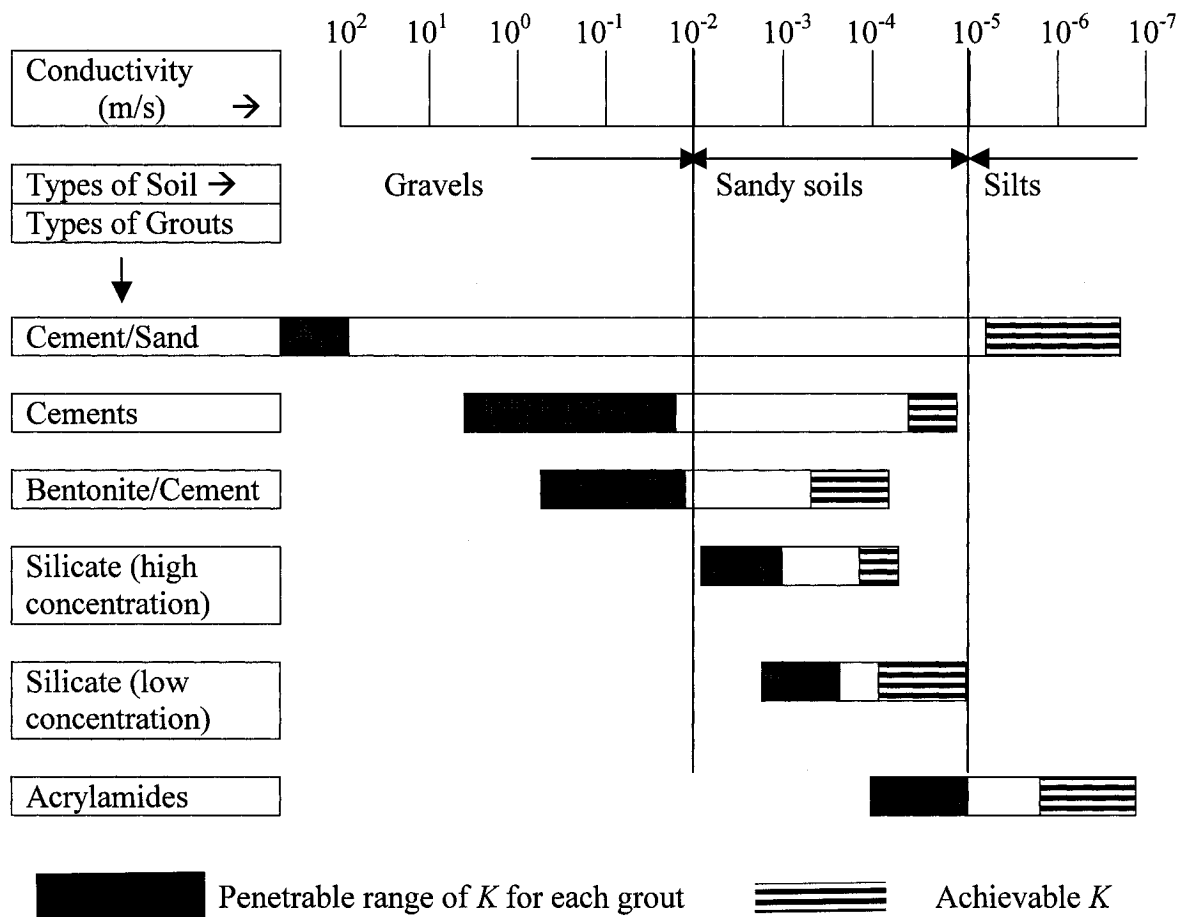
Figure. 1.1: Penetrability of grouts in soils and indicative range of achievable hydraulic conductivities (K) (adapted from Karol, 1990)

Chemical grouts have been used in geotechnical, construction and water sealing applications. However, researchers have focused attention on the application of chemical grouts for waste containment during the last two decades (May *et al.,* 1986; Mitchell and Rumer, 1997; Mitchell and Van Court, 1997). The use of gelling solutions is also a common practice in the field of petroleum engineering during secondary oil recovery. Chemical solutions are injected into the petroleum formations such that these solutions enter high hydraulic conductivity zones and reduce their hydraulic conductivity once the solution gels. Then the oil trapped in low hydraulic conductivity zone is flushed out through water injection techniques. Various solution types that are used in enhanced oil

3

recovery include xanthan-chromium gel system (Avery *et al.*, 1986; Hubbard *et al.*, 1988; Dolan, 1989; Hejri, 1989; Hejri *et al.*, 1989; Jousset *et al.*, 1990), polyacrylamide/chromium system (McCool *et al.*, 1988; Todd 1990; Todd *et al.*, 1991; Marty *et al.*, 1991) and colloidal silica system (Jurinak and Summers, 1991; Seright, 1992, 1993).

1.3 MOTIVATION FOR THE RESEARCH

Groundwater contamination poses serious risk to the environment and in turn to human health. Waste containment through grout/slurry barriers has become a very important step in waste management and site remediation programs of regulatory agencies, as the search for more cost effective clean up technologies continues (Inyang, 1999). Since cleanup technologies, when available for subsurface contaminants, can be costly and time consuming, it is necessary to examine other possible and cheaper ways to reduce the risk and protect human health and environment at the contaminated sites (Pearlman, 1999). Subsurface containment barriers are an important method of limiting and/or eliminating the movement of contaminants through the subsurface. A completely contained contamination zone can be used as an in situ reactor vessel in which new and/or slow in-situ remediation technologies can be tried without the usual risks associated with unbounded treatment zones (Inyang, 1999). Unlike in situ treatment systems, in which the treatment parameters could be altered to observe the effects, in situ containment systems present very few opportunities for conducting sensitivity analysis for various system parameters in the field.

Barriers may be used either as an interim or as a permanent step for containment of wastes. There are various types of subsurface barrier technologies available commercially (Pearlman, 1999). However, there are two main concerns: 1) barrier continuity and 2) barrier performance. Once installed, these subsurface barriers must have a hydraulic conductivity equal to or less than the design value (Rumer and Ryan 1995). Currently there is no method of guaranteeing the continuity of a subsurface barrier (Sullivan *et al.*, 1998). Proper emplacement of a subsurface barrier is critical to ensure overall effectiveness of the containment system. One of the main reasons for uncertainty

4

in the integrity and attainment of the design hydraulic conductivity is the soil heterogeneity. This problem can only be addressed through quantitative modeling of performance using field parameters and adopted laboratory data that has been scaled up temporally and spatially (Inyang, 1999). Thus, there is a need for the development of mathematical tools to simulate the grouting phenomena, identify the critical processes and establish their relative importance. Also, models are useful in evolving rational design and assessing the uncertainty of barrier performance in the presence of soil formation heterogeneities. The utility of such a mathematical model would be of great value for a broader area of rational design of grouting than just the environmental containment. Before designing, it is necessary to understand the physics of grout injection into porous media and to represent the physics of gelation and other relevant processes with the help of experimental and modeling studies.

1.4 OBJECTIVES OF THE STUDY

The main objectives of the present study are:

- To conduct laboratory-based experiments of grout injection into porous media to understand the grouting physics.

- To develop a numerical model to simulate chemical grout injection, with emphasis on colloidal silica grouting, and the resulting profile modification.

- To determine the interplay between the grouting processes such as gelation, shear thinning, filtration and viscous fingering.

- To determine numerically the effect of heterogeneity on chemical grouting.

1.5 SCOPE OF THE RESEARCH

The present study is designed to advance our knowledge of the physics of chemical grouting and the processes occurring during grout injection into porous media through experimental investigations and numerical modeling. Colloidal silica (Bindzil 40/170 produced by M/s Eka Chemicals, USA) is chosen as a chemical grout for the present study. Experiments are performed on colloidal silica grout injection into sand columns to make quantitative measurements and qualitative observations to decipher the physics of grouting. This research also aims to develop a chemical grouting model using a

5

groundwater flow simulation code - MODFLOW (McDonald and Harbaugh, 1988; Harbaugh and McDonald, 1996) and reactive transport simulation code - RT3D (Clement and Johnson, 2003), with modifications to simulate the chemical grouting processes. Though gelation equations related to colloidal silica have been incorporated in the code, adaptability of the code to other gelling liquids is demonstrated by incorporating the gelation equation of sodium silicate grout in the reaction module. The model results are (i) verified against an analytical solution developed in this study, (ii) validated against the results obtained from a numerical model published in the literature. The grout model is used to analyse the experimental data of sodium silicate grout injection in a sand column as reported in the literature. The grout model is also used to analyse the observations made in the colloidal silica grout injection experiments performed as part of this study to better understand the processes that govern the grouting injectivity.

1.6. ORGANIZATION OF THE DISSERTATION

The dissertation is organized into five chapters.

Chapter I presents a general introduction to the subject, motivation, objectives and scope of the research.

Chapter II reviews the literature on chemical grouting, gelation under shear, experimental and numerical investigations of chemical grouts and other gelling liquids.

Chapter III presents the experimental work carried out in this study.

Chapter IV presents the mathematical model development including governing equations, solution techniques, assumptions and limitations. The chapter also presents the details on verification and validation of the model, as well as other numerical investigations on different processes such as gelation, mixing, grout aging, dispersion and heterogeneity.

Chapter V presents the summary, conclusions and recommendations for future research.

6

CHAPTER 2
LITERATURE REVIEW

2.1 INTRODUCTION

Karol (1990) is perhaps one of the most important textbooks that covers most aspects of chemical grouting. Littlejohn (2003) presented an excellent historical perspective on chemical grouting. The processes occuring during the transport of gelling solutions through porous media may be described in terms of either microscopic processes such as aggregate size distributions, pore throat size distributions, evolution of aggregate sizes, etc. (Todd, 1990), or macroscopic processes such as viscosification, shear thinning and filtration (Bryant *et al.,* 1998; Chauveteau *et al.,* 2001). It is important to understand the interplay of these processes within the soil and related parameters to predict grout flow (Dwyer, 1994). The present chapter includes the literature review on the experimental and mathematical modeling studies of chemical (colloidal silica in this case) grouting, processes influencing the grouting process and problems encountered in attempting to represent the physics in grout modeling.

2.2 COLLOIDAL SILICA

2.2.1 Properties

Colloidal silica (CS) is a stable dispersion of discrete particles (commonly termed as sol) of amorphous silica (Iler, 1979). Stable in this case means that the solid particles neither settle nor agglomerate at a significant rate. If the liquid is water, the dispersion is called aquasol or hydrosol. The CS particles are approximately uniform and size ranges between 2-100 nm (Persoff *et al.,* 1999). CS is made by extracting alkali from sodium silicate using ion exchange resin (Yonekura, 1997). The colloid, thus produced, is unstable. It is stabilized by a negative charge on each particle by either of the two popular methods: (i) by raising pH, or (ii) by isomorphous substitution of alumina for silica on the particle without stabilization (Persoff *et al.,* 1999). The colloids formed in this way have electric double layer ions around the surface. Two-dimensional representation of a dehydrated and hydroxylated colloidal silica particle is presented in Figure 2.1.
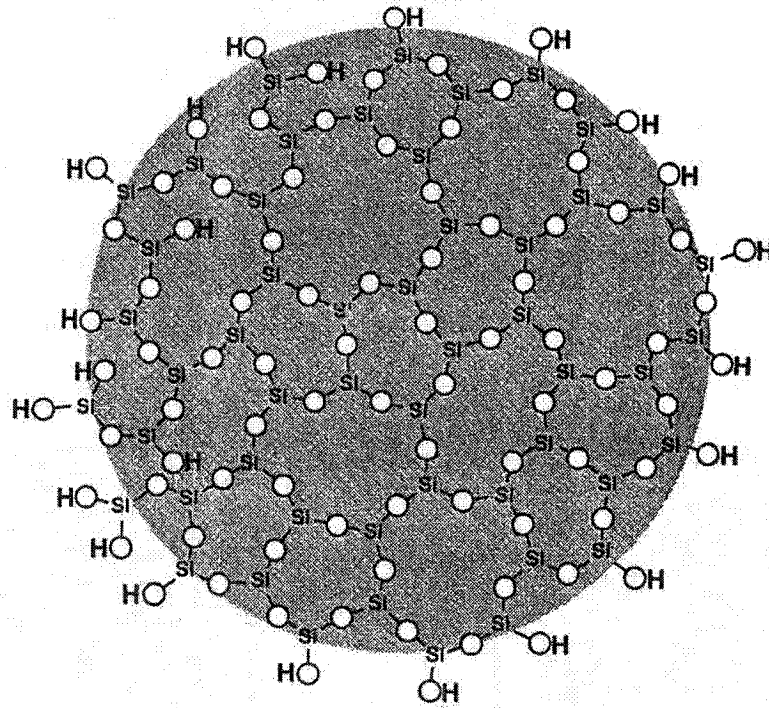
Figure 2.1: Two-dimensional representation of a dehydrated but fully hydroxylated colloidal silica particle. The fourth oxygen coordinated with *Si* is above or below the plane of the paper (Bergna, 1994).

(Reprinted with permission from Bergna (1994), American Chemical Society through their letter dt. August 19, 2004)

CS has been investigated for grouting use because of its low viscosity and the absence of the syneresis problem, which occurs with sodium silicate (SS) grouts (Yonekura and Kaga, 1992). Typically, solids content in SS grout is 40 % by wt. with a viscosity of 200 cP. Hence it needs dilution before grouting. Whereas, CS with solids content of 40 % by wt. has viscosity around 16 cP (LUDOX series) and it is less than 15 cP for CS formulations of Eka gel (Bindzil series). Various CS formulations available commercially are either aqueous based or glycol (organo) based. Colloidal silica is manufactured under LUDOX series and NYACOL series by E.I. du Pont and Nyacol Inc., under aqueous and glycol base respectively. Eka gels (Bindzil series) produced by M/s Eka Chemicals are aqueous based solutions. Properties of different CS formulations are summarized in Table 2.1.

8

Table 2.1: Properties of different colloidal silica formulations

Properties	Ludox-SM	Ludox-HS40	Ludox-TM	Bindzil 40/170
Silica (as SiO2), % by wt.	30	39-41	50	40
SiO2/Na2O (by wt)	50	89-101	220	200
Particle charge	Negative	Negative	Negative	Negative
pH	10.0	9.2-9.9	9.0	9.5
Viscosity (cP) @25°C	5	45	37	<15
Average particle size (nm)	7	12	22	20
Specific surface area (m^2/g)	360	198-258	140	170
Density (g/cm^3)	1.22	1.292 –1.312	1.40	1.30

Source: Iler, 1979; Grace & Co, 2003; Eka Chemicals, 2004

2.2.2 Applications

Colloidal silica gels were applied for geotechnical, environmental and enhanced oil recovery operations during secondary recovery of petroleum applications through experimental, in situ and modeling investigations. Jurinak and Summers (1991) were the earliest researchers to explore CS gels in the reservoir field to control water in petroleum recovery. They were searching for a gel system that (i) could be injected into soils having low permeability (<1mD), (ii) had controllable gel time, (iii) was stable in typical operating environments, (iv) was easily injectable, and (v) posed minimal safety handling and environmental problems. They narrowed down their search to silica based systems as these systems could satisfy the above mentioned objectives. Of these silica systems, they finally selected colloidal silica gels over conventional sodium silicate gels because of robust gel time control with variation in salinity and pH. They also investigated the effect of CS grout concentration ranging from 5 to 30 % by wt. on the reduction in hydraulic conductivity in sand packs having initial permeabilities of 1 to 3 Darcies and obtained permeabilities of 1 mD when the sand packs are treated with 4 % by wt. colloidal silica gel solution. Liang *et al.* (1992) and Seright (1995) investigated the reduction of oil, gas and water permeabilities in their efforts to develop secondary

9

petroleum recovery technology using different gels including CS. Seright (1992, 1993) also investigated the effect of rock permeability on gelation. Seright (1992) obtained post-treated soil permeabilities of 10-30 μD when injected with 10 % by wt. colloidal silica solution. His findings are in agreement with those of Jurinak and Summers (1991).

Yonekura (1997) presented an overview of the different silicate based gels including CS and post-grouted soil properties such as compressive strength and durability. Yonekura and Kaga (1992) reported the use of CS for soil stabilization. Gallagher (2000), Gallagher and Mitchell (2002) and Liao *et al.* (2003) investigated the use of colloidal silica for the mitigation of liquefaction. In a further study, Gallagher and Koch (2003) investigated the delivery of colloidal silica to stabilize the soils from liquefaction through their sand box model experiments and found that 1.5 to 2 pore volumes were needed to achieve the adequate coverage.

CS has triggered the interest of researchers who had investigated its use for protecting groundwater quality (Noll *et al.*, 1992; Persoff *et al.*, 1994, 1995; Finsterle *et al.*, 1994, 1997; Moridis *et al.*, 1995, 1999; Durmusoglu and Corapcioglu, 2000; Kim and Corapcioglu, 2002a,b). Noll *et al.* (1992), while trying to determine the potential use of LUDOX colloidal silica (developed by Du Pont) as an innovative remediation technology, investigated the limits under which LUDOX sol could be gelled and would remain gelled in situ for long periods of time. Environmental application of LUDOX is an outgrowth of a technology developed by Cononco Inc. (especially by Jurinak and Summers, 1991) for oil field applications. Noll *et al.* (1992) investigated the factors affecting gel time, achievable degree of permeability (hydraulic conductivity) reduction, to assess the ability to stabilize metals and elucidate the adsorptive capacity of the LUDOX gel. Lowest gel times were achieved in the pH range of 6-7. They reported that the sand packs treated with 5 % by wt. (~2 % by volume) LUDOX sol yielded hydraulic conductivity of 10^{-9}-10^{-10} m/s, which means four to five orders of reduction. Researchers at Earth Sciences Division, Berkeley (Persoff *et al.*, 1994, 1995; Finsterle *et al.*, 1994, 1997; Moridis *et al.*, 1995, 1999), while trying to develop viscous liquid barrier technology, investigated colloidal silica applications extensively. Persoff *et al.* (1999)

10

observed that grouts with CS concentrations of 7.4 % by wt. (3 % by volume) or more achieved statutory requirements of hydraulic conductivity of barriers, *i.e.*, 10^{-9} m/s. The gel barrier formation in the unsaturated zones was investigated experimentally (Durmusoglou and Corapcioglu, 2000) and numerically (Kim and Corapcioglu, 2002a,b).

2.3 GELATION

Iler (1979) described gelling as "a process where the particles are linked together in branched chains that fill the whole volume of sol so that there is no increase in the concentration of silica in any macroscopic region of the medium." Thus, gelation or gelling of colloidal silica involves colloidal particles linking together and forming three-dimensional chains or networks (Iler, 1979; Bergna, 1994). A schematic diagram of gelation and flocculation is shown in Figure 2.2. Electrolytes are added to destabilize the stable colloids and in turn achieve gelling. Due to the formation of chains, sol medium becomes more viscous resulting in solidification by the networks of particles. In order for the chain of silica particles to form, silica particles with sufficiently low charge on the surface should collide (Iler, 1979). When they collide with each other, siloxane (Si-O-Si) bonds are formed and hold these particles together as shown in Figure 2.1.
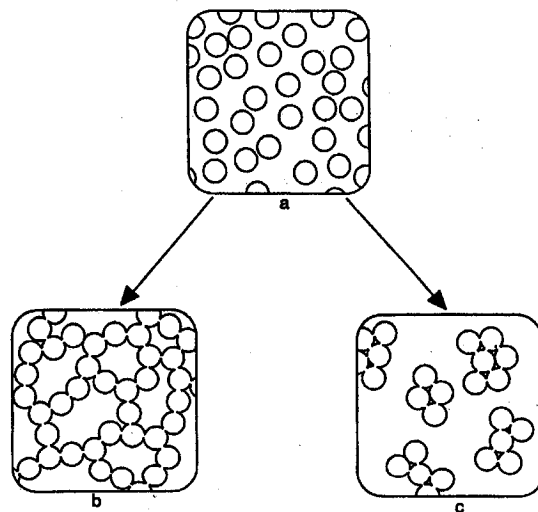
Figure 2.2: Schematic representation of gelation and flocculation Silica
gel (a) sol, (b) gel and (c) flocculation and precipitation
(Reprinted with permission from Iler (1979). Copyright (1979) Wiley, USA)

11

Gelling time depends on the ionic activity. No aggregation occurs if the concentration of electrolyte is generally less than 0.1-0.2 N depending on silica concentration (Iler, 1979). The CS solution viscosity increases due to controlled gelation process induced by the addition of a concentrated brine solution (Persoff *et al.*, 1999). When the CS sols are gelled, the gel becomes more viscous and then develops rigidity. The gel fills the volume originally occupied by the water.

2.4 GEL TIME CONTROL

Gel-time is the time from the moment reaction has started (*i.e.*, when the brine and CS sol are mixed) to the time that the grout solution is completely immobile. Gel-time is a qualitatively described rather than a specific measurable state. Sydansk (1990) classifed gelation process into 11 stages. The grout was considered to be fully gelled, when the grout solution is completely immobile. Gallagher (2000) defined the gelation as a state at which the marble ball in the grout containing vial takes 15 seconds to reach the bottom when the grout containing vial was turned upside down. For the purpose of numerical modeling, Kim and Corapcioglu (2002a) considered the grout to be fully immobile when the viscosity reaches 10^{10} times the viscosity of water. Rate of gelling is proportional to the total surface area of silica particles. Surface area is proportional to size of the particles. As the particle size decreases, the total surface area increases. Therefore, other factors being equal, sols having the same ratio of concentration to particle diameter gel at about same rate (Iler, 1979). Gel formation is proportional to the hydroxyl ion concentration and hence the pH of the solution (Iler, 1979). Figure 2.3 presents the effect of pH and salts on the gel formation. In the case of silica with pH less than 3.5, salts (electrolytes) have little influence on the rate of gelling. In the case of most commercial silica bearing negative charge, with pH greater than 3.5, reaction with salts reduces the net repulsion effect and accelerates gelling (Iler, 1979). From Figure 2.3 it may be observed that gel formation increases for silica with pH varying between 3-5. For the case of pH above 6, even though hydroxyl ions are available in abundance, fewer collisions between silica particles result in a slow rate of gelation.

12

In a recent study, Persoff *et al.,* (1999) showed that gel time was also controlled by the concentration of silica, concentration of added brine, in addition to pH. Based on their experiments to study the effect of dilution, Persoff *et al.,* (1999) found that with increasing concentration of silica and/or the concentration of brines the gelling is achieved quickly. Faster gelling was achieved at neutral pH compared to basic pH. They also reported that CS grouts with 19.7 % silica or more (in LUDOX SM formulations) reached gel time target without pH adjustment. Neither strength nor hydraulic conductivity of colloidal silica grouted samples was changed in the presence of organics at low concentration (approximately 5 % organics such as TCE, CCl4, aniline). From the experiments where soil was added to still grout solution, the presence of soil was found to reduce the gel time (Persoff *et al.,* 1999; Durmusoglu and Corapcioglu, 2000).
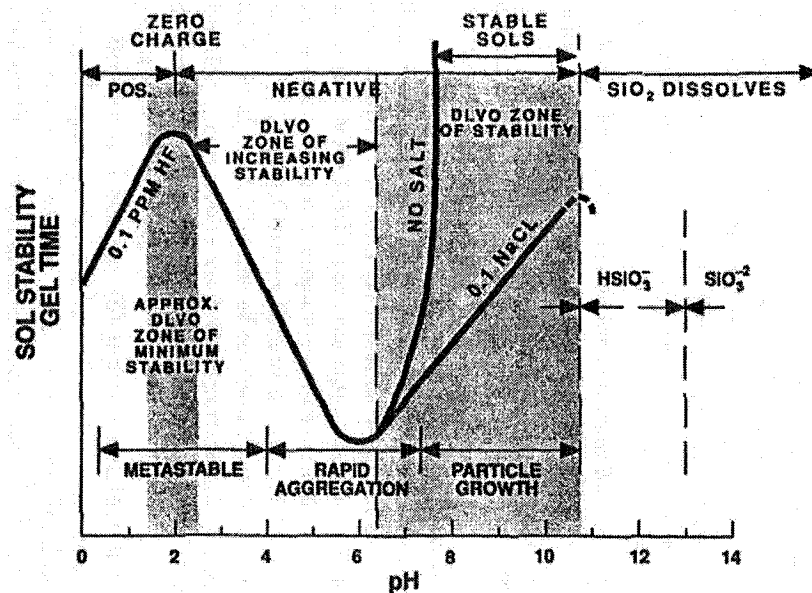
Figure 2.3: Effect of pH on the gel time of the colloidal silica-water system (Reprinted with permission from Iler (1979). Copyright (1979) Wiley, USA)

Karol (1990) studied the gel time control vis-à-vis soil layering. A schematic diagram of the grouted soil with layers is presented in Figure 2.4. In order for the grout to enter the soil formation with alternate layers of high and low hydraulic conductivity, it is advantageous to set a short gel time. The grout solution that enters the high permeable

13

layers gels and reduces their hydraulic conductivity, sometimes close to or less than that of low permeable layers. If the grout injection is continued, grout solution then enters low conductivity layers as well. On the other hand, when only low hydraulic conductivity soils are present, it is necessary to have a longer gel time to enable the grout to be transported to farther locations in the formation. In any case the gel times should not be longer than the injection time (Karol, 1990). If the grout is not gelled completely, after injection is stopped, there is a risk of dilution due to groundwater movement either at the outside boundary of the grout bulbs or at the contact between the grout bulbs resulting in the formation of seams. This has an adverse effect on impermeable barrier formation than when grouting is used for strengthening or mitigation of liquefaction purposes.
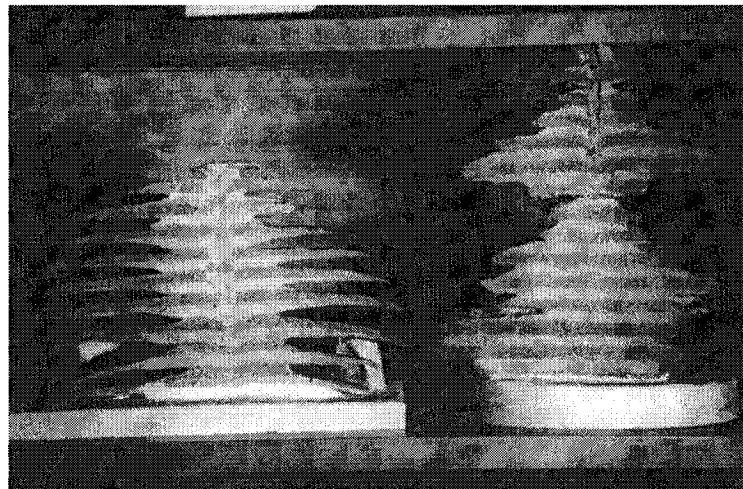
Figure 2.4: Grouting in layered soils: long gel time vs. short gel times (Karol, 1990).

2.5 CHEMICAL GROUTING MODELING

Numerical models were been developed for simulating the injection of gelling solutions into porous media in the areas of geotechnical (Honma, 1984; Bouchelghem and Vulliet, 2001a,b; Gallagher, 2000; Gallagher and Mitchell, 2002), geoenvironmental *i.e.,* environmental containment (Noll *et al.,* 1992; Finsterle *et al.,* 1997; Moridis *et al.,* 1999; Kim and Corapcioglu, 2002a,b), and secondary oil recovery process (Sorbie *et al.,* 1985; Hubbard *et al.,* 1988; Todd, 1990). These models combined the analysis of fluid flow and

14

mass transport of grout solution to obtain flow field and concentration distribution. Gelation was represented as a reaction term in the transport equation. The governing equations for the combined flow and mass transport were solved using a variety of numerical techniques such as finite difference (Guo and Langevin, 2002), finite element (Voss and Provost, 2002), integrated finite difference (Oldenburg and Pruess, 1995) and finite volume (Frolkovic and Schepper, 2001) methods.

2.5.1 Flow and Transport Coupling

Solute concentration in the fluid affects the transport in porous media (Ackerer *et al.*, 1999) in environmental problems like seawater intrusion into coastal aquifers (Pinder and Cooper, 1970; Frind, 1982), leakages from landfills (Frind, 1982; Oostrom *et al.*, 1992), deep-well disposal of toxic and radioactive wastes in salt rock formations, transport of dissolved solids in agricultural fields (Deverel and Fujii, 1988) and Henry and Elder problems (Oldenburg and Pruess, 1995). In these cases flow and solute transport problems were interlinked and posed non-linearity. The degree of non-linearity depends mainly on the concentration of solutes, which also affects density and viscosity of the fluid system.

Analysis of solute transport problems in porous media involves solving the flow problem and then solving the transport problem using the flow field obtained from the solution of the flow problem. However, in case of problems such as the present one, the fluid changes its viscosity state as a function of reaction time and concentration of grout cross-linker. The increased viscosity modifies the flow field, which in turn affects the concentration field. Thus the flow and transport modeling of gelling solutions in porous media is a coupled system. The coupling between flow and transport problems involves two parts (Oldenburg and Pruess, 1995; Diersch and Kolditz, 2002). In the first stage the velocity from the flow problem is used in the solution of the advection part of the transport solution. The second part involves the dependence of hydrodynamic dispersion on the velocity field, which is obtained from the flow problem solution.

15

Since the literature was limited on viscous coupled systems, analogy was drawn from density dependent coupled systems. Diersch and Kolditz (2002) stressed the importance of non-linearity due to coupling when the fluid density is strongly dependent on concentration and pointed out that the results could be quite contradictory depending on degree of non-linearity. The set of problems of this category were referred to as density dependent and/or viscosity dependent flow and transport problems. There have been several studies on the numerical solution of density dependent systems (Frind, 1982; Galeati et al., 1992; Oldenburg and Pruess, 1995; Kolditz et al., 1998; Ackerer et al., 1999; Younes et al., 1999). They differ in the way the coupling between the flow and the transport problem is simulated and the solution techniques used.

Based on the way the flow and transport are combined, modeling studies reported so far may be classified into fully coupled, partially coupled and decoupled approaches (Galeati et al., 1992, Oldenburg and Pruess, 1995, Boufadel et al., 1997). In the fully coupled systems, the flow and transport variables were solved for pressures and concentration fields simultaneously for any given time step (Oldenburg and Pruess, 1995). In the remaining classes of problems, flow and transport problems were solved sequentially. In case of decoupling, the flow problem was solved once and the transport problem was solved for the entire simulation period using the same velocity field. An implicit assumption in this approach was that the concentration did not affect the density and viscosity, and hence the flow field. This might be true in cases where salinity concentration was less than 5 % (Oldenburg and Pruess, 1995) or grout concentration was less than 2 % (Gallagher, 2000). When the density and viscosity were affected by concentration, the flow and transport problems could be solved sequentially in a partially coupled approach. The following stepwise procedure was followed:

1. The flow problem was solved and flow field is obtained.
2. Using the flow field from above, the transport problem was solved.
3. Based on the density and viscosity variations due to changed concentration field, a new flow field was calculated.
4. Using the new flow field, the transport problem was solved.

16

There were two types of solution schemes in the partially coupled approach. First of the two partial coupling approaches reported in the literature, referred to as iterative coupling, is where flow and transport problems are solved sequentially. The solution process was continued until the difference in heads and concentrations between any two successive iterations was less than the tolerance limit. Then the solution process proceeded to the next time step and so on. In the second approach, referred to as non-iterative coupling, for a given time step the flow field was solved by incorporating density and viscosity variations as a function of concentration field obtained in the previous step. Thus, the effect of change in density and viscosity obtained in this time step were used to solve the flow and transport problems for the next time step (Galeati *et al.*, 1992; Boufadel *et al.*, 1997). The simulation progressed until the end of the simulation period.

The studies that followed the iteratively coupled approach used Picard iterative (Younes *et al.*, 1999), modified Picard iterative and Newton-Raphson techniques (Oldenburg and Pruess (1995). Some of the studies preferred Picard schemes with first order of convergence, to Newton-Raphson scheme with second order of convergence because of stability, even though Picard schemes call for higher computational effort (Boufadel *et al.*, 1997). The advantage of using the fully coupled system was its accuracy, while simulations with no-coupling gave highly inaccurate results (Galeati *et al.*, 1992; Oldenburg and Pruess 1995; Boufadel *et al.*, 1997). The iterative coupling gave reliable results, whereas the results from non-iterative coupling were close to the ones obtained from iteratively coupled system at significantly lower computational effort (Galeati *et al.*, 1992; Boufadel *et al.*, 1997). Both fully coupled and iteratively coupled solutions required more than one iteration, which means there was a need for excessive computational effort.

2.5.2 Geotechnical Applications

Honma (1984) was the first one to present a mathematical model for simulating injection and distribution of sodium silicate (SS) chemical grouting. Honma adopted what is known as an iteratively coupled approach where the flow problem was solved first and

17

then the transport problem was solved using that flow field. The simulation was repeated until the end of injection period. The viscosity increase was represented by an exponential equation. Honma analyzed the grouting problem in one, two and three dimensions. Modeling results were compared to the experimental observations of SS grout injection into a sand column and 3-D point injection. Honma observed that the injection pressure profiles obtained from one-dimensional simulation of sodium silicate grout injection into a sand column and the experimental observations differed significantly. Honma concluded that the time dependent viscosity relationship did not represent gelation in porous media and considered only a concentration dependent viscosity function.

A recent modeling study by Gallagher (2000) focused on colloidal silica application for passive soil stabilization. The objective was to determine the conditions under which grout could be injected as far as possible into the soil formation in saturated groundwater flow system as a carrier. This study used a groundwater flow simulator, MODFLOW (McDonald and Harbaugh, 1988) and solute transport code MT3D (Zheng, 1991). In this study, hydraulic conductivity was divided by two (i.e., initial viscosity of grout), to incorporate the effect of grout solution viscosity. The flow field was generated only once and used for the remaining simulation of transport of grout in the saturated groundwater system. Hence, this modeling study may be categorized as a no coupling system. This was based on the assumption that the decoupled approach was appropriate if the injected grout is of very low concentration and very little change in hydraulic conductivity may be expected. Gallagher (2000) recommended that future modeling studies include the variations in hydraulic conductivity in the soil formation i.e., in addition to inter-layer heterogeneity in hydraulic conductivity, intra-layer heterogeneity should be incorporated.

2.5.3 Environmental Containment Applications

Noll et al., (1992) was the first study to be reported in the area of modeling of colloidal silica (LUDOX SM Sol) for environmental containment. The study involved injection of CS grout solution into a bench-scale sand box. Since the LUDOX did not react with the sand and behaved like a conservative tracer, they demonstrated the possibility of using

18

conventional numerical groundwater flow and transport models. They used MODFLOW (McDonald and Harbaugh, 1988) for flow simulation and MT3D (Zheng, 1991) for grout transport and distribution. They reported that the post-excavated grouted bulb sizes obtained from the model and the bench-scale sand box experiment were similar, though the results were not presented explicitly. They also reported that the grout injection resulted in four orders of magnitude reduction in hydraulic conductivity. Although the reported conclusions were interesting, several details on their model development were missing. It was not clear how the viscosity effects were incorporated. Also, there was no mention about how the changes in flow field due to viscosity change were incorporated.

Researchers at Earth Sciences Division, University of California, Berkeley, as part of their efforts to develop Viscous Liquid Barrier (VLB) technology using colloidal silica, modeled the colloidal silica grouting into the porous media (Finsterle *et al.*, 1994, 1997; Moridis *et al.*, 1999). They developed a grouting model based on an existing numerical simulator TOUGH2. TOUGH2 (Pruess, 1991) is a numerical simulator for non-isothermal flows of multicomponent multiphase fluids in porous and fractured media. The solution scheme is based on a fully coupled approach. Finsterle *et al.*, (1994, 1997) and Moridis *et al.*, (1999) developed equations of state for the gelation and solidification of grout once placed in the soil. They investigated using a specially designed CS formulation (DP5880).

Moridis *et al.*, (1999) compared the optimization based design, aimed at achieving design parameters that maximize uniformity and minimize hydraulic conductivity of the barrier, with that of the standard engineering practice. Their design based on optimization met the functional requirements of barriers such as (1) hydraulic conductivity $< 10^{-9}$ m/sec and (2) barrier thickness of 1.0 m. The design based on standard engineering practice did not achieve the above two design objectives along the entire barrier. Moridis *et al.* (1999) reported that the hydraulic conductivity values obtained through numerical modeling studies and those obtained from the post-grouted in situ values were in agreement. However, the paper did not report the hydraulic conductivity data of grouted soil obtained in the field.

MSE Tech (2001) conducted a modeling study using PORFLOW simulator (ACRi, 1994, 1999) to predict the unsaturated flow around soil grouted with CS. PORFLOW is a general purpose simulation software for transient or steady-state multiphase flow, heat, salinity and mass transport in multiphase, variably saturated porous or fractured media with dynamic phase change. They used Nyacol NP 6010 CS formulation. The modeling study indicated that the infiltration rate would be reduced from 0.3048 m/yr to 0.0017 m/yr against the design objective of 0.04 m/yr. This reduction in infiltration rate is more than 23 times the design objective. The field investigations also revealed a similar trend in reduction in the hydraulic conductivity, although it varied with depth below ground.

More recently Kim and Corapcioglu (2002a,b) reported the modeling of colloidal silica gel barrier formation. Their model development was based on a two-phase approach - gel and sol phases. The gelling model that they proposed was different from the gel time curve proposed by Finsterle et al. (1994, 1997) and Moridis et al. (1999). Kim and Corapcioglu (2002a,b) used Nyacol 1440 colloidal silica formulation. They observed, in general, that the increase in the total colloidal silica release yielded a better performance i.e., higher reduction in hydraulic conductivity.

2.5.4 Secondary Recovery of Petroleum Applications

Todd (1990) reviewed the three models that were published until that time. They included the Winfrith model (Sorbie et al., 1985), UTCHEM based model (Hortes, 1986) and modified model based on black oil simulator, BOAST (French and Gao, 1988). Sorbie et al. (1985) modeled the transport of a multicomponent gelling system using a convection-dispersion equation system. Hubbard et al. (1988) investigated the transport and gelling of xanthan-chromium system experimentally and numerically. They used the method of lines technique of Sorbie et al. (1985) to solve the system of equations. Hubbard et al. (1988) analyzed the results obtained on core flow experiments using the mathematical model to understand the different processes. They had to consider strong adsorption of xanthan gel in order to match the numerical model results with the experimental observations. Todd (1990) and Todd et al., (1991) proposed linear

displacement and radial models to simulate the gelation of polyacrylamide-chromium system. They solved the pressure and mass transport equations for ten chemical species, which were expected to control the gelation along with equations for kinetics of reaction, rheology and filtration. Todd's model was based on the filtration (a hypothesis proposed by McCool *et al.,* 1991) of aggregates resulting in porosity reduction and hence hydraulic conductivity reduction. The filtration is defined as a function of pre-gel cluster growth and entanglement density of gel networks. The parameters for these processes are very difficult to obtain in practice. The model considered the spatial variation in the grout age.

2.6 AUXILIARY EQUATIONS

2.6.1 Gelation Modeling

When colloidal silica (CS) solution mixes with a brine solution (NaCl, $CaCl_2$, $FeCl_3$), the viscosity of the solution increases and finally gels. The time taken from the instant brine is added to CS solution to the time it gels is called gel time. Gel time depends on solids (silica) concentration in the solution, pH and brine concentration. Gelation is a complicated process. Incorporating all the kinetics including formation of chains as proposed by Todd (1990) is very difficult and requires extensive computational power. There have been several models to describe gelling with varied complexity. Sorbie *et al.* (1985) modeled gelation as a simplified first order reaction between polymer and cross-linker. They calculated mass ratio of the reactant as stoichiometric ratio instead of calculating the reaction coefficient. Hubbard *et al.* (1988) proposed a two-stage reaction model for gelation of xanthan/chromium gel system. In the first stage chromium uptake takes place and later aggregation and gelation takes place. Todd (1990) presented an in situ gelation model based on kinetics. It included many of the process parameters including particle size distribution. However, due to the need for several input parameters, it is not popularly used (Finsterle *et al.,* 1997).

There are different models proposed in the geotechnical and geoenvironmental literature to represent the gel viscosity increase with time (Honma, 1984; Finsterle *et al.,* 1997; Kim and Corapciouglu, 2002a,b). When the injected solution gels, the viscosity increases and modifies the physical and chemical characteristics of the porous formation (Finsterle

21

et al., 1997). In order to avoid the unwanted reaction/interaction with in situ soil, there is a need for a grout that is least affected by the soil physical and chemical characteristics such as pH, salinity, *etc.* In such cases there is no need for modeling (geo)chemical reactions. Kim and Corapciouglu (2002b) suggested that the soil be pre-flushed with brine solution in order to achieve controlled gelation. If it is not possible to pre-inject brine solution, use of surface modified CS is recommended. Moridis *et al.,* (1999) and Persoff *et al.,* (1999) used specially formulated surface modified CS in their studies. The gelation models outlined in the literature are briefly described below:

(i) Honma Model

Honma (1984) presented functional approximations for the gel time data for three different compositions of sodium silicate and calcium chloride. The generic equation for the ratio of the viscosity of grout to the viscosity of water (μ_r) can be expressed as

$$\mu_r = \mu_{ro}\left(1 + \zeta t\right)\left[\exp\left\{\frac{\sigma t}{geltime - t}\right\}\right] \tag{2.1}$$

where μ_{ro} = initial relative viscosity (initial grout viscosity/μ_{water}); ζ and σ are empirical fitting parameters corresponding to gel time.

Three relations correspond to different gel times are presented in the following table.

Table 2.2: Viscosity relations of Honma (1984)

Gel Time (t) (Sec)	Relation
1200	$\mu_r = 5.91\left(1 + 3x10^{-5}t\right)\left[\exp\left\{\frac{0.773t}{1200 - t}\right\}\right]$
2220	$\mu_r = 2.27\left(1 + 2.2x10^{-4}t\right)\left[\exp\left\{\frac{0.293t}{2220 - t}\right\}\right]$
4200	$\mu_r = 1.00\left(1 + 1.8x10^{-4}t\right)\left[\exp\left\{\frac{0.19t}{4200 - t}\right\}\right]$

22

These relations were obtained based on the measurements of viscosity during gelation of grout in batch experiments. Honma questioned the use of time dependent viscosity for gelation when the solution is in motion. Based on the numerical analysis using time dependent viscosity relation, the required pressure heads for injecting grout solution at a constant rate should have increased exponentially. However the experimental investigations showed only a linearly varying trend. When the grout solution with a gel time 6 minutes (in an unagitated condition) was injected into the soil column, grout could be injected until 43 minutes. During this period Honma (1984) did not observe an exponential rise of required grout injection pressures, instead he found an approximately linear increase in injection pressure. Honma (1984) attributed this linear trend of injection pressures to the delay in gelation of grout due to the combined effect of agitation caused by motion of grout and dilution during the grout permeation through the porous media. The dilution at the grout front was observed to be significant.

(ii) Berkeley Model

Finsterle *et al.* (1994, 1997), based on the viscosity measurements of Moridis *et al.* (1994) during gelling, proposed a gel time curve of exponential form:

$$\mu_{gel} = a_1 + a_2\ exp\ (a_3 t) \tag{2.2}$$

where μ_{gel} = viscosity at a given time t after gel reaction is initiated, a_1, a_2 and a_3 are fitting parameters. For a gel time of one hour, the values for parameters a_1, a_2 and a_3 are 3.22×10^{-3} Pa.s, 2.82×10^{-3} Pa.s and 1.35×10^{-3} Pa.s respectively (Moridis *et al.*, 1999). Relative viscosity μ_r can be obtained by dividing μ_{gel} with the viscosity of water.

(iii) Kim and Corapciouglu Model

Kim and Corapciouglu (2002a,b) proposed a two component based (solution phase and gel phase) kinetic gelation model. Gelation rate was expressed as a function of concentration of CS and brine concentration. Durmusoglu and Corapcioglu (2000) reported that the rate of increase in viscosity depends on the concentration of CS. Kim

23

and Corapcioglu (2002a) proposed a gelling reaction for a closed system (*i.e.*, no dilution due to mixing with water) based on solution phase and gel phase of the colloidal silica as

$$\frac{\partial F_s}{\partial t}\bigg|_{reaction} = -r_1 F_s \left(F_s C_{cs} + F_g C_{cg} \right) = -k_1 F_s C_{co} \tag{2.3}$$

where r_1 = gelation reaction rate coefficient; F_s, F_g = volumetric fraction of sol and gel phase; C_{cs}, C_{cg}=concentration of colloidal silica in sol and gel phases; C_{co}=colloidal silica concentration.

Based on Iler's (1979) observation that the viscosity rises steeply when the developed gel phase occupies half the volume of the solution, Kim and Corapcioglu (2002a) calculated reaction coefficient r_1 as

$$r_1 = \frac{\ln 0.5}{-t_{0.5} C_{co}} \tag{2.4}$$

where $t_{0.5}$ = time it takes from the initiation of the reaction to the time when gel phase occupies half the volume of the solution.

Kim and Corapcioglu (2002a) found that temporal viscosity measurements for different NaCl concentration fall on the same curve when plotted with respect to normalized time (t^* =$t/t_{0.5}$). They proposed an exponential function for viscosity as a function of normalized time.

$$\mu_{gel} = \mu_s - 0.3 \left[\exp(0.734) \right]^{0.01} + 0.3 \left[\exp \left\{ 0.734 * \exp \left(6.5 t^* \right) \right\} \right]^{0.01} \tag{2.5}$$

where μ_{gel} = viscosity of gel mixture; μ_s = viscosity of sol phase; μ_s at t^* =0.0 corresponds to the initial viscosity of the sol phase. The above equation holds when there was no dilution. However, in reality, dilution does take place. In such cases, viscosity is generated by the gel phase and was determined by the volumetric fraction of gel phase only and not by CS concentration. The viscosity in Equation 2.5 expressed in terms of gel phase is given as

24

$$\mu_{gel} = \mu_s - 0.3\left[exp(0.734)\right]^{0.01} + 0.3\left[exp\left\{0.734\left(1-F_g\right)^{6.5/ln(0.5)}\right\}\right]^{0.01} \qquad (2.6)$$

For the purpose of numerical calculations they assumed that if the gel phase viscosity reaches 10^{10} g cm^{-1} s^{-1}, it is considered to have reached complete gelation. Relative viscosity μ_r can be obtained by dividing μ_{gel} with the viscosity of water.

2.6.2 Effect of Shear

(i) Shear Thinning

A survey of literature on the polymer solutions which are in motion during gelation indicated that there is a breaking in networks of molecules due to shearing action while they flow through pores. This results in viscosities lower than those obtained when gelling polymer solutions are in an undisturbed condition. The viscosities may be higher than the initial viscosity of the solution. The phenomenon of reduction in viscosity when subjected to shear was called shear thinning (Krieger and Dougherty, 1959; Cross, 1965). Effect of shear was extensively studied in the area of polymer solutions. However, there were no studies reported in the area of grouting.

When the sols are under gelation, there are two opposite forces acting on the system, one is the formation of flocs, and the other is disruption by the shear forces. Thus, shearing sets up a competition between formation of networks of chains into clusters of growing sizes and disruption of the clusters by hydrodynamic forces (Carvalho and Djabourov, 1997). Some researchers studied the effect of shear on gelation experimentally (Raghavan and Khan, 1995), while others studied this effect both experimentally and theoretically (Carvalho and Djabourov, 1997).

(ii) Studies on Effect of Shear on Gelation in Porous Media

Gel treatments are not easy to control because of inadequate knowledge of physico-chemical characteristics of the porous media. Chauveteau *et al.* (2000) stated that "the physics of gelling under shear as well as the chemistry of cross-linkers in aqueous

25

solutions are complex and still not well understood." They proposed two mechanisms to explain the plugging of porous media due to gelling, *viz.,* (i) pore throat bridging by micro-gels formed in situ then growing in size as they move through the porous medium, and (ii) pore throat bridging from the progressive increase in thickness of a gelled surface layer.

Chauveteau *et al.* (2000) observed four successive steps during their experimental studies on cross-linking of polymers under shear *viz.,* induction period, pre-gel period, micro-gel size limitation and micro-gel consolidation period. The gel time was strongly dependent on shear at high shear rates, while it was less dependent at low rates. The rupture by the torque exerted by shear flow determines the size of the micro-gels. The maximum shear stress reached at the end of cross-linking did not depend on the applied shear rate in the diffusion controlled regime. But the same increased with shear rate in the convection regime.

Hejri (1989) and Hejri *et al.* (1989) investigated the effect of low shear rates *i.e.,* frontal velocities of 3-6 ft/day, whereas Jousset *et al.* (1990) examined the effect of medium and high shear rates, *i.e.,* frontal velocities in the ranges of 12-120 ft/day. For a given shear rate in the low range, Hejri *et al.* (1989) and Hejri *et al.* (1993) reported that flow resistance was increased as permeability (expressed in L^2 dimensions) decreased. When the shear rate was decreased, flow resistance was found to increase. Jousset *et al.* (1990) reported that location of the region of high flow resistance varied linearly with shear *i.e.,* frontal advance rate. The magnitude of the resistance was correlated with frontal velocity.

2.6.3. Shear Gelation Models

The popular viscosity-shear rate relations used in the literature include (i) Cross model (1965), (ii) Meter equation (Bird *et al.,* 1987), (iii) Carreau model and Carreau-Yasuda models (Bird *et al.,* 1987) and (iv) Chauveteau model (Chauveteau *et al.,* 2000).

(i)   Cross model

Cross (1965) derived the relation between viscosity (μ) and shear rate (γ) as

$$\mu = \mu_\infty + \frac{\mu_0 - \mu_\infty}{1 + \alpha\gamma^{n_c}}$$ (2.7)

where μ_∞ = viscosity of solution at infinite shear rate, μ_0 = viscosity of solution at zero shear rate, α = a constant associated with the rupture of linkages, n_c = Cross model exponent, given as 2/3.

(ii)   Meter Equation

Another popularly used equation for expressing viscosity as a function of shear rate, referred to as Meter equation, is given as

$$\mu = \mu_\infty + \frac{\mu_0 - \mu_\infty}{1 + (\frac{\gamma}{\gamma_{1/2}})^{p-1}}$$ (2.8)

where p = empirical parameter, $\gamma_{1/2}$ = shear rate at which viscosity is $\mu_0/2$.

(iii)   Carreau Model and Carreau-Yasuda Models

Carreau-Yasuda model is given as

$$\frac{\mu - \mu_\infty}{\mu_0 - \mu_\infty} = \left[1 + (\lambda\gamma)^d\right]^{\frac{(n-1)}{d}}$$ (2.9)

where λ = time constant, n = power law exponent which describes slope in $\mu(\gamma)$ curve and d = dimensionless parameter that describes transition from zero shear rate region to power law region. The Carreau model is obtained when μ_∞ =0.0 and d = 2, and is given as

$$\mu = \mu_0\left[1 + (\lambda\gamma)^2\right]^{\frac{(n-1)}{2}}$$ (2.10)

27

(iv)   Chauveteau Model

Chauveteau *et al.*, (2000) expressed the shear rate dependence of the viscosities in terms of power laws as:

$$\mu \ \propto \gamma^{-(1 - m_{ch} - n_{ch})} \qquad\qquad (2.11)$$

The exponents m_{ch} and n_{ch} are positive and depend on the shape and rigidity of the polymeric species as well as their concentration. Value of $(m_{ch} + n_{ch})$ is expected to reach a maximum of 0.7-0.8 for strongly entangled system with an excess of cross-linker giving strong rigidity.

Essentially these models are of similar nature with minor variations. Each of these models was applied to different gel systems. Hence, choice of these models may be made based on the specific experimental investigations. Lopez *et al.* (2003) preferred the Cross model over the Carreau-Yasuda model because it has fewer fitting parameters. However, Lopez *et al.* (2003) used a form of truncated power law due to the inability of the Cross model in providing an analytical solution to relate pressure drop to effective viscosity in a single capillary. Using truncated power law viscosity (μ_{eff}) as a function of shear rate is given as

$$\mu_{eff} = max \ [\mu_\infty \ ; \ min \ (C\gamma^{n-1}; \ \mu_0)] \qquad\qquad (2.12)$$

where C and n are shear viscosity coefficient and exponents; μ_∞ and μ_0 are the viscosities at infinite shear and no shear respectively.

2.6.4 Shear Rate Models

The common approaches used in determining the shear rate were the capillary bundle approach, network approach and oscillatory viscometer approach (Wreath *et al.*, 1990). The capillary bundle approach approximates that the porous media consisted of bundles of straight non-interacted capillaries of uniform size. In this approach, for a given flow rate, constant pressure drop takes place. However, the interconnections between pores

28

and pore throats yield shear rates larger than those obtained through the capillary bundle approach (Wreath et al., 1990). They summarized different studies that related shear rate and apparent viscosity. In a porous medium, average macroscopic shear rate can be defined as

$$\gamma = C\frac{q}{\sqrt{k\phi}} \tag{2.13}$$

where q = Darcy velocity; k = intrinsic permeability and ϕ =porosity. The proportionality constant (C) is expressed in different forms.

One of the popularly used forms is

$$C = \left(\frac{3n+1}{4n}\right)^{\frac{n}{n-1}} \tag{2.14}$$

where n = exponent in the power law viscosity relation.

By combining the capillary bundle approach and power law, Cannella et al. (1988) have defined this term as

$$C = C_c\left(\frac{3n+1}{4n}\right)^{\frac{n}{n-1}} \tag{2.15}$$

where C_c =shear rate coefficient. The coefficient C_c is obtained by fitting the model to the experimental observations. All the studies summarized by Wreath et al. (1990) introduced the shear rate coefficient to match the model results with the experimental observations. After surveying different studies, Lopez et al. (2003) reported that C "is a function of both the bulk rheology and pore structure and that there is no theory that can predict its value reliably." Summarizing the literature, they reported that C varied between 1 and 15 for different pore structures.

2.6.5 Mixing

During its transport through a groundwater system, the grout gets diluted after mixing with water. This was also observed by Honma (1984). Commonly used mixing rules were (i) linear and (ii) power law mixing rules. They were given by Koval (1963), Finsterle *et al.* (1994) and Kim and Corapcioglu (2002a).

Linear mixing rule:

$$\mu_l = X_{gel}\mu_{gel} + (1 - X_{gel})\mu_w \qquad (2.16)$$

Power law or quarter power mixing rule:

$$\mu_p = \left(\frac{X_{gel}}{\mu_{gel}^{1/4}} + \frac{(1 - X_{gel})}{\mu_w^{1/4}} \right)^{-4} \qquad (2.17)$$

where X_{gel} = fraction of grout concentration, $\mu_{l\ or\ p}$ = viscosity of the grout after mixing with water due to dilution –subscripts l and p refer to linear and power law mixing rules, μ_{gel} = viscosity of the grout according to gel time relation (Equation (2.1), (2.2) or (2.6)) and μ_w = viscosity of water present in the porous media. Suitability of either of the mixing models needs to be determined based on the laboratory experiments.

2.7 EXPERIMENTAL STUDIES OF INJECTION OF GELLING LIQUIDS INTO POROUS MEDIA

Honma (1984), while analyzing the pressures required to inject sodium silicate grout at a constant flow rate, found that the experimentally observed pressures are in disagreement with those obtained from modeling studies when time dependent gelation relationships given in Table 2.2 are used. When the grout gel viscosity expressed as a function time, a relationship obtained from laboratory measurements of viscosity during grout gelation under still conditions, was employed in the modeling study, the injection pressures were

30

observed to increase exponentially. Honma (1984) performed experiments on sodium silicate grout injection into a sand column and a point injection in a cube shaped sand box. The experimental observations of injection pressures followed almost a straight line pattern. Honma reported that it was possible to inject grout for 2580 seconds (43 minutes) even though the gel time of the grout was only 360 seconds (six minutes). Honma believed that the discrepancy was due to slowing in gelation caused by agitation and turbulence of the flow.

Colloidal silica grouting into soil was investigated through column experiments (Durmusoglu and Corapcioglu, 2000), two-dimensional tank experiments (Durmusoglu and Corapcioglu, 2000; Gallagher, 2000) and field investigations (Moridis et al., 1995; Persoff et al., 1995). Most of these studies aimed at studying viability of colloidal silica injection for barrier formation. Gallagher (2000) however focused on achieving gel times such that the grout was spread as far of possible.

In the area of enhanced oil recovery, various gel systems investigated include polyacrylamide/Cr (McCool et al., 1988; Seright, 1992), Xanthan/Cr (Hubbard et al., 1988; Jousset et al., 1990), polyacrylamide-aluminum citrate (Seright, 1994; Ranganathan et al., 1997) and formaldehyde system (Seright, 1992; Bryant et al., 1998). McCool et al. (1988), Jousset et al. (1990) and Ranganathan et al. (1997) reported the process of filtration of micro-gels during their transport through porous media. Seright (1995) also observed similar phenomenon of stripping of polymer and cross-linker at the inlet section. Bryant et al. (1998) performed experiments on phenol-formaldehyde system and concluded that one or more of the viscosification, shear thinning and filtration processes play an important role in the injectivity of gel solutions through slim tube (8 mm diameter) sand column experiments. They also reported that occurrence of filtration is strongly correlated to the age of the gelants (gel constituents).

2.8 VERIFICATION AND VALIDATION OF NUMERICAL MODELS

Numerical simulation results need to be examined for their reliability and accuracy. Verification and validation are the two main phases of model testing in order to assess the

31

accuracy of the simulation results (Roache, 1994, 1998; Barron and Latypov, 1995; Oberkampf and Trucano, 2002).

2.8.1 Verification

Verification was defined, by the Society of Computer Simulation (SCS) (Schlesinger, 1979), as "substantiation that a computerized model represents a conceptual model within specified limits of accuracy." In this process, results produced by the numerical simulation code were checked to ensure that the code is approximating the governing differential equations (Barron and Latypov, 1995; Oberkampf and Trucano, 2002). Major sources of errors in numerical simulations were insufficient spatial and temporal discretization and insufficient iterative convergence (Oberkampf and Trucano, 2002). Major steps in assessing how well the numerical model approximated the differential equations are (Barron and Latypov, 1995): grid refinement studies, comparison with analytical solutions and benchmark numerical solutions and a posteriori error estimations.

Herbert *et al.* (1988), Oldenburg and Pruess (1995) and Diersch and Kloditz (2002) investigated the importance of spatial grid resolution on the converged solution for density dependent coupled flow-transport problems. Oldenburg and Pruess (1995) refined the grid until the results were not found to vary any further. It is, however, not feasible to refine grids many times and run simulations due to computational and other limitations. In such cases the Grid Convergence Index (GCI) method suggested by Roache (1994) and applied by Zhao *et al.* (2000) provided a systematic way to estimate the errors resulting from the use of coarse grids. Oldenburg and Pruess (1995) and Ackerer *et al.* (1999) implemented an adaptive time-stepping approach. Depending upon the number of iterations it takes to reach convergence, the time step is either increased or decreased. From the numerical experiments, Ackerer *et al.* (1999) suggested that, for coupled systems, when the ratio between the time step for flow and time step for advective step was three, simulations were efficient. Oldenburg and Pruess (1995) and Ackerer *et al.* (1999) stressed the importance of convergence criteria. In case of coupled problems, there were two different convergence criteria that one needs to consider *i.e.*, one was for the coupling between flow and transport equations and the other criterion was for the

32

iterative solver (Ackerer *et al.,* 1999). These studies adopted a formulation scheme referred to as residual formulation to maintain exact mass balance at the elemental level. Oldenburg and Pruess (1995) suggested convergence criterion of 10^{-5} for the residual of the mass accumulation terms between any two iterations.

2.8.2 Validation

Validation, on the other hand, is "a process of determining the degree to which a model is an accurate representation of the real world from the perspective of the intended uses of the model" (American Institute of Aeronautics and Astronautics, 1998). During this process, numerical model results are compared to either the field/experimental observations or the results of an already verified and validated numerical model. The process of validation determines the degree to which the model mimics the essential physics of the real world problem (Barron and Latypov, 1995). Roache (1998) described verification as "solving the equations right" and validation as "solving the right equations."

2.9 MODELING HETEROGENEOUS HYDRAULIC CONDUCTIVITY

Flow and transport in heterogeneous porous formation was one of the most extensively investigated topics because spatial variability in hydraulic characteristics in geological formation affects the evolution and the spreading of contaminants in groundwater system. Soil heterogeneity results from natural processes that govern the formation of soil deposits having variable stretches or layers of different soil hydraulic properties. Also, heterogeneities result from the order of difference between horizontal and vertical hydraulic conductivities. Even when the soil is seemingly homogeneous, there exist thin lenses of different soil layers. Hydraulic conductivity is the main property that affects the flow and transport processes and it was known to vary by several orders of magnitude. The hydraulic conductivity was considered random (Freeze, 1975; Dagan, 1989; Gelhar, 1994; Hassan *et al.,* 1998) and its variability was described in a stochastic way (Elfeki *et al.,* 1997). Hydrogeologists, in their stochastic analyses, considered the aquifer as one of the possible outcomes of several possibilities or scenarios having the same statistical

33

properties. Each of these possibilities, called realizations, has a set of physico-chemical characteristics (Delhomme, 1979; Dagan, 1986; Gelhar, 1986).

Stochastic modeling in geoscience, reservoir engineering and hydrology involves the generation of synthetic geologic architecture and/or property field data, depending on the problem dimension, running flow and/or transport simulations to get the results (Haldorsen and Damsleth, 1990). To describe the random hydraulic conductivity, joint probability density functions between all points in space were to be known (Hassan et al., 1998). Starting from the reportedly first paper on describing heterogeneous hydraulic conductivity using lognormal distribution (Law, 1944), a large volume of literature followed this approach (e.g., Warren and Price, 1961; Freeze, 1975; Hassan et al., 1998). The logarithm of hydraulic conductivity of the heterogeneous porous formation was considered to be a random space function that is statistically homogeneous (Freeze, 1975; Hassan et al., 1998). If the log transformed hydraulic conductivity followed a Gaussian distribution, then the first two moments, mean and covariance, were sufficient to describe the RSF (Hassan et al., 1998).

Geostatistical approaches were used for predicting hydrogeological properties. They comprised of a collection of techniques for the analysis of spatially correlated data (Journel and Huijbregts, 1978; American Society of Civil Engineers, 1990a,b; Lin et al., 2000). There were two popular geostatistical techniques: interpolation and simulation. Interpolation techniques such as, Kriging (Journel and Huijbregts, 1978; Kitanidis, 1997), statistically gives the Best Linear Unbiased Estimate (BLUE) at a given location or the best estimate for a given area or volume (Hicks, 1996). Kriged values exhibit lower variation than the actual variability (Lin et al., 2000; Hicks, 1996). Although interpolated maps capture the large-scale lateral variation, they were smooth and did not reflect the realistic variability. Also, in problems such as ore estimations it was enough to know the average estimate. However, in hydraulic conductivity distribution determination, it is important to know not only the mean value and but also variability. In such situations, geostatistical simulations were used to preserve the variability.

34

Geostatistical simulation attempts to preserve the statistics (histogram, semi-variogram and scattergram) of the observed data and hence realizations generated through simulations were more realistic (Hicks, 1996; Goovaerts, 1999). Depending on whether the simulations honoured the observed data, they were classified into conditional or unconditional simulations. If the simulation honoured not only the statistics such as mean and variability but also the actual data, it was called conditional simulation. In cases where the simulations preserve only the statistics and not the observed data, it was called unconditional simulation. Simulation tries to maintain the variability in the generated data. Variability was incorporated by introducing the noise on to the interpolated surface. Noise was systematically added to the interpolated surface according the model.

There were several techniques reported in the literature for generating the realizations (Deutsch and Journel, 1998). They include turning bands method (Bras and Rodriguez-Iturbe, 1985), spectral technique (Montoglou and Wilson, 1982; Naff *et al.*, 1998a,b) and sequential Gaussian simulation (Goovaerts, 1999). Goovaerts (1999) compared the space of uncertainty generated by four of the most commonly used algorithms: Sequential Gaussian Simulation (SGSIM), Sequential Indicator Simulation (SISIM), p-field simulation and Simulated Annealing (SA). Goovaerts reported that SGSIM yielded the most accurate prediction, among various algorithms, of long-term response for the problem chosen. Goovaerts also found that SGSIM yields both large goodness statistics and small local uncertainty. Hence it should be preferred for the generation of hydraulic conductivity maps.

2.10 CONCLUSIONS

Chemical grouting is being investigated as an environmental containment technological option for the two decades. Sodium silicate and polyacrylamide are the two popularly used chemical grouts. While sodium silicate based grouts are environmentally safe, they suffer from poor gel time control and syneresis. Polyacrylamide offers better gel time control. But they suffer from environmental and health concerns. In the light of these problems with sodium silicate and polyacrylamide grouts, quest for new chemical grouts led to the identification of colloidal silica grouts. Colloidal silica was reported as a promising alternate for sodium silicate as a chemical grout. Colloidal silica is

35

environmentally benign, has better gel time control and has no syneresis problem. Hence further investigations are needed.

Researchers in the recent past have investigated the applicability of colloidal silica based grouts through numerical modeling and field applications. However these studies have not reported the processes that are occurring during grout injection. Although Gallagher (2000) investigated numerically and experimentally, the author had adopted decoupled approach and recommended the use of coupled approach. Based on the literature review, it was identified that the modeling studies on the injection of chemical grouts (including sodium silicate and colloidal silica) into porous media did not consider the effect of shear, which was known to effect gelation. The modeling studies reported in the literature on the colloidal silica grouting did not perform experimental studies with an aim to understand the processes that effect grout injection and generate data to validate the modeling results.

CHAPTER 3
EXPERIMENTAL STUDY

3.1 GENERAL

Experimental work is vital in understanding the physics and generating data to validate models, especially in the absence of sufficient field data. Measurement of material properties such as viscosity of grout solution and soil hydraulic characteristics is essential not only to understand the behaviour of the grout, but also to develop the functional relationships for use in modeling studies. This chapter presents the details of the experimental work carried out in order to test the materials, better understand the physics and generate data to validate the model. Based on the discussions in the previous chapter, the important issues in chemical grouting are grout material, grout medium, gelation characteristics, flow and transport of gelling grout and grouted soil characteristics. The experimental work in the current chapter is focused along these issues. The chapter is organized into sections on materials, viscosity measurements of colloidal silica in the presence and absence of shear effect, colloidal silica grout injection into sand columns and determination of hydraulic conductivity of grouted sand. Experimental hardware and measurement procedures are presented in the respective sections.

3.2 MATERIALS

In this study, grout solution and grout media are the two main materials involved. The grout medium used in this study is fine sand. The grain size distribution of the sand is presented in Figure 3.1. The average grain size (d_{50}) and geometric standard deviation (σ_g) were estimated as 0.20 mm and 1.28 respectively. Once the column was packed with sand, the hydraulic conductivity was determined using falling head method. Soil hydraulic conductivity ranged between 2.7 x 10^{-4} m/s and 3.3 x 10^{-4} m/s with an average hydraulic conductivity of 3.06 x 10^{-4} m/s. Grout solution consists of a mixture of colloidal silica solution and NaCl solution. Bindzil 40/170 grade colloidal silica solution (provided by M/s Eka Chemicals, USA) is used for the experimental study. The important physico-chemical properties of Bindzil 40/170 formulation are presented in Table 2.1. In the present study, reagent grade NaCl (BDH, USA) was used to make both

10 % by wt. solution for mixing with colloidal silica solution and 2.5 % by wt. solution for preflushing in all the tests. When the 10 % by wt. NaCl solution is mixed with colloidal silica solution, the resultant grout mixture will have 2.5 % by wt. concentration of NaCl. Thus when the grout mixture is injected into the saturated column that is preflushed with 2.5 % by wt. NaCl solution, the diffusion of NaCl solution due to concentration difference could be avoided.
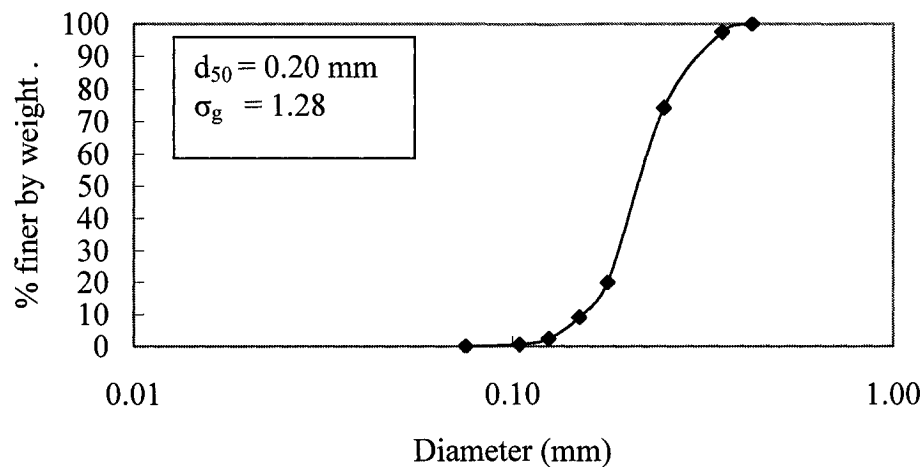
Figure 3.1: Grain size distribution of sand used for experiments in this study

3.3 GELATION CHARACTERISTICS

When the grout polymer solution (Bindzil 40/170 colloidal silica in this case) is reacted with a cross-linker (NaCl brine solution), the resultant solution becomes viscous and eventually a gel, semi-solid or solid due to the formation of networks of particles linking together. Viscosity increases with time, from the instant the colloidal silica is reacted with brine solution, needs to be determined experimentally in order to represent the gelation process in the model. Jansson (2003) of Eka Chemicals provided the viscosity data obtained during gelation under no shear for three different compositions of Bindzil 40/170 and NaCl, *i.e.*, 4:1, 5:1 and 6:1 at three different temperatures, *i.e.*, 10, 20 and 30° C. Ratios indicate weight fractions of Bindzil 40/170 to 10 % by wt. sodium chloride solution. The viscosity data were measured using Brookfield synchro-lectric viscometer with LV spindles and UL adapter. The viscosity data are presented in Figure 3.2. These

38

profiles indicate that gel time is dependent on concentration of polymer solution, brine concentration and temperature. The gel time is found to increase with reduction in the brine concentration in the final mixture. This is because the gelation is slow in ionically less active solutions. The grout is found to gel more quickly at $30^\circ C$ because of higher ionic activity at higher temperatures. Despite varying time evolution of viscosity for different compositions, all these solutions achieved similar final gel viscosities. Hence in field applications, the engineer may choose a specific composition depending upon the site and design requirements of gel time.

Bindzil 40/170: NaCl (10%)
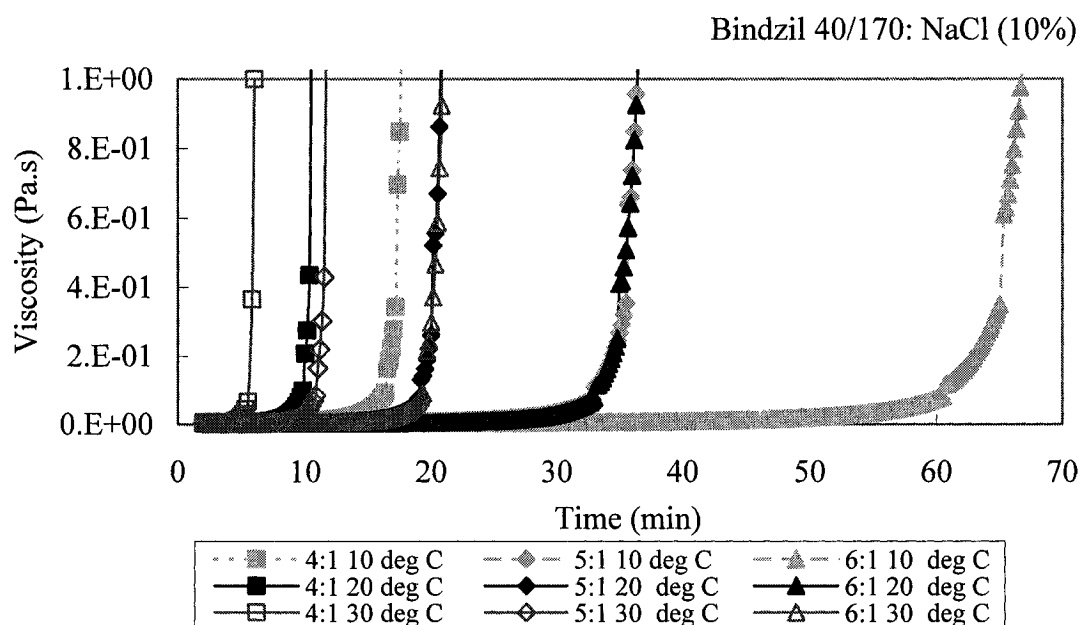
Figure 3.2: Colloidal silica grout viscosity profiles during gelation under no shear for different compositions at different temperatures. Ratios indicate weight fractions of Bindzil 40/170 to 10 % by wt. sodium chloride solution

3.4 GELATION UNDER SHEAR

3.4.1 Viscosity Measurements

Apparent viscosity of the grout in porous media during its flow is less than the viscosity of the grout in an unagitated condition. This reduction in viscosity is attributed to one of

39

three reasons – (i) break in the networks of particles (Carvalho and Djabourov, 1997), (ii) flow induced order in the solution structure such as compression resulting from elongation of polymers and/or micro-gels in the normal direction (Chauveteau et al., 2000) or (iii) densification of gel fraction (Drabarek et al., 2002) if the gelling polymer solution is in motion. Despite different explanations, it is generally agreed that delay in gelation is the result of shear. The dynamic action on the solution due to motion was represented in terms of shear rate having units $[Time]^{-1}$. Shear rate is a function of velocity of the flow (Lopez et al., 2003). Raghavan and Khan (1995) observed that the viscosity of the gelling solution decreased as the shear rate increased and then recovered easily as the shear rate decreased or ceased. They also noted that the viscosity of gel increased suddenly, once the shear was removed. Thus it may be noted here that the viscosity at any instant of time during gelling may be higher than the original or initial viscosity. However, it would be less than the viscosity that the polymer would have had, had the solution been allowed to gel in an unagitated condition, without shearing.

Of the several compositions used by Eka Chemicals as presented in the previous section, the formulation corresponding to gel time of 600 seconds was chosen to further investigate the effect of shear. The compositions corresponding to approximate gel time of 600 seconds or more produce homogeneous gels. The composition corresponding to this gel time consists of reaction of Eka gel (Bindzil 40/170) solution and 10 % by wt. brine (NaCl) solution in the ratio of 4:1 by weight at 20° C. This composition was used in the present experimental study for measuring viscosity evolution when the solution was subjected to shear. The viscosity measurements were carried out by Prof. D. DeKee's research group at Tulane University. These measurements were made using an AR-2000 research grade rheometer manufactured by TA instruments. Concentric cylinder method had been used to measure the viscosities. A concentric cylinder attachment with immersed height of 42 mm, stator radius of 15 mm and rotor radius of 14 mm was used for these measurements. The gap between the cup and the tip of the cone was 5920 μm.

In order to understand the effect of shear on gelation, viscosities were measured at three different shear rates of 1 s^{-1}, 50 s^{-1} and 500 s^{-1}. The viscosity data from these three experiments are plotted in Figure 3.3. The curves labeled as 2, 4 and 6 correspond to the viscosity measurements at shear rates 1 s^{-1}, 50 s^{-1} and 500 s^{-1}. These shear rates correspond to the most commonly experienced groundwater velocities. The viscosity data corresponding to 600 seconds of gel time from Figure 3.2 are also plotted in Figure 3.3. The latter graph clearly demonstrates the effect of shear on gelation. These profiles are similar to the ones obtained for gelation of biopolymer under shear (Carvalho and Djabourov, 1997) and colloidal silica (commercial grade LUDOX) gelation under shear (Hanley *et al.*, 1999). For a given composition, for each of the shear rates there exists a certain maximum viscosity limit. The higher the shear rates, the lower the maximum viscosity. Viscosity remains constant until the time close to the gelation time (induction period as explained by Chauveteau *et al.*, 2000) and increases steeply in a very short span of time (pre-gel period) for the case when there is no shear. When the shear was applied, the viscosity profiles followed the no shear viscosity profile for a while and deviated from there to reach a maximum limit that was lower than the no shear profile. After attaining a peak (micro-gel size limitation), the viscosity started to decrease.

Colloidal silica particles form networks until the solution reaches peak viscosity. During this phase, networks are formed while resisting shear. After a certain stage, the peak viscosity is as shown for each of the shear viscosity profiles in Figure 3.3. The networks of particles cannot resist shear and undergo one of the three processes *viz.*, break in networks, flow induced order in solution structure or densification. As a result, the bulk viscosity starts decreasing. The breaking of networks of colloidal silica particles into small networks (blobs) continues until an equilibrium state between the gelation and shear is reached. At this stage, the polymer (grout) solution viscosity is lower than the maximum viscosity for the given shear rate. Hanley *et al.* (1999) reported that gel viscosity, after reaching a peak, reduced monotonically to 10 % of the peak viscosity.

41

Viscosity (Pa.s)

1.E+02
1.E+01
1.E+00
1.E-01
1.E-02
1.E-03
1.E-04
1.E-05
1.E-06

1.E-02   1.E-01   1.E+00   1.E+01   1.E+02   1.E+03

Time (minutes)
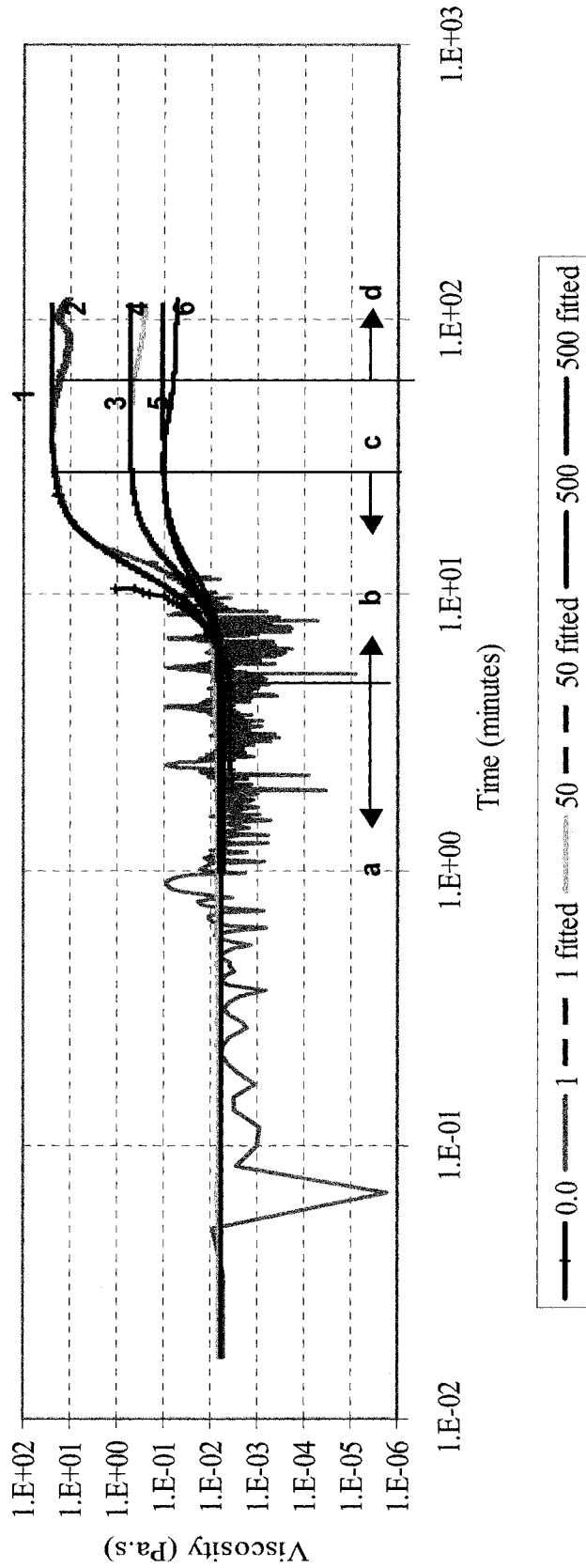
a. Pre-gel period   b. Induction period   c. Micro-gel size limitation   d. Micro-gel consolidation period

0.0 — 1   1 fitted   50 — 50 fitted   500 — 500 fitted

Figure 3.3: Viscosity profiles during gelation when the grout solution is subjected to shear. Gel mixture consists of colloidal silica (Bindzil 40/170) and 10% NaCl in the ratio of 4:1. This composition corresponds to 600 seconds gelation time at zero shear.

(The numbers on legend box refer to shear rates expressed in terms of 1/s. Shear rate of 0.0 refers to viscosity measurements made without shear application. Curves 1, 3 and 5 refer to fitted and 2, 4 and 6 refer to experimental profiles of viscosity.)

42

3.4.2 Shear Gelation Model

The viscosity increase during gelation under shear needs to be incorporated in the model in order to simulate the flow and transport of grout (gelling) solutions. As discussed in the literature review, different models to represent gelation have been reported. Due to the difficulty in representing the physics based reaction equation of Todd (1990) to determine gel viscosity increase, recourse had been made to fit an empirical equation based on laboratory data to calculate the viscosity as a function of time and concentration (Finsterle et al., 1994; Kim and Corapciouglu, 2002a,b). The present study also followed the same procedure and a non-linear regression equation was fit to the experimental measurements of viscosity corresponding to three shear rates. The relation estimates the viscosity as a function of shear and reaction time. A perusal of viscosity data during gelation under shear shows that, for each case, there is a minimum viscosity (i.e., initial viscosity) which is the same for all the three cases, and a maximum viscosity corresponding to each of the shear rates. There is a smooth transition between these two limits. These viscosity profiles resemble the moisture profiles in unsaturated zones. Hence, an expression of the same form as the one used by van Genuchten (1980) for the unsaturated zone moisture profiles (Equation (3.1)) was fit to the data (Equation (3.2)).

$$\frac{\theta - \theta_r}{\theta_s - \theta_r} = \frac{1}{\left(1 + [a(\psi)]^b\right)^c} \qquad (3.1)$$

where θ = moisture content at any instant

θ_r = residual moisture content

θ_s = moisture content at saturation

ψ = soil water pressure head

a, b and c are the fitting parameters

A non-linear regression expression similar to Equation (3.1) as given below was fit for the data shown in Figure 3.3. Equation (3.1) was modified to represent the viscosity as:

$$\frac{\log(\mu_{gel}) - \log(\mu_{min})}{\log(\mu_{max}) - \log(\mu_{min})} = 1 - \frac{1}{\left(1 + \left[s_1 \, (t/60)\right]^{s_2}\right)^{s_3}} \qquad (3.2)$$

where μ_{gel} = viscosity at any instant of time

       μ_{max} = maximum viscosity achieved for a given shear rate

       μ_{min} = viscosity at the beginning of the reaction

       t = reaction time $i.e.,$ time since the reactants are mixed

       s_1, s_2 and s_3 are the fitting parameters for the shear viscosity relation

When the viscosity data is represented in non-dimensional form as per the left side term of Equation (3.2), all the three viscosity profiles fall on the same curve. The above equation was fit to the non-dimensionalised viscosity data as a function of time and the fitting parameters were determined using least squares method. The gelation time in an unagitated condition was 600 seconds. When the time 't' was represented in seconds, the values obtained from least squares fitting for s_1, s_2 and s_3 are 0.854, 1.775 and 10.419 respectively.

Unlike in moisture profiles where the maximum moisture content (θ_s) in Equation (3.1) is known ($i.e.,$ 1.0), the maximum viscosity for a given shear rate is not known. Hence an expression for the maximum viscosity as a function of given shear rate was developed using a linear regression on log transformed viscosity data as a first step. Maximum viscosity (μ_{max} plotted on a log scale) as a function of the shear rate is shown in Figure 3.4 and is represented as

$$\mu_{max} = 22.41 \, \gamma^{-0.8863} \qquad (3.3)$$

where γ = shear rate [T^{-1}].

44
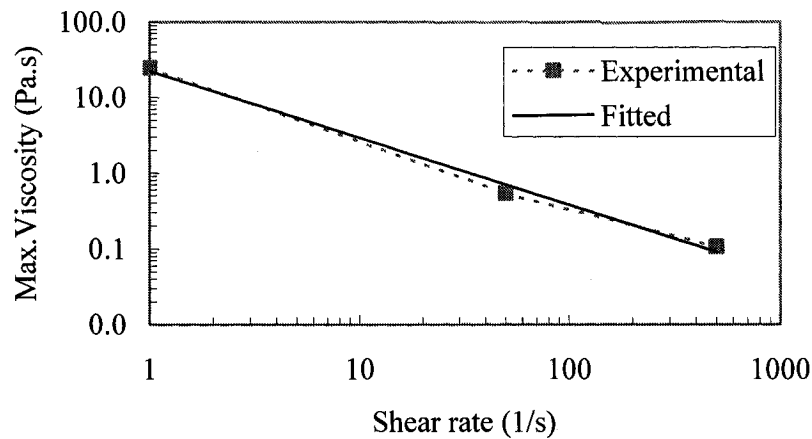
Figure 3.4: Relation between shear rate and maximum achievable viscosity

3.5 COLUMN EXPERIMENTS

In the present study, experiments on the colloidal silica grout mixture injection into sand columns were carried out. Normally, experiments are performed with either of the two boundary conditions *viz.,* (i) constant pressure head or, (ii) constant flow rate. In the case when the grout is injected at constant pressure head, the grout fluxes through the column are recorded. On the other hand, when the grout is injected at constant flow rate, the pressures required to maintain the constant flux are recorded. In the present study, grout was injected at a constant flow rate and the required injection pressures to maintain the constant grout flow were recorded to analyse the grouting processes. The experiments were performed on two types of columns. The first column was of 500 mm long and had an inner diameter 30.16 mm. The experiments performed using this column were, here onwards, referred to as column experiments. One experiment was performed on the second column, a steel tube having a diameter of 6.5 mm, referred to as slim-tube experiment. The details on the slim tube experiment were presented in section 3.7.

45

3.5.1 Experimental Setup

A schematic diagram of the experimental setup is presented in Figure 3.5. Photograph of the setup is presented in Figure 3.6. An acrylic transparent tube of 500 mm length and 30.16 mm diameter was filled with fine sand, whose particle size distribution was described in section 3.2, to a height of 450 mm. Both ends of the sand are equipped with Teflon™ screen followed by glass wool. Glass wool is placed on both the ends of the sand to avoid any leakage of sand from the column and Teflon™ screen was used to hold the glass wool and sand together rigidly. A spring is positioned above the Teflon™ screen such that the sand is under compression when the top of the column is closed in order to hold the sand in place and to avoid any possible drifting or pushing from the bottom when the grout is injected under pressure. The top end of the column is maintained at atmospheric pressure. A pressure gage and/or transducer fitted at the entrance of the grout solution into the column are used to record the pressures required to inject the grout solution at a constant rate. The pressures were expected to increase with the increase in grout viscosity as the reaction between colloidal silica and NaCl progressed with time.

Two peristaltic pumps were used in series to inject the grout. The first pump (ismatec MV pump, Cole-Parmer model no. 7332-00) had the facility to pump multiple lines at a predefined flow rate. This pump had a regulator to ensure the desired flow rates. The second pump in the series (Cole-Parmer Masterflex pump model no. 7524-10 fitted with PTFE tubing attachment model no. 77390-00) also regulated the flow rate. This second pump can inject up to an injection pressure head of about 150 m, while the first pump cannot inject at such high pressure. The capacity of the second pump to inject at higher pressures was necessary in order to inject the grout after the gelation time (including the delay caused by the shear effect) had elapsed. The outflow from the second pump was connected to the bottom of the column and pressure gage attachment.

At the start of the experiments, carbon dioxide gas was injected from the bottom in order to flush out any air, which may contain different gases leading to trapped air bubbles inside the column (Sugita and Gillham, 1995). The higher solubility of carbon dioxide in water aids in avoiding the risk of trapped air bubbles in the porous medium. After about

46
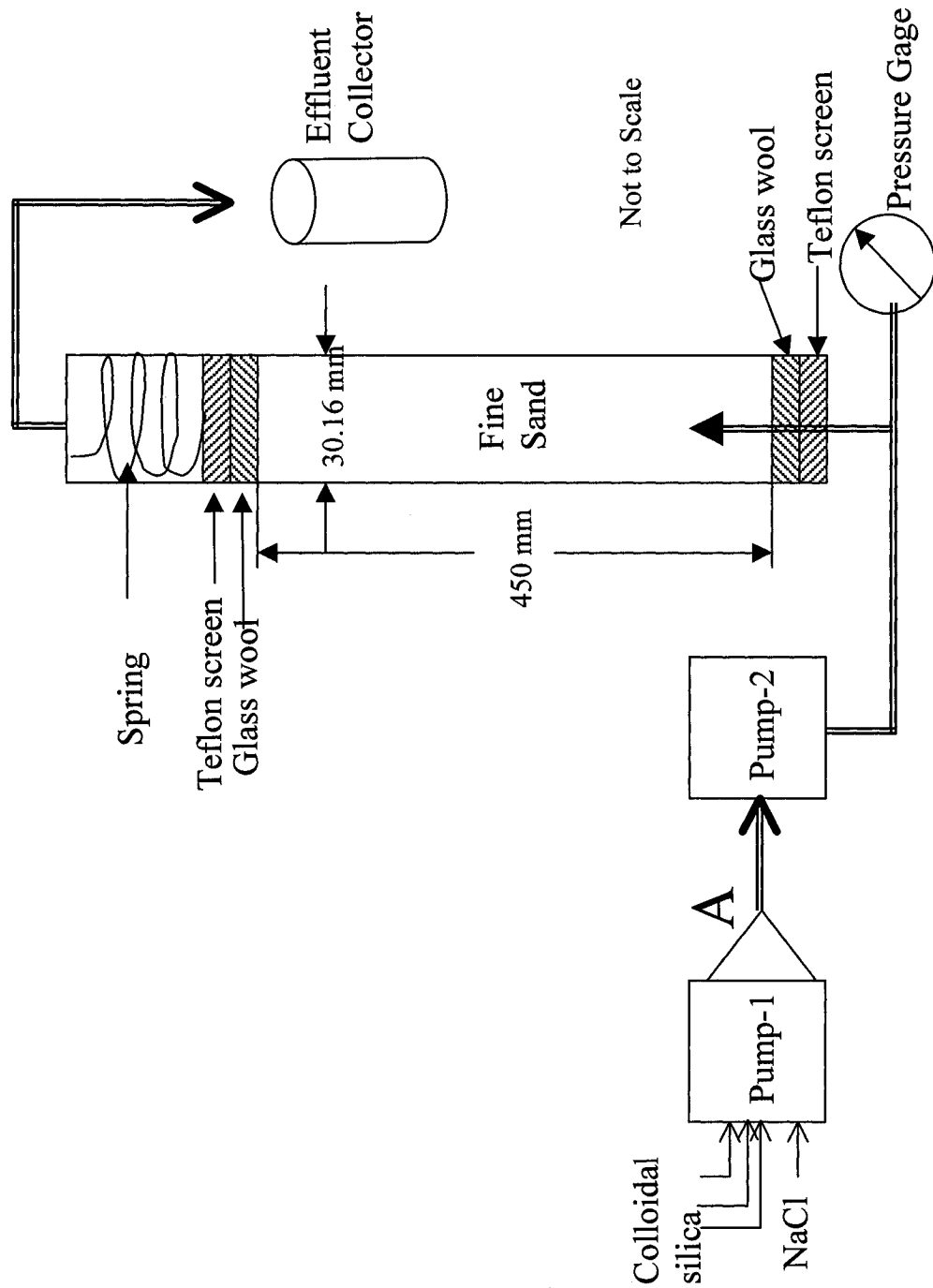
Figure 3.5: Schematic diagram of the experimental setup of grout injection to sand column

47
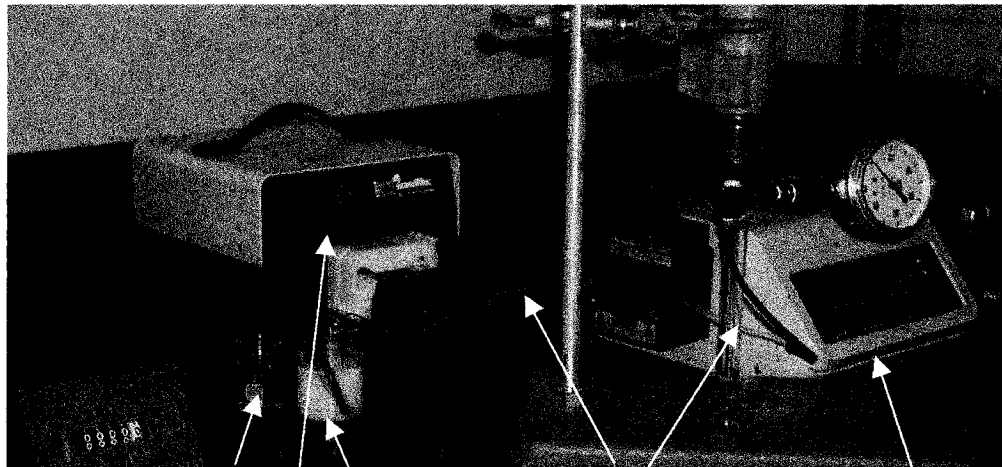
Stopwatch NaCl Pump 1 Colloi-   a   Teflon tube   Pump 2
                           dal silica
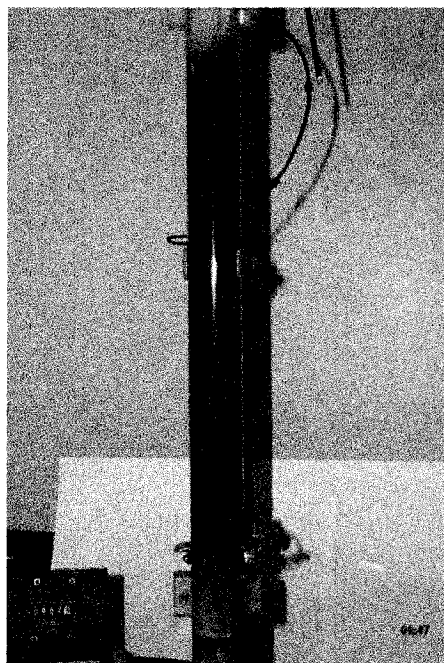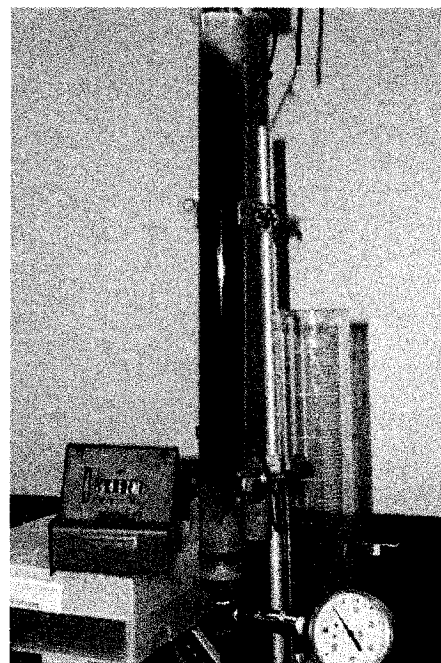
(i)   (ii)

b

Figure 3.6: Photographs of experimental setup. a) Pumps, gage, stopwatch, b) columns
            preflushed with dyed sodium chloride solution (i) experiment 1-2 and
            (ii) experiment 1-3

48

1800 seconds of carbon dioxide flushing, 10-15 pore volumes of deaired water was injected into the column (Swartz and Schwartz, 1998) to fully saturate the column and make it devoid of air bubbles. The grout solution was prepared using colloidal silica (Bindzil 40/170 as received from the manufacturer *i.e.,* 40% by weight of solids) and NaCl (10 % by weight) in the weight ratio of 4:1. The NaCl concentration in the mixture solution is 2.5 %. To minimize the dispersed grout front, the column was preflushed with 2.5 % NaCl solution, which was equivalent to the expected NaCl concentration in the injected grout solution. The NaCl preflush was recommended (Finsterle *et al.,* 1994; Persoff *et al.,* 1999; Kim and Corapcioglu, 2002a,b) in field operations to minimize or avoid the unwanted reaction of colloidal silica with other salts in soil. The column was preflushed with 2-3 pore volumes of NaCl solution to ensure that the entire column was filled with NaCl solution. Following the NaCl preflush, a mixture of colloidal silica and 10 % by wt. of NaCl solution in the ratio of 4:1 by weight was injected into the sand column. Time zero was assigned to the time at which the solutions were mixed. The pressures required to inject the grout at a constant rate were measured using a pressure gage and/or transducer with increasing passage of time.

3.5.2 Classification of Experiments

The experiments performed using the 30.16 mm diameter column, referred to as column experiments, may be classified into three groups *i.e.,* Set-1, Set-2 and Set-3. Four experiments were conducted under Set-1 and five experiments each were performed under Set-2 and Set-3. The experiments categorized under Set-2 and Set-3 were performed using the same batch of colloidal silica solution about ten months after the Set-1 experiments. Thus, the colloidal silica solution used for the Set-2 and Set-3 experiments was produced at a significant time prior to performing these experiments. The colloidal silica solution, with time, undergoes some changes such as reduction in surface area of particles due to agglomeration. The grout injection pressures were recorded using a pressure gage for the experiments under Set-1 and Set 2. A pressure transducer with digital display was added to the system during the experiments of Set-3 and the pressures were recorded using both the pressure gage and the transducer. Both the pressure gage and the transducer were calibrated using a dead weight tester before and

49

after each test. A summary of different experiments and their conditions is presented in Table 3.1.

Set-1 Experiments

Four experiments grouped under this set were performed based on the procedure described in section 3.5.1. The grout solution (consisting of colloidal silica and NaCl solution) was injected at a flow rate of 2 ml/min for the first three experiments. The flow rate was reduced to 1.3 ml/min in the fourth experiment. Another difference between the first three experiments and the fourth experiment was that the saturated sand column was not preflushed with NaCl solution in the fourth experiment. Each of the first three experiments was aimed at recording grout injection pressures, and grout distribution patterns for comparison of numerical model results against experimental observations. During the first experiment (referred to as Expt-1-1), performed without any dyes in the grout solution, only pressures were recorded. The pressure readings were recorded every 60 seconds and the time interval was reduced during the last couple of hundred seconds when the injection pressures were increasing steeply. As indicated in Table 3.1, the experiments in this group were performed using Milli-Q water.

In order to verify the grout concentration distribution patterns, the second and third experiments (referred to as Expt-1-2 and Expt-1-3) were performed, under the same conditions as the first experiment, with dyed solutions that do not affect gelation. In Expt-1-2, three different dyes *viz.,* green, red and blue were used. The NaCl solution used for preflush was coloured with the green dye (Figure 3.6b(i)). When the green dyed NaCl front reached about two-thirds of the column height, the injection of colloidal silica and processes, red dye was added to the grout solution being injected at 1760 seconds. The injection of red dyed solution was continued until 3240 seconds and at that point in time, the colour of the injected solution was changed to blue. Again at 5280 seconds, the blue NaCl solution mixture (without any dye) was started. This mixture had a white colour of colloidal silica (as seen at the bottom of the column in Figure 3.6b(i & ii)). During this

50

Table 3.1: Summary of different experiments and their conditions

Experiment Id	Colloidal Silica	Purpose	Pre-flush	Dye	Type of Water Used	Application Rate (ml/min)	Mean Velocity $\bar{v} = \dfrac{q}{n}$
Set-1							$\times 10^{-4}$ m/s
Expt-1-1	As soon as received	Pressures	Yes	No	Milli-Q	2.0	1.165
Expt-1-2	As soon as received	Pressures & Patterns	Yes	Yes	Milli-Q	2.0	1.165
Expt-1-3	As soon as received	Patterns	Yes	Yes	Milli-Q	2.0	1.165
Expt-1-4-NPF-Slow	As soon as received	Pressures	No	No	Milli-Q	1.3	0.757
Set-2							
Expt-2-3	Aged 10 months	Pressures & Patterns	Yes	Yes	Tap water	2.0	1.165
Expt-2-4	Aged 10 months	Pressures & Patterns	Yes	Yes	Tap water	2.0	1.165
Expt-2-5	Aged 10 months	Pressures & Patterns	Yes	Yes	Tap water	2.0	1.165
Expt-2-7	Aged 10 months	Pressures & Patterns	Yes	Yes	Tap water	2.0	1.165
Expt-2-8	Aged 10 months	Pressures & Patterns	Yes	Yes	Tap water	2.0	1.165
Set-3							
Expt-3-0	Aged 10 months	Pressures	Yes	No	Milli-Q	2.0	1.165
Expt-3-1	Aged 10 months	Pressures	Yes	No	Milli-Q	2.0	1.165
Expt-3-2	Aged 10 months	Pressures	Yes	No	Milli-Q	2.0	1.165
Expt-3-3	Aged 10 months	Pressures	Yes	No	Milli-Q	2.0	1.165
Expt-3-5NPF	Aged 10 months	Pressures	No	No	Milli-Q	2.0	1.165

51

process, the injection pressures were recorded. In order to capture the important dyed solution was replaced by red dyed solution. Thus, the dye sequence consisted of green (preflushing NaCl solution), white (grout mixture without dye), red (grout mixture with red dye), blue (grout mixture with blue dye) and red (grout mixture with red dye).

Expt-1-3 was carried out under the same conditions, essentially to understand the grout distribution pattern inside the column but the pressures were not recorded. In this case, the dye injection scheme was slightly changed. The column was preflushed with blue dyed NaCl solution. Figure 3.6b(ii) shows the column preflushed with blue dyed NaCl solution followed by white coloured colloidal silica grout solution. The injection of red dyed grout solution was started at 3000 seconds as opposed to 1760 seconds in the earlier test (*i.e.,* much later than the Expt-1-2). When the ratio between the viscosities of two different stages of grout solution was large, the observed fingers were likely to be distinct and thinner with smaller diameter. After the experiment was over *i.e.,* when the grout front has reached the top of the sand in the column, the column was cut into four sections in order to observe the grout patterns, mainly to investigate the finger patterns.

The last experiment in this group labeled as Expt-1-4-NPF-slow, was performed to understand the effect of preflush on the grout injection. All the experimental conditions were the same as the Expt-1-1 and Expt-1-3 except the flow rate and NaCl preflush. The grout was injected at a rate of 1.3 ml/min. Unlike the other three experiments, the column was not preflushed with 2.5 % NaCl solution. Thus this experiment had the effect of two different components *i.e.,* slow injection rate and absence of preflush. The details of the results are presented in section 3.6.

Set-2 and Set-3 Experiments

As mentioned earlier, five experiments were performed in each set using aged colloidal silica solution. All the experimental conditions were the same as the ones followed for experiments Expt-1-1 and Expt-1-3 except the type of water used. The difference between the experiments grouped under these categories was that de-aired tap water was used for experiments grouped under Set-2 and milli-Q water was used for the

52

experiments in Set-3. One of the five experiments grouped under Set-3 was performed without NaCl preflush while the remaining four experiments were performed with NaCl preflush to investigate the effect of preflush on the aged grout injection. The experiments performed under Set-2 are labeled as Expt-2-3, Expt-2-4, Expt-2-5, Expt-2-7 and Expt-2-8. The ones grouped under Set-3 are labeled as Expt-3-0, Expt-3-1, Expt-3-2, Expt-3-3 and Expt-3-5-NPF. As explained in the previous section, NPF refers to no preflush.

3.6 COLUMN EXPERIMENT RESULTS AND DISCUSSIONS

3.6.1 Grout Distribution Patterns

Figure 3.7a,b present the grout distribution patterns at different times for Expt-1-2. The colour of the grout reflects grout age. The effect of small heterogeneity can be observed at the interface between the dyed and the undyed NaCl used for preflush. Similar effects are also observed at the interface between the dyed preflush and the undyed grout solution. It can be noted from Figure 3.7a that the grout solution front is fairly stable because higher viscosity solution is displacing a lower viscosity solution.

From Expt-1-2, the grout solution dyed in red was first observed at the bottom of the sand column at 1860 seconds, *i.e.* 100 seconds after the red dyed grout was introduced. Therefore, the grout age is 100 seconds. The red colour zone persisted as a small patch at the bottom after which no indication of red dyed grout solution could be found on the surface of the column as shown in Figure 3.7a. At 2250 seconds the red coloured grout solution is observed at 210 mm from the bottom of the sand column. This means it took approximately 380 seconds to travel 210 mm, whereas it took 1546 seconds for the undyed grout to travel the same distance. This is approximately a quarter of the time it took for the undyed grout to displace the NaCl solution in the pores and reach that height. When the grout was injected initially to displace NaCl solution, the grout travelled as a plug flow displacing NaCl solution throughout the cross-section (*i.e.*, high viscosity solution displacing low viscosity solution), whereas red dyed grout injected long after the gel time of initially injected grout solution, traveled as fingers. By the time red dyed grout was injected, the grout in the pores had already reached gel time. At that time,

53
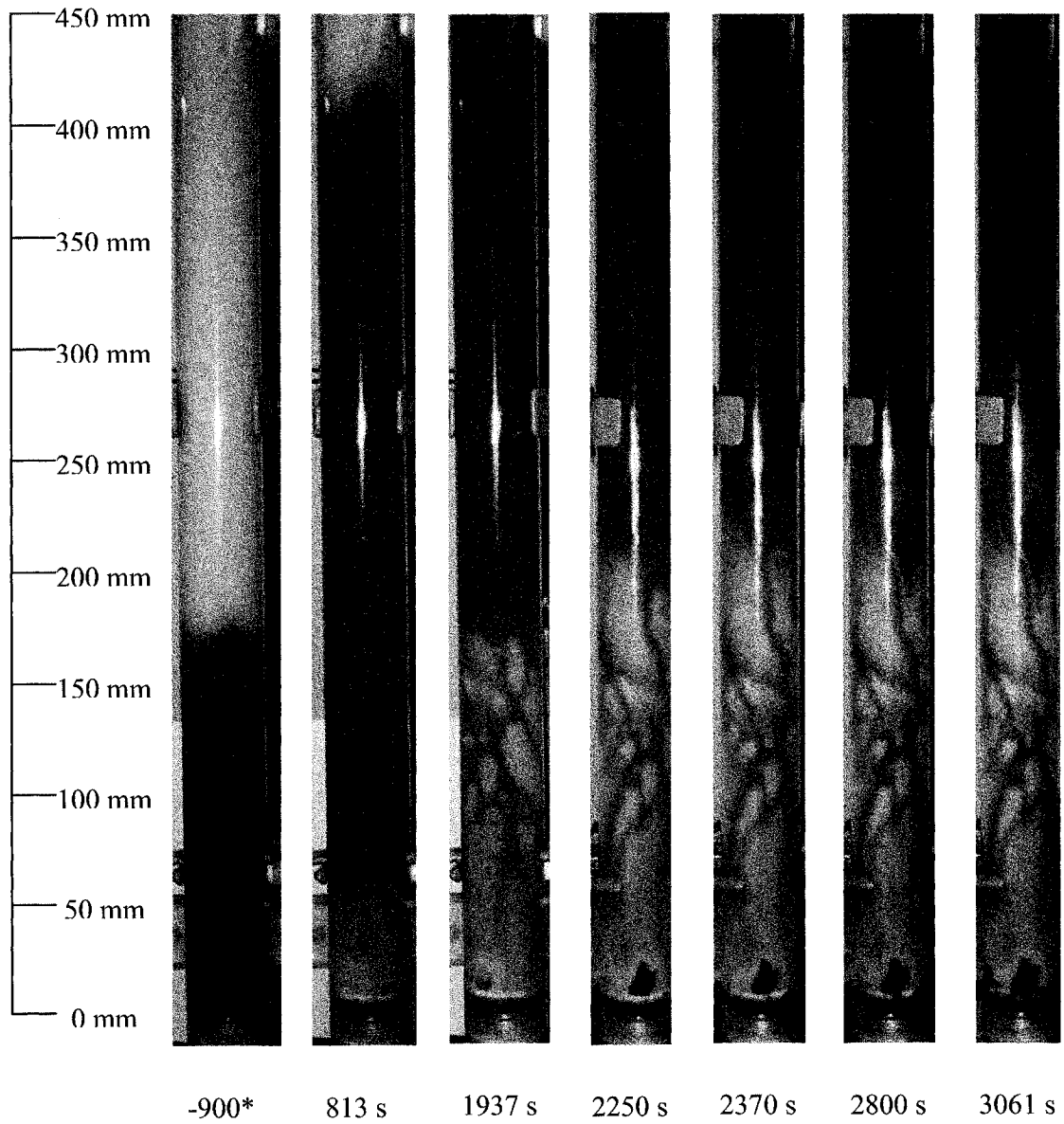
Figure 3.7a: Grout distribution at different times in the sand column during colloidal silica grout injection for Expt-1-2

(–900* refers to 900 seconds prior to the mixing of grout)

54
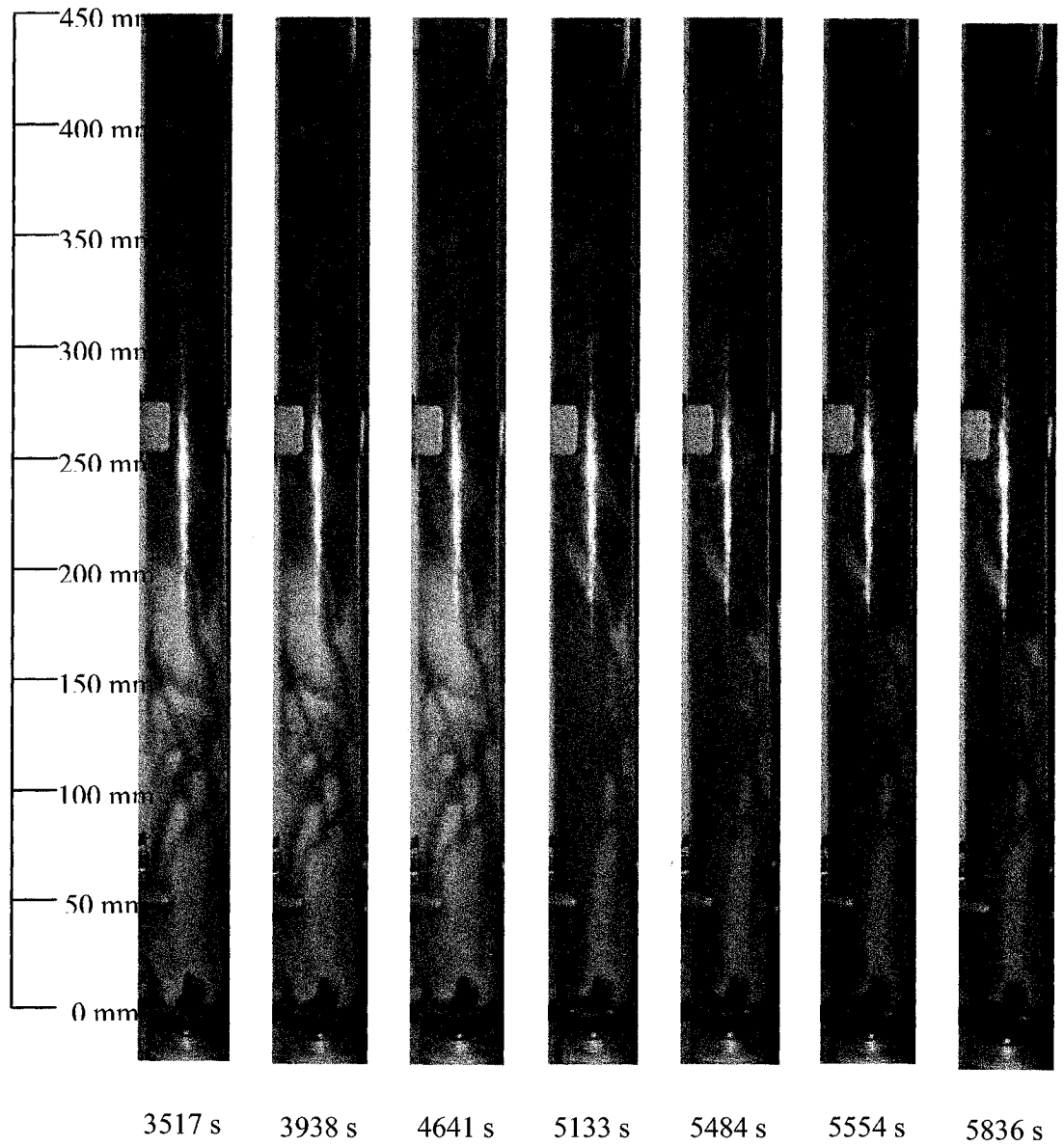
Figure 3.7b: Grout distribution at different times in the sand column during colloidal silica grout injection for Expt-1-2

55

fresh grout with very small grout age, *i.e.*, low viscosity, triggered the formation of fingers because of the flow instability of a lower viscosity displacing higher viscosity solution. Thus, this difference in time of travel was because the red dyed grout traveled as fingers and reached the grout front quickly. This was confirmed when the column was cut into pieces at different cross-sections after experiment Expt-1-3 as discussed in subsequent paragraphs.

At 3240 seconds, the red dyed grout solution was replaced by the blue dyed solution. The blue dyed grout also followed patterns similar to that followed by the red dyed grout solution, *i.e.*, the red patch observed at the bottom of column at 1860 seconds was covered by blue dyed solution. There was no sign of blue dyed solution along the column. The blue grout was observed on the surface at 300 mm from the bottom at 3720 seconds. Thus, it took 480 seconds for the grout to reach 300 mm in the column. If the time (~100 seconds) it took for the grout to reach the bottom of the sand column is subtracted from 480 seconds, the time it took for the grout to travel from the bottom of the column to 300 mm into the column is 380 seconds. This means that blue grout was also traveling through fingers smaller than the fingers through which the red dyed solution travelled. The younger grout travelled approximately six times faster than the undyed solution and about 1.5 times faster than the red dyed colloidal silica grout mixture. After reaching the front, the red dyed and blue dyed grouts were spread throughout the cross-section.

Based on the observations on grout arrival at different heights with time, one can attempt to calculate the mean velocity of grout flow through the fingers. The grout injected at the beginning had traveled as a plug flow. As mentioned earlier, it took 1546 seconds for the grout to travel 210 mm. This corresponds to a velocity of 1.2×10^{-4} m/s. During the time interval between 1860 seconds and 2250 seconds, the red dyed grout had traveled as a finger. From the dyed grout patterns, it is observed that it took 390 seconds to travel 210 mm. The average linear velocity is calculated as 5.4×10^{-4} m/s. Similarly from the observation of blue dyed grout patterns during 3240 seconds and 3720 seconds, the average linear velocity through the finger is calculated as 7.9×10^{-4} m/s. The increase in

56

velocities implies that the finger size is shrinking with time. These changes reflect the dynamic nature of the grout fingering process. It may be noted that these velocities are average linear velocities based on first order calculations because processes such as shape, size and tortuosity of the grout fingers are not considered in calculating these velocities.

At the front, the younger grout displaced the already existing grout to make its way forward. The conceptual model of the same is shown in Figure 3.8. Figure 3.9 shows this phenomenon as observed in experiment Expt-1-3. From Figures 3.8 and 3.9, it should be noted that the grout travelled through the finger was much younger than the grout around the finger. Due to the mobile nature of the grout, the younger (i.e., less viscous) grout displaced the older grout and occupied the pore space in the finger. The finger formation and growth shown in Figure 3.8 corresponds to the grout age. The finger is behind the grout front. The grout front indicated in the figure referred to the grout concentration. It may be noted that the concentration of the grout behind the grout front varies between 0.9-1.0 times the injected grout concentration. However, the ages of the grout vary. The age of the grout in the finger is significantly lower than that of the grout around the fingers.

At 4641 seconds the blue dyed grout formed a patch to the left of the initial patch at the bottom of the column as shown in Figure 3.7b. The blue dyed grout spread all along the left side of the internal surface of the column and eventually formed a finger. This is an indication that at this time, the viscosity of grout in the finger that was catering to the flow through the column had increased sufficiently that the resistance to the flow of the grout solution through the finger had increased substantially. Consequently, the younger grout with blue dye developed a new finger through the weakest zone which was along the left side internal surface (wall) of the column. Thus, the formation of new fingers showed the dynamic nature of the grout finger development process. At 5280 seconds, the solution had been changed to red dyed mixture. The red dyed solution also followed the wide finger formed by the blue dyed injection on the left side of the column.

57
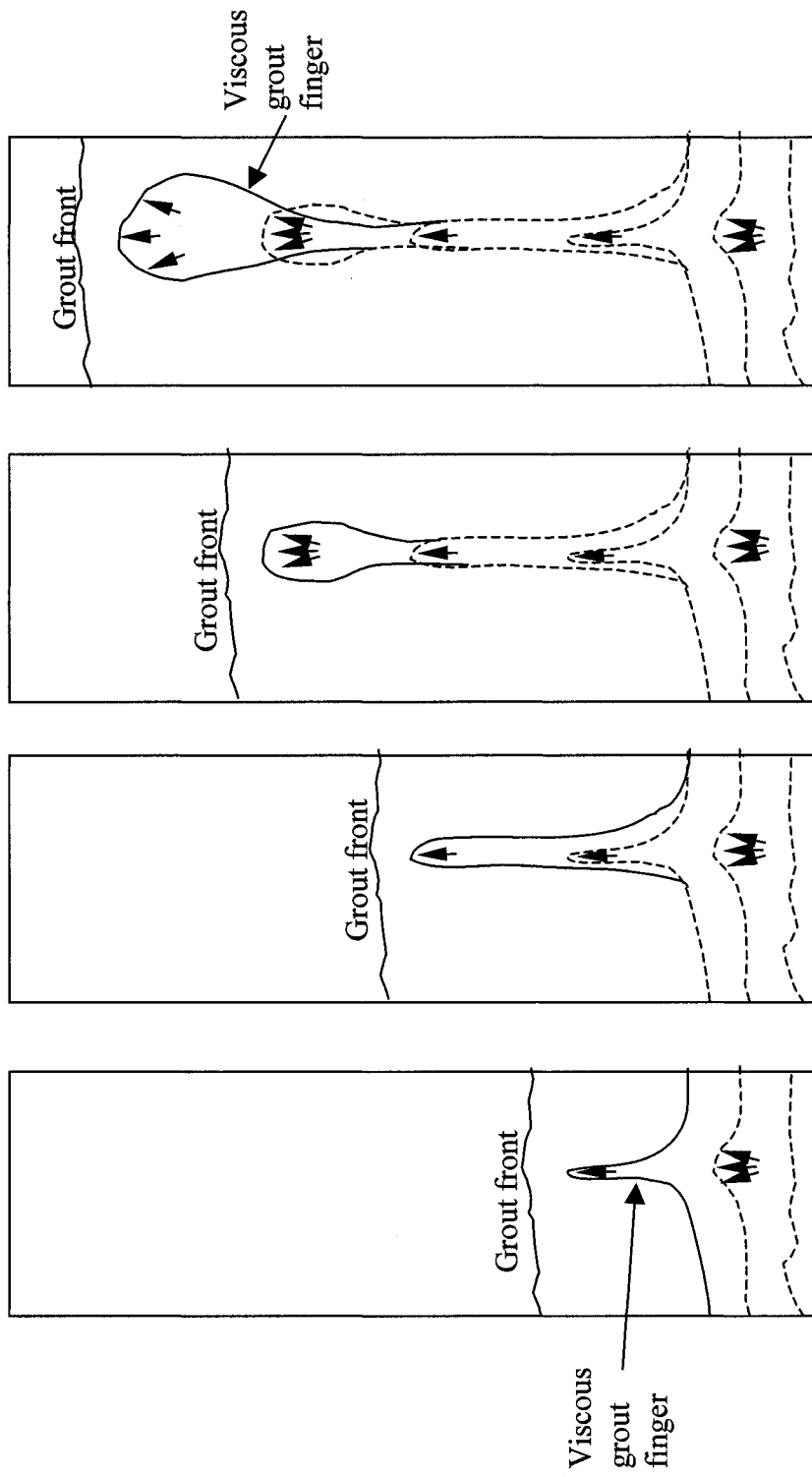
Figure 3.8: Conceptual model of fingering process in the column and grout bulb formation behind the grout front The finger corresponds to the age. The grout front corresponds to the concentration.

58
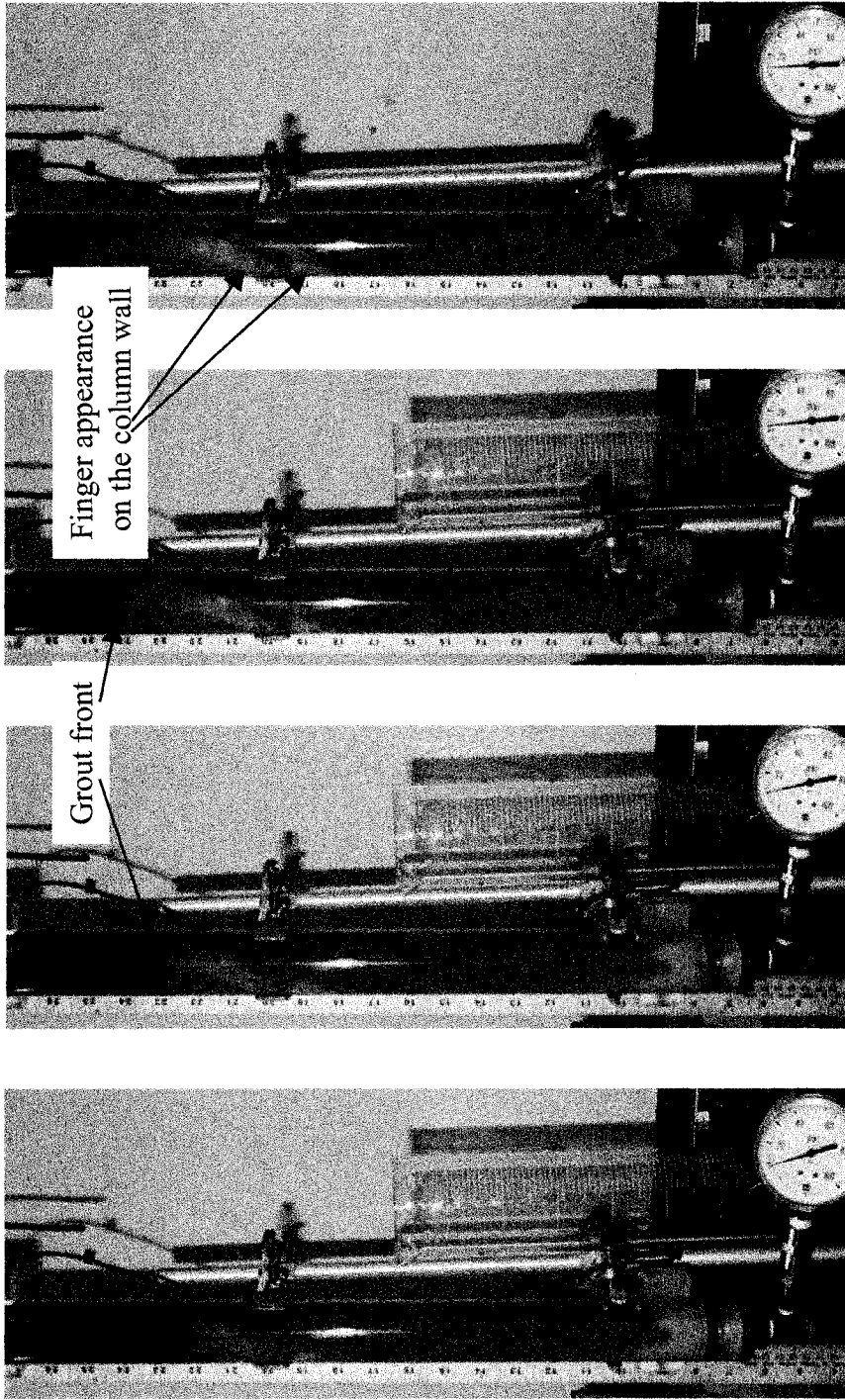
Figure 3.9: Experimental images of fingering process in the column and grout bulb formation behind the grout front as observed in experiment Expt-1-3.

59

Experiment 1-3 was performed along similar lines of experiment 1-2. However, dyed grout solution was injected at different times. The grout distribution patterns were similar in many ways. After the completion of experiment 1-3, the sand column was cut into five pieces along the cross-section at 100 mm, 200 mm, 320 mm, and 440 mm from the bottom of the sand column. Figure. 3.10 shows the formation of fingers in these cut sections of the column. At 100 mm from the bottom of the sand column, the younger grout (red coloured) formed as a core. The same core was found to be splitting into different fingers of 7 mm size in the next section of the column at 200 mm. At 320 mm, red dyed grout was found to be spreading all around the column. This was because the grout, which traveled through the fingers, had reached gelation. As a result, the ability to puncture through the front reduced and the grout, which had travelled through the finger, had spreaded across the cross-section. This is evident from the cross-section (b) in Figure 3.10. When the fingers reached near the top (~300 mm from bottom), they are coalesced while trying to spread laterally. The grout fingers are formed due to flow instabilities generated during the displacement of high viscous grout solution by the low viscous grout solution. Once the fingers are formed, it is assumed that grout flow occurs only through the fingers. In such a situation, the velocities are calculated at 100 mm and 200 mm cross-sections based on the cross-sectional areas shown in Figure 3.10(ii). The area of the finger at 100 mm cross-section is estimated based on the measurements of finger core dimensions as 125 mm^2. Similarly, the total area of the fingers observed at 200 mm cross-section is determined to be 112 mm^2. The consequent average linear velocities at these sections are calculated as 6.7×10^{-4} m/s and 7.4×10^{-4} m/s at these two sections, respectively.

The present section described the grouting physics with based on visual observations. The following subsection presented the discussion on the observed pressure heads. These grout injection pressure heads were interpreted in terms of pressures at the grout injection point under different conditions and processes occurring the column.

60
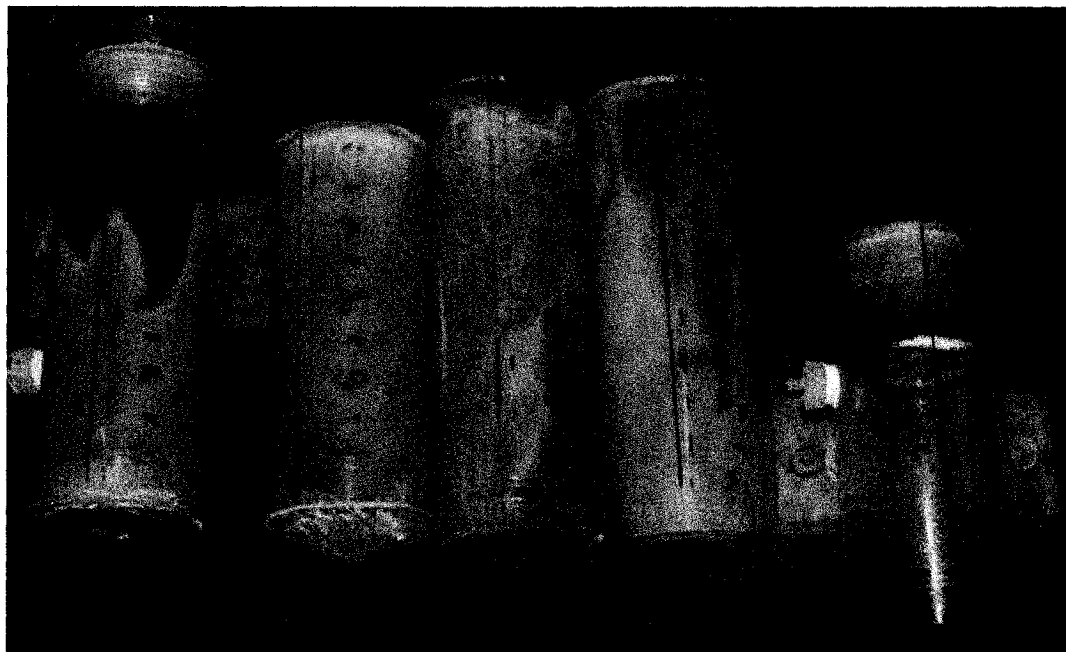
a
(0-100 mm)

b
(100-200 mm)

c
(200-320mm)

d
(320-440 mm)

e
(440-450mm)

i
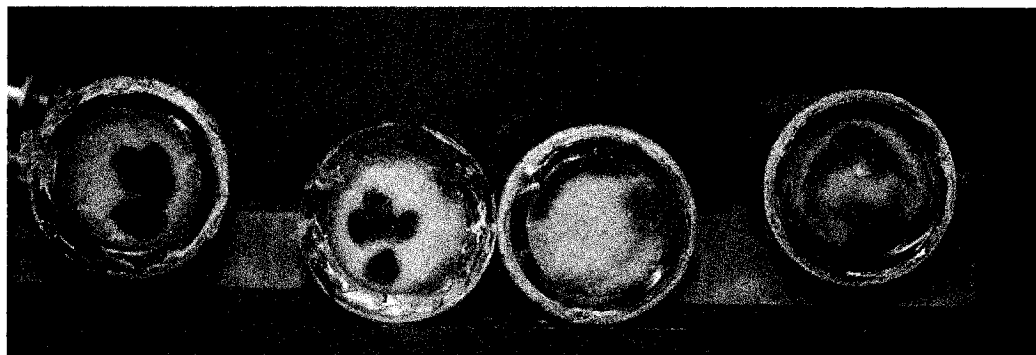
a
(100 mm)

b
(200 mm)

d
(320 mm)

e
(440 mm)

ii

Figure 3.10: Grout distribution at different cross-sections in the grouted column showing
fingers as obtained in Expt-1-3: (i) top view along the length of the column
at different intervals (ii) cross-sectional views at various heights

61

3.6.2 Grout Injection Pressures

The processes occurring during grouting were interpreted based on the grout injection pressures. It may be observed that even though the gel time of the grout formulation was 600 seconds, it was possible to inject grout until about 4000 seconds during Expt-1-1 and 6000 seconds during Expt-1-2. This delay may be explained in terms of the processes occurring in the grout injection column. Bryant *et al.,* (1998) reported that the main processes that govern the flow during injection of gelling liquids were viscosification, shear thinning and filtration. In addition to these three, the present experiments reveal the formation of viscous fingering, which was not reported in earlier studies. The grout injection would be affected due to any of these processes or a combination of these processes. Viscosity and filtration cause increase in grout injection pressures while shear thinning and viscous fingering reduces the pressure increase for a given flow rate. Therefore an analysis of injection pressures was essential to understand the physics of grout injection.

The pressures required to inject grout at a constant flow rate were recorded with increasing time and are plotted in Figure 3.11. The increase in grout injection pressure followed a mild slope until a certain time (~3200 seconds in this case) followed by a rather steep increase in a short duration. The two regions reflect the state of grout within the pores and the processes that were contributing to the pressure increase. During the time period over which the pressure profiles followed a mild increase, the grout was slightly viscous and the increase in viscosity was low. Consequently, the pressure increase was less. For convenience, the mild slope region may be divided into different sections. The first section is from the time the reaction was initiated until the time equal to gel time under no shear. The second section is the interval between the no shear gel time to the time at which viscosity in shear gelation curve attains a peak. The pressure increase during this time was only due to viscosity, which followed a mildly sloped straight line. The approximately linear pressure increasing trend during this time indicated that only viscosity might be contributing to the pressure increase. The pressure increase during this time was mainly due to head loss in the finger(s) and grouted soil around the finger(s). Since the grout age was still close to the gel time, the increase in

head loss through the column was due to viscosity increase only. The increase in pressure, during the initial phase or until the onset of finger(s), was governed by the highest viscosity at any cross-section along the column.

Once the viscous finger was formed, the majority of the flow took place through the finger. As long as the time it took for the grout to reach from the bottom of the sand column to the top of the finger was less than or equal to the gel time, the head loss curve was mildly sloped. This corresponded to the role of viscosity. From 3200 seconds till the end of the experiment, pressure increase was due to the combined effects of viscosity and filtration. The pressures increased very steeply in a short time when the grout approached gel state. By 3200 seconds, the finger head (front end of the finger behind the grout front) started to gel because by this time the grout age was close to gel time. The injectability of the grout in the porous media even at higher pressure was a clear indication that the macromolecules or pre-gels or micro-gels were still mobile, though possessing a relatively high viscosity.
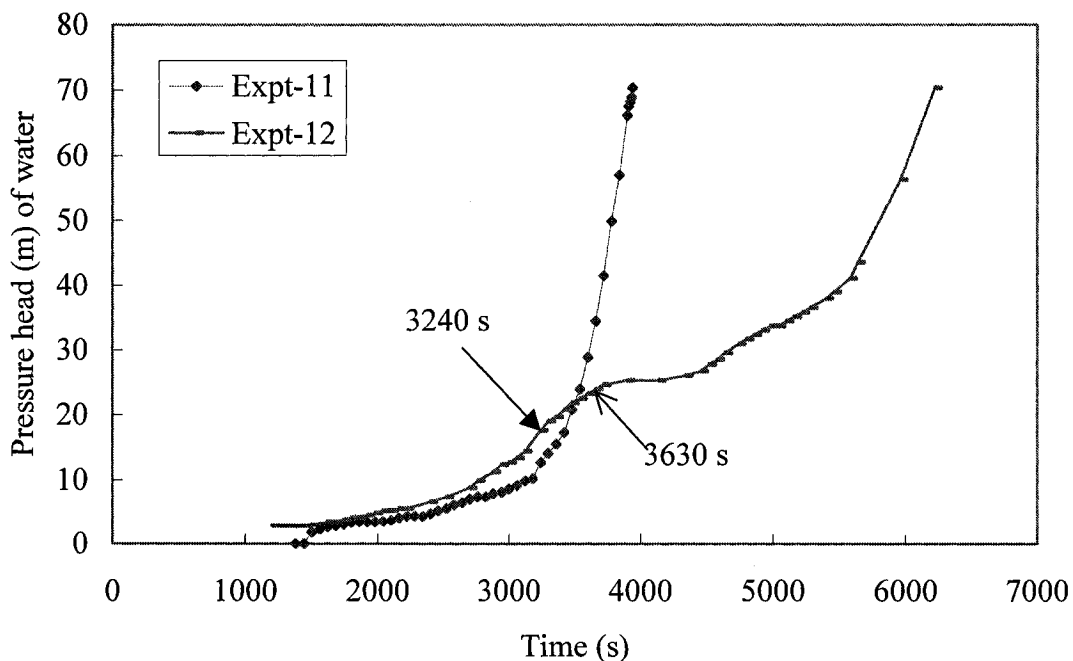
Figure 3.11: Pressures required to inject colloidal silica grout into sand columns at a constant flow rate of 2 ml/min

63

A fairly good match between the pressures for experiments Expt-1-1 and Expt-1-2 up to 3240 seconds showed the repeatability of experiments. After 3240 seconds, the slope of the grout injection pressure curve for Expt-1-2 was reduced until 5580 seconds, after which the injection pressure profile increased in slope. At 3240 seconds of the Expt-1-2, the colloidal silica was mixed with NaCl solution having a concentration of 9.2 % by wt. instead of 10 % by wt. The resulting grout solution had NaCl concentration of 2.3 % by wt. instead of 2.5 % by wt., which was used in Expt-1-1. This indicates that a very small percentage difference in NaCl solution affects the gelation process. As the pressure increase was slowed down, the NaCl concentration in the injected solution was restored to 10 % by wt. NaCl solution. Once the NaCl concentration was restored at 3630 seconds, the pressures increased steeply after 4340 seconds. The experiment also demonstrated the opportunity to correct the composition of the grout if the field engineer finds a delay in gelation of the grout in comparison to design gel time.

Figure 3.12 shows the pressures (labeled as Expt-NPF-slow) obtained for both NaCl preflush and no preflush cases. NPF indicates that the column was not preflushed and slow refers to reduced grout injection rate. The grout was injected at a rate of 1.3 ml/min as opposed to 2 ml/min in all other experiments. Since the flow rate was less, the gelation should have been quicker because of lower shear rate. However, the pressure profile is less steep than that obtained from Expt-11. This indicates that even though the shear rate was less, gelation had been delayed due to the absence of preflush. Thus the grout injection process was affected by the preflush. It is clear from the Figures 3.11 and 3.12 that a small change in NaCl concentration or a change in preflush conditions can sufficiently affect the gelation process. We can use this fact to adjust the NaCl concentration depending upon the gelation behaviour in the field.

Set-2 Experiments

The colloidal silica solution used for this set of experiments was the same batch solution used for Set-1 experiments. The NaCl solution was prepared with de-aired tap water for these experiments. Since the colloidal silica solution was about ten months older than that

64
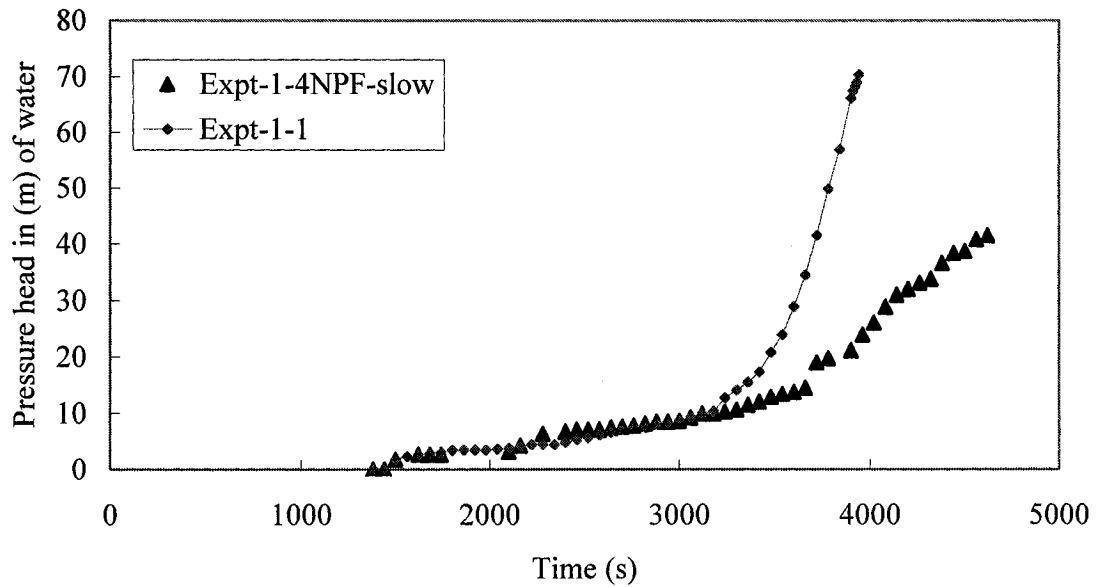
Figure 3.12: Grout injection pressures: effect of NaCl preflush

used for Set-1, vial experiments were performed to estimate the gel time. From the vial experiments, it was found that the gel time was increased to about 1500 seconds as opposed to 600 seconds for the grout composition used in Set-1 experiments. Thus, it took 900 seconds longer (*i.e.,* 2.5 times longer than the initial gel time) for the same colloidal solution to reach gelation. The pressures measured for the Set-2 experiments (*i.e.,* Expt-2-3, Expt-2-4, Expt-2-5, Expt-2-7 and Expt-2-8) during the grout injection into the sand column are presented in Figure 3.13. The figure also shows the profile obtained from Expt-1-1 to facilitate comparison of the profiles obtained for different cases. The required injection pressure head profiles varied significantly. The occurrence of the steep portion of the pressure profile reflecting the matured flow patterns and the time taken to reach 70.3 m of injection pressure are taken as the measures for comparison of different cases. The matured flow patterns are achieved when the gelation, viscous fingering and filtration effects were simultaneously playing their roles on the pressures at the grout injection point. The steep increasing portion of the profiles occurred between 3200 seconds and 4000 seconds.

65
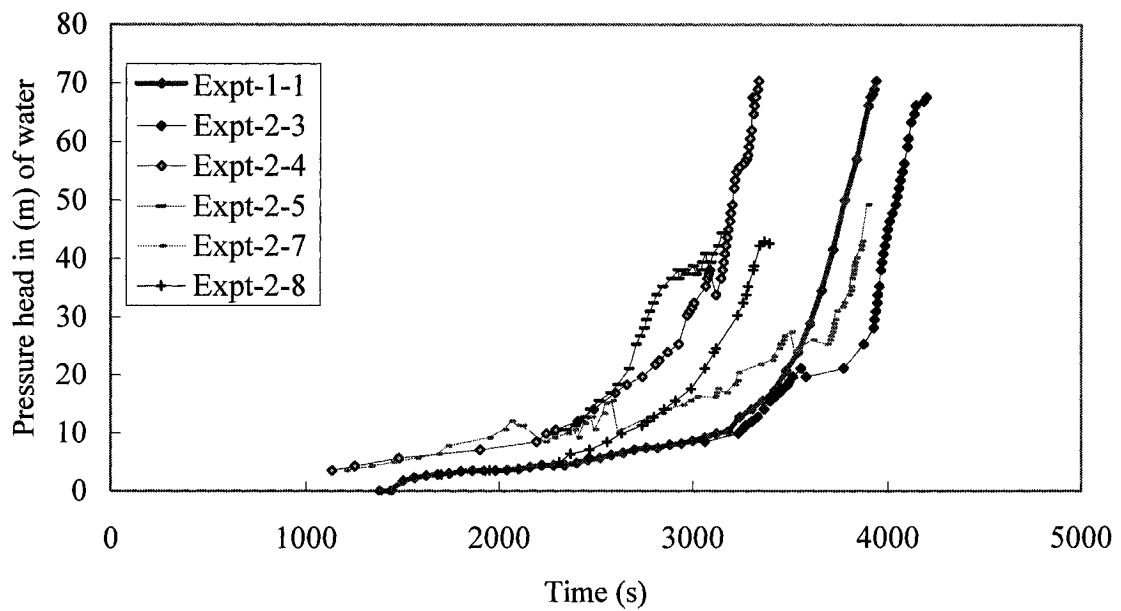
Figure 3.13: Grout injection pressure profiles: effect of tap water

(Note: Expt-2-8 is discontinued due to leakage at 3360 seconds)

Even though all the experimental operating conditions were the same, these pressure profiles seemed to differ significantly. The pressure profiles from these experiments, however, followed the same trend as the one observed from Expt-1-1. Ideally, these steep portions of the profiles should have occurred later than that of the Expt-1-1 because of the use of ten months old colloidal silica solution for which gelation time was longer. However these profiles lie on both sides of the profile of the Expt-1-1. There could be two major factors for these variations. The first and the most important parameter that is understood to have an affect is the salt content in the deaired tap water. Based on the Expt-1-2 in Set-1, the grout gelation process and injection pressures are found to be very sensitive to the small variations in salt concentration. The second factor might be the soil stratification achieved during the packing of the sand column. Though the sand particles were fairly uniform sized and the packing process was the same, variation in stratification could affect the grout injection pressures. Another important aspect of these profiles is the occurrence of the kink in the pressure profiles observed in experiments Expt-2-4, Expt-2-5, Expt-2-6 and Expt-2-7 in the injection pressure head range of 20 m – 40 m.

66

This kink might be the result of readjustment of grout blobs at higher pressures as a result of the movement of blocked grout blobs.

Set-3 Experiments

The experiments performed under this set were similar to the conditions used in Set-2 except that milli-Q water was used for saturating the column, for preparing 2.5% by wt. NaCl solution used for preflush and for the 10% by wt. NaCl solution used for the grout reaction. These experiments were labeled as Expt-3-0, Expt-3-1, Expt-3-2, Expt-3-3 and Expt-3-5-NPF (see Table 3.1). The pressure head profiles obtained from the experiments are plotted in Figure 3.14. These pressure profiles show mildly sloped trends, unlike the steeper slopes observed in the experiments of Set-2 and Expt-1-1.
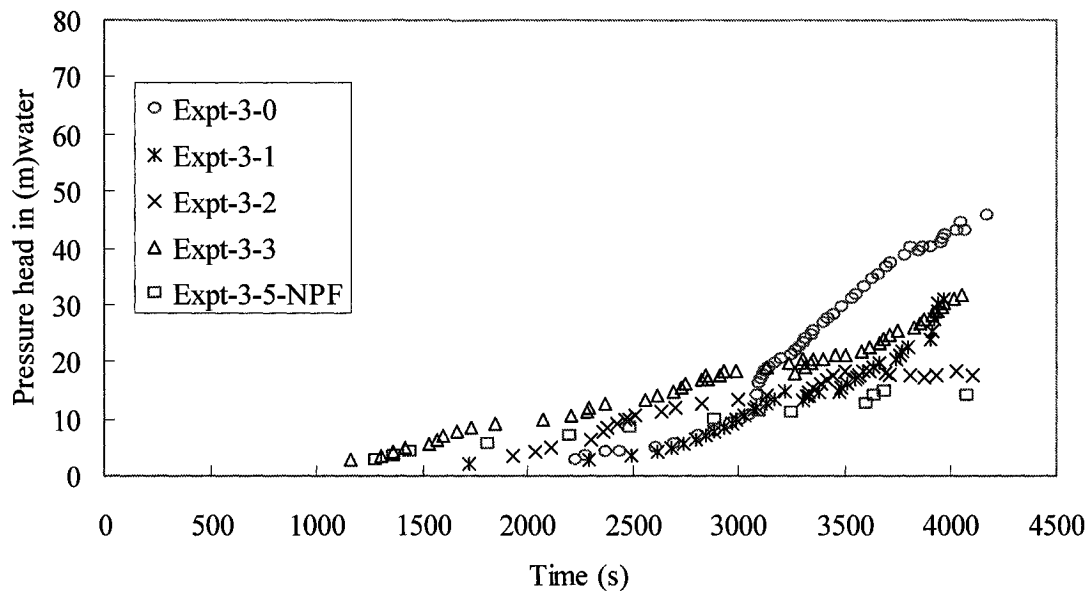
Figure 3.14: Grout injection pressure profiles obtained when milli-Q water is used

Regardless of the shape of the pressure head increase profile, the final pressure heads obtained just before the front exited the sand column are lower than that of Expt-1-1. This shows that the gelation was slower than that of Expt-1-1 because of the use of older colloidal silica solution. The surface area, a measure of colloidal silica particles in suspension, played an important role in the gelation. As the time since the colloidal silica is produced to the time it is used increases, surface area of the particles reduces due to

67

aggregation between the particles, which in turn leads to longer gelation or the need for higher NaCl concentration.

Due to the absence of salts in the milli-Q water, the gel time was expected to be longer than the gel time obtained when tap water was used. The pressure heads corresponding to Expt-3-0 and Expt-3-1 followed the pressure head profile obtained from Expt-1-1 up to about 3100 seconds and followed a different path after that. The final pressure from Expt-3-1 and Expt-3-3 are coincided. The profile obtained from Expt-3-2 approached steady state after 3500 seconds. The final pressure obtained for this experiment is the lowest among the four experiments of Set-3.

Figure 3.14 also shows the injection pressure profile obtained from the experiment where the column was not preflushed with NaCl solution (Expt-3-5-NPF). As expected, the final pressure obtained from this experiment was lower than those obtained from all other experiments even though the injection pressures during the early time was slightly higher than those observed during the experiments Expt-3-0 and Expt-3-1. Figure 3.15 shows the pressure profiles from Expt-1-1, Expt-1-4NPF-Slow, Expt-3-1 and Expt-3-5-NPF. This plot shows the comparative trends of the grout injectivity under the cases of grout solution made of fresh and older colloidal silica and the effect of NaCl preflush. Thus, Figure 3.15 demonstrates that the increase in duration between the time of colloidal silica production and its usage, and preflush affects the grout injectivity.

3.6.3 Grout Age - Experimental Artifact

Age of the grout that enters the bottom of the soil column effects the grout injection process. This is the time taken for the grout to travel through the tubing before entering the bottom of the sand column, since the reactants are pre-mixed. This age was observed as 350 seconds when the white coloured colloidal silica grout solution (without any dye) was injected after the preflush. When the red dyed grout solution was injected in Expt-12 (as shown in Figures 3.7a,b), the time it took from the instant colloidal silica and NaCl solutions were mixed to the time red dyed solution reached the bottom of the sand column was only 100 seconds, *i.e.,* grout age at the time of injection was only

68

100 seconds as opposed to 350 seconds at the beginning of the experiment. This was because when the grout was injected at the beginning, grout replaced the water in the tubings and fittings. However, by the time the red coloured dye was injected, the grout in the tubing and fittings started gelling and there was only a thin channel left for the fresh grout to be injected. This is very important in the analysis in determining the initial conditions and will be reflected in modeling. The younger grout will have lower viscosity which affects the injectivity. If we do not consider the reduced age of the grout at the bottom of the sand, we tend to assign higher viscosity to the grout solution at that time of entry into the sand.
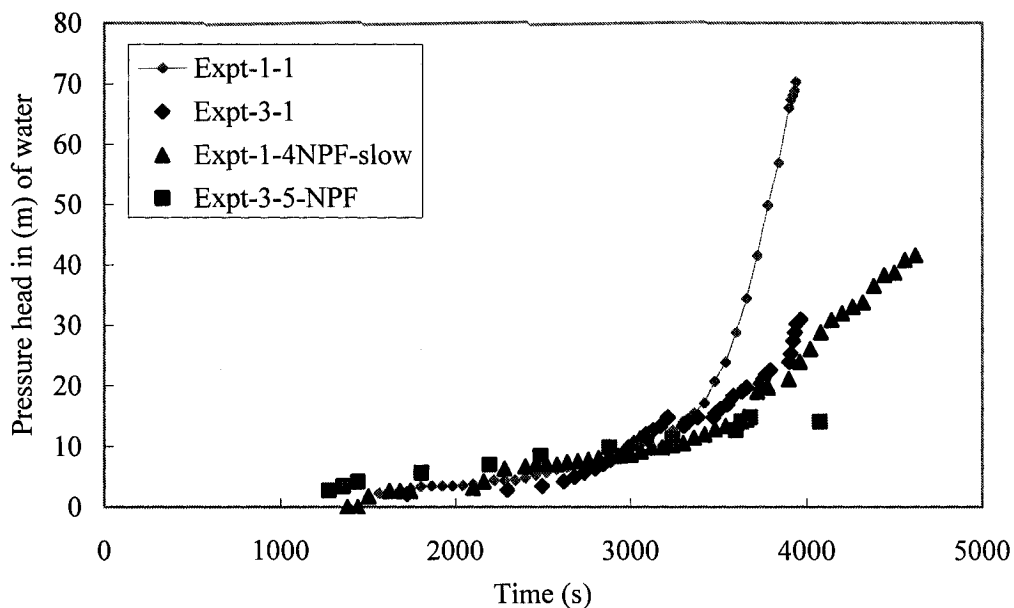
Figure 3.15: Grout injection pressure profiles: effect of preflush

3.7 SLIM TUBE EXPERIMENT

The pressure distribution profile obtained from the column experiment described in the previous section was complicated due to viscous fingering. In order to minimize this complexity, the grouting problem needs to be analysed in a column without the occurrence of the fingering process. Bryant *et al.* (1998) performed a similar experiment, named it as slim tube experiment, using an 8 mm diameter tube to identify the contribution of each of the processes such as viscosification, shear and filtration. A

69

column with a diameter smaller than or equal to the finger diameter was chosen to eliminate viscous finger formation. In the present study, a slim tube experiment was performed to better understand the physics during the grout injection into the column. A steel tube of 6.5 mm diameter was filled with the same fine sand described in section 3.2. The experimental setup was the same as that shown in Figure 3.5. In order to subject the gelling grout to the same shear rate as applied in the 30.16 mm diameter tube, the flow rate was scaled proportionate to the cross-sectional area, that is,

$$q = \frac{Q_1}{A_1} = \frac{Q_2}{A_2} \qquad \therefore \quad Q_1 = Q_2 \frac{A_1}{A_2} \tag{3.4a}$$

$$Q_{6.5} = Q_{30.16} * \left(\frac{A_{6.5}}{A_{30.16}} \right) = 2 \frac{ml}{min} * \left(\frac{6.5}{30.16} \right)^2 = 0.093 \frac{ml}{min} \tag{3.4b}$$

However, this flow rate is so small that there is a risk of grout being gelled even before it reaches the bottom of the sand in the column. Hence it was determined that the colloidal silica grout having 600 seconds gelation time needed to be injected at a rate somewhere between 0.4 and 0.5 ml/min in order the grout front to reach somewhere between half and two-thirds of the slim tube. Based on the measurements of the grout outflows over a period of 5 min, grout injection rate was determined as 0.46 ml/min. The required injection pressures were recorded every 30 seconds between 1080 and 1500 seconds and every 15 seconds from there on in order to capture the profile of steep increase in pressure. These pressure heads required to inject the grout as a function of time are plotted in Figure 3.16. Also plotted on the figure are the viscosity profiles correspond to gelation (i) under no shear (shown in solid diamonds) and (ii) when the grout was subjected to shear (shown in solid squares). Since it was possible to inject the grout solution until about 1200 seconds beyond the gelation time of 600 seconds, it may be understood that there was a delay in gelation, which may be attributed to shear effect. By the time the grout solution reaches the bottom of the sand column (slim tube), the grout viscosity is more than 100 times that of water viscosity. Therefore, filtration could have started affecting the grout injection. This is reflected by the change in slope of the

70

pressure profile either at point "A" or point "B" as shown in Figure 3.16. These results are used, as discussed in the next chapter, to analyse the grouting process for the case where the grout was injected into sand column that has no fingering effect.
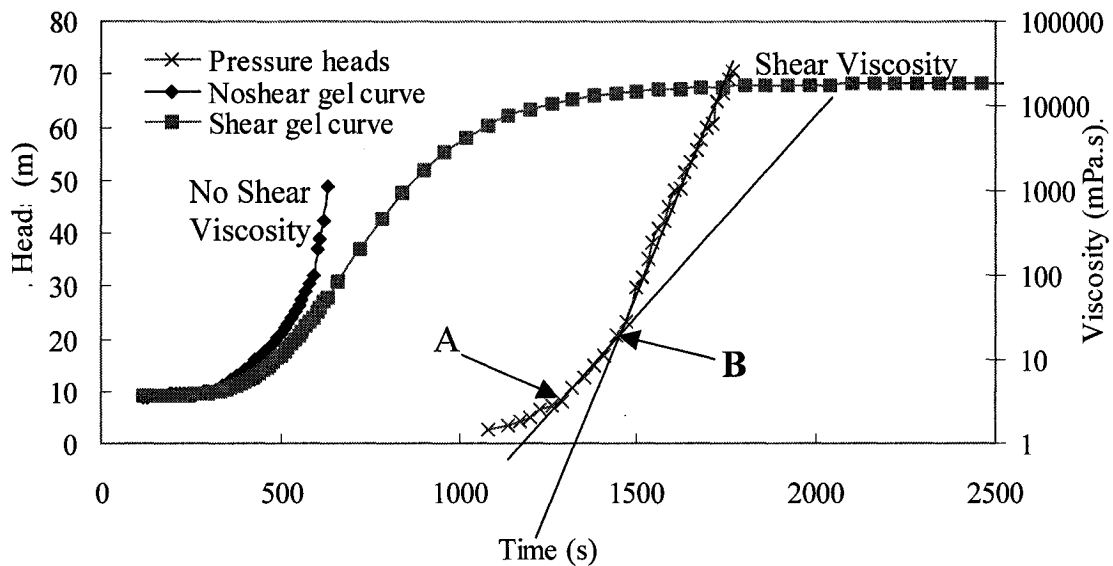
Figure 3.16: Grout injection pressure profiles for slim tube experiment and viscosity profiles during no shear and shear gelation

3.8 GROUTED SAND TESTING

3.8.1 Method

Fine sand (described in section 3.2) samples grouted with colloidal silica and NaCl solution mixture were tested for their imperviousness. Three samples consisting of colloidal silica of 40 %, 20% and 10 % by weight were prepared. Since the grouted sand was expected to have very low hydraulic conductivity, conventional testing might not yield the accurate estimate of hydraulic conductivity of grouted sands. Hence the grouted sand samples were tested using a porometer (manufactured by Porous Material Inc., NY). The schematic diagram of the porometer test is presented in Figure 3.17. In this test, the grout soil sample was cast in the porometer sample holder as shown in Figure 3.18. Once the grout was set, the sample was placed in the porometer sample holder and was covered

71
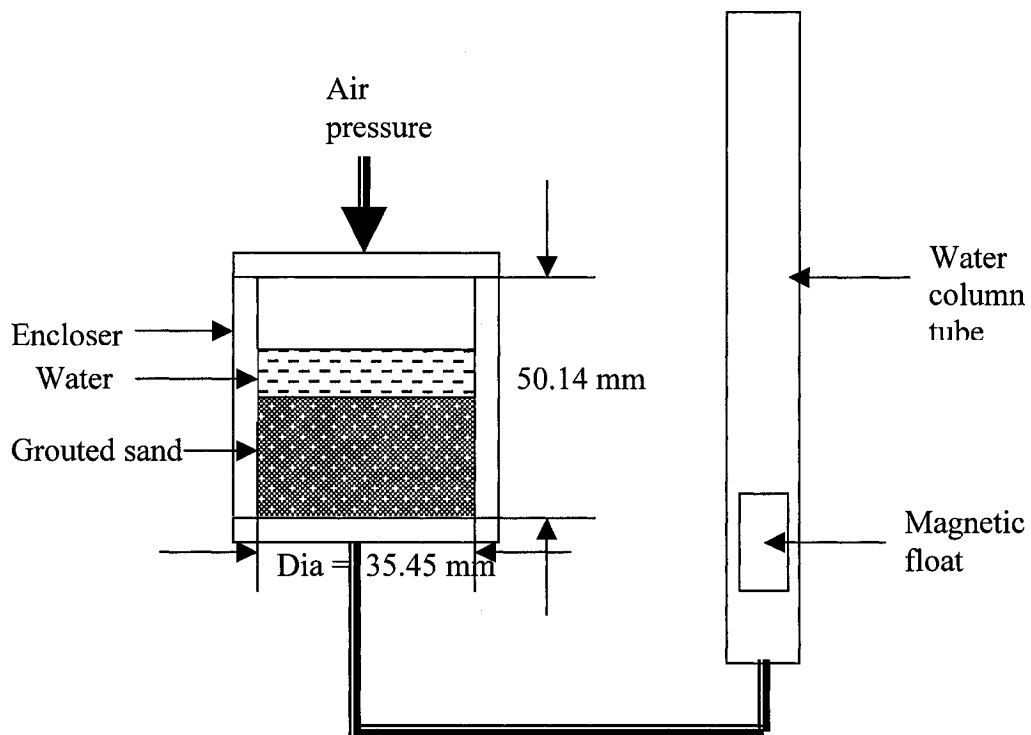
Figure 3.17: Schematic diagram of the porometer
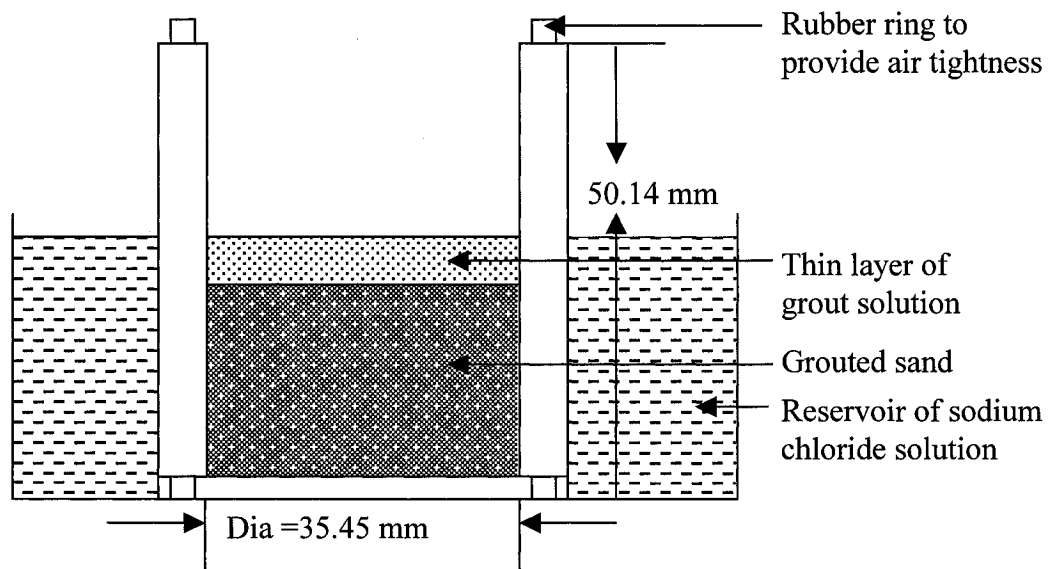
Figure 3.18: Porometer sample holder placed in a sodium chloride solution for casting grouted sand sample for testing its hydraulic conductivity

72

with the airtight cap. The test involved applying pressures from the top and forcing water flow through the sample. The bottom of the sample holder was connected to the bottom of the tube containing a magnetic float. The position of the float represents the pressure head at the bottom of the sample. The pressure of 0-351.6 m (*i.e.*, 500 psi) is graduated with a resolution of 1 in 20,000. The volume of water flowing through the sample was also noted.

Sample preparation involves placing the soil sample holder on top of filter paper, pouring grout solution followed by sand. Sand was poured into the grout solution in order to fill the pores completely with the grout and without any voids. The filter paper at the bottom protects from draining out of grout solution and the sample holder was placed with the rubber ring at the bottom. Then a reservoir of NaCl solution was created around the sample holder as shown in Figure 3.18. The levels of NaCl solution outside the sample holder and the grout mix on top of the soil sample were maintained at the same level. This exterior NaCl solution level will avoid any draining of the grout mix. The NaCl in the outside water will help prevent any diffusion or dilution of NaCl that exists in the grout soil mixture within the soil sample holder. The sample was kept in this condition until long after gel time in order to let the grout gel completely before it was fixed in the porometer for hydraulic conductivity testing.

Once the sample holder was placed in the porometer, depending upon the flow rate through the soil sample, the magnetic float placed in the tube moves up and down. The applied pressure, water column heads at the bottom of the sample and the flow rates were recorded until the difference between any consecutive observations was constant for at least three readings. The sample preparation procedure was repeated for the cases where the fine sand was grouted with 20 % and 10 % by wt. colloidal silica and corresponding NaCl solutions. Hydraulic conductivities of the grouted sand for the three cases were determined and are been given in Table 3.2.

3.8.2 Analysis

These grouted sand hydraulic conductivity tests help not only in obtaining the estimate of the minimum hydraulic conductivity that can be obtained corresponding to each of the colloidal silica concentrations, but also obtaining the relation between porosity (or porosity reduction) and hydraulic conductivity. The expression is given as

$$\left(\frac{\phi_g}{\phi_o}\right)^x = \left(\frac{k_g}{k_o}\right) \tag{3.5}$$

where ϕ_o and ϕ_g are porosity of the original soil medium and new porosity after reduction due to grouting respectively, k_o and k_g are permeability before and after grouting, x is a fitting parameter. Porosity after grouting is estimated as

$$\phi_g = (\phi_o - \phi_{cs}) \tag{3.6}$$

where ϕ_{cs} = volume fraction occupied by colloidal silica= X $(\rho_{bulk}/\rho_{solids})$, X =colloidal silica solids concentration, ρ_{bulk} = bulk density of the colloidal silica solution, ρ_{solids} = density of colloidal silica solids.

Table 3.2: Hydraulic conductivities of sand grouted with different compositions of grout mixture and evaluation of Equation (3.5) proposed by Clement et al. (1996)

Colloidal Silica (CS)	Porosity occupied by CS	New porosity (ϕ)	Observed Grouted sand K	Observed (K/K_o)	Calculated (K/K_o) from Eqn (3.5)	K_{obs}/K_{cal}
Solids % by wt	(ϕ_{cs})	$1-\phi_{cs}/\phi_o$	(m/s)	$(4)/K_o$	$(\phi/\phi_o)^{19/6}$	(5) / (6)
(1)	(2)	(3)	(4)	(5)	(6)	(8)
40	0.32	0.2	8.12×10^{-8}	3.52×10^{-6}	6.11×10^{-3}	5.76×10^{-4}
20	0.16	0.6	3.163×10^{-6}	1.38×10^{-4}	1.98×10^{-1}	6.93×10^{-4}
10	0.08	0.8	5.408×10^{-6}	2.35×10^{-6}	4.93×10^{-1}	4.76×10^{-4}

74

Clement *et al.* (1996) derived a similar theoretical expression relating porosity and permeability corresponding to change in physical properties of porous media due to microbiological colloidal accumulation in the porous media. Clement *et al.* (1996) determined the power "x" in Equation (3.5) as 19/6, whereas Civian (according to Todd, 1990) determined it to be 3.

Grouted sand hydraulic conductivities measured using the porometer and estimated from Equation (3.5) are compared as shown in Table 3.2. They differ by four orders of magnitude. In order to understand better, the ratios of the observed and calculated values are also tabulated in Table 3.2. It is found that there is a need for a proportionality constant that related porosity ratios and permeability ratios for different colloidal silica grout. This observation is based on only one type of sand. Hence it is necessary to test the grouted sand for different types of sands before confirming the proportionality factor. These conductivity data are useful in the model to assign the lowest hydraulic conductivity that the soil can be achieved for a given grout concentration.

3.9 CONCLUSIONS OF EXPERIMENTAL STUDIES

The experimental work performed in this chapter may be classified into three categories, *viz.,* viscosity measurements, grout injection into columns and grouted sand testing. The grout viscosity data were reported for two cases *i.e.,* gelation under no shear and gelation under shear. The gel times were found to be shorter as the concentrations of colloidal silica and sodium chloride increased. The gel times were also found to reduce with the increasing temperatures within the range of observed temperatures, *i.e.,* 10-30° C, at which gel viscosities were measured. Gel viscosities were found to reduce with the increase in shear rate. The increase in viscosity was minimal until the gel time corresponding to no shear gelation and increase was steep within a short duration. After reaching peak gel viscosities, they started to reduce. A gelation model was developed to express viscosity as a function of shear rate and time. The shear gelation model was used in the numerical modeling studies reported in the next chapter.

The column experiments were performed to investigate the processes occurring during the colloidal silica grout injection into the sand in these columns. The two different columns used for these experiments had diameters 30.16 mm and 6.5 mm. The column experiments performed in this chapter were grouped into three categories based on the age of the colloidal silica solution used and the type of water used. It was possible to inject the grout in both the cases until long after the gel time corresponding to no shear gelation. This was a clear indication that the shear was affecting the grout injection pressures. The viscous fingering had affected the grout injection process in the 30.16 mm diameter column. The smaller diameter column experiment, referred to as slim tube experiment, was aimed at obtaining the injection pressure head data in the absence of fingering formation within the column. The grout solutions injected into the 30.16 mm column were dyed with different colours. The visually observed dyed grout patterns helped in understanding the processes occurring during the grout injection into the sand column. The age of the colloidal silica solution and the type of water affected the grout injection. The grout injection process was found to be very sensitive to the salt content.

The hydraulic conductivities of the sand filled with different grout compositions were measured to determine the lowest achievable hydraulic conductivity for different colloidal silica concentrations. This was useful in specifying the lowest hydraulic conductivity for a given concentration in the modeling studies.

CHAPTER 4
MATHEMATICAL MODEL

4.1 MODEL DESCRIPTION

Chemical grouting of colloidal silica (CS) solution into porous media was simulated by coupling MODFLOW (McDonald and Harbaugh, 1988; Harbaugh and McDonald, 1996) and RT3D (Clement, 1997; Clement *et al.,* 1998; Clement and Johnson, 2003) and adding modules for gelling and grout reaction time. MODFLOW is a three-dimensional groundwater flow simulator used to determine the flow field. RT3D is a modular computer code for reactive multi-species transport in 3-dimensional groundwater aquifers. When the grout reactants are mixed, the viscosity changes with concentration of grout and its age. In general, grout age is the time elapsed since the grout reaction is initiated. However, grout does not age (*i.e.,* does not cure) unless there is a minimum grout concentration. Hence, a grout aging function, which incorporated a threshold concentration, was incorporated to prevent spurious gelation. This was achieved by numerically retarding gelation if the grout concentration falls below a specified minimum concentration.

Gel viscosity was indirectly incorporated in MODFLOW by changing the hydraulic conductivity (*K*) in each cell based on gel viscosity. Gel viscosity was calculated as a function of grout reaction time (grout age), grout concentration and shear rate. The structure of the grout model is presented as a flow chart in Figure 4.1. MODFLOW is called from RT3D periodically to update the flow field using the changing *K*-field. Using velocity fields generated by MODFLOW, transport of grout solution in the porous media is simulated using RT3D. The velocity field is then updated at regular intervals using MODFLOW and the computation for transport is repeated. Two modules, *i.e.,* GROUT_AGE and GROUT_GEL, were added to the RT3D and MODFLOW code system. GROUT_AGE, added as a reaction module under RT3D, determines and keeps track of grout age. GROUT_GEL, incorporated as part of MODFLOW, calculates grout viscosity as a function of grout age and grout concentration, and modifies the *K*-field.

Start RT3D model

Read grouting model data, well injection pattern, etc. → Set up using GMS 3.1

Call MODFLOW
Read in flow problem, K-field, etc

GROUT_GEL Module in MODFLOW
Calculate K-field based on grout concentration, age and shear

Calculate hydraulic heads using MODFLOW for velocity field for next time step

Return to RT3D to simulate grout injection to obtain grout concentration

GROUT_AGE – a reaction module to determine grout age

If
stress periods>=stress period # and, time steps >=time step #

Yes

No

Stop

Stress Period: *time interval during which all conditions (i.e., injection rate, grout concentration, location, etc) remain the same. Each stress period may have one or more time steps*

Figure 4.1: Flow chart of grouting model process

78

GROUT_GEL module allows choosing any of the gelation models presented in Chapter 2 and 3 and also incorporates the option to include or ignore the shear effect on viscosity. The shear effect on the colloidal silica gelation was incorporated in the GROUT_GEL module through the inclusion of shear gel viscosity equation (Equation (3.2)) developed in Chapter 3.

A summary of governing equations, constitutive relationships, solution techniques and other related information on the model formulation is presented in sections 4.2-4.7. The manuals for the respective codes, MODFLOW (McDonald and Harbaugh, 1988; Harbaugh and McDonald, 1996) and RT3D (Clement, 1997; Clement *et al.*, 1998; Clement and Johnson, 2003) provide further details. This chapter also presented the modules developed to simulate grout aging and gelation. Following these sections, the numerical modeling studies are presented. They are classified into (i) verification and validation of grout simulation model and (ii) analysis of data obtained from the colloidal silica grout injection into porous media to understand the effect of various parameters and processes.

The grout model was verified against an analytical solution, developed in this study to calculate the head loss through a soil column for a constant grout injection rate assuming that there is no dispersion. As part of validation, model results were compared against the results obtained from the numerical model results of Honma (1984). The grout model was used to analyse the observations on (i) the sodium silicate grout injection into a sand column experiment of Honma (1984) and, (ii) colloidal silica grout injection experiments carried out in this study. Numerical modeling studies were focused on issues such as the effects of grid size, effect of decoupling, heterogeneity, longitudinal and transverse dispersion, in addition to process related issues, *viz.*, effect of mixing rule, effect of shear-based gelation model and effect of minimum concentration in the grout aging function. The modeling studies were aimed at understanding the physics of grouting, the processes taking place and identifying the parameters.

4.2 GOVERNING EQUATION: RT3D

The partial differential equation describing the fate and transport of contaminants of species k in three-dimensional transient groundwater flow systems adopted in the development of RT3D was given by Zheng and Wang (1999), Clement (1997), Clement *et al.* (1998) and Clement and Johnson (2003) and is presented below:

$$\frac{\partial \left(\phi C^k \right)}{\partial t} = \frac{\partial}{\partial x_i}\left(\phi D_{ij} \frac{\partial C^k}{\partial x_j} \right) - \frac{\partial}{\partial x_i}\left(\phi v_i C^k \right) + q_s C_s^k + \sum R_n \tag{4.1}$$

where ϕ = porosity of the subsurface medium, dimensionless
C^k = dissolved concentration of species k, [ML^{-3}]
k = 1,2,....m aqueous phase (mobile) species
x_i = Cartesian coordinate, $x_1=x$, $x_2=y$, $x_3=z$, [L]
D_{ij} = hydrodynamic dispersion coefficient tensor, [L^2T^{-1}]
v_i = seepage or linear pore water velocity in the x_i direction, [LT^{-1}]; it is related to the specific discharge or Darcy flux (q_i) through the relationship, $v_i = q_i / \theta$
t = time, [T]
q_s = volumetric flow rate per unit volume of aquifer representing fluid sources (positive) and sinks (negative), [T^{-1}]
C_s^k = concentration of the source or sink flux for species k, [ML^{-3}]
$\sum R_n$ = chemical reaction term, [$ML^{-3}T^{-1}$]

Equation (4.1) states that for a control volume the change in the mass storage (both dissolved and sorbed phases) at any given time is equal to the difference in the mass inflow and outflow due to dispersion, advection, sink/source, and chemical reactions. The first, second and third terms on the right side of Equation (4.1) describe the effect of dispersion, advection and source/sink respectively. The last term on the right hand side of Equation (4.1) represents general biogeochemical reactions on contaminant fate and transport such as aqueous-solid surface reaction (sorption), first-order rate reaction or any other user defined chemical reaction.

80

4.3 GOVERNING EQUATIONS: MODFLOW

The governing differential equation (McDonald and Harbaugh, 1988; Harbaugh and McDonald, 1996) describing groundwater flow in three-dimensions is given as

$$\frac{\partial}{\partial x}\left(K_{xx}\frac{\partial h}{\partial x}\right) + \frac{\partial}{\partial y}\left(K_{yy}\frac{\partial h}{\partial y}\right) + \frac{\partial}{\partial z}\left(K_{zz}\frac{\partial h}{\partial z}\right) + q_s = S_s\frac{\partial h}{\partial t} \tag{4.2}$$

where K_{xx}, K_{yy} and K_{zz} = hydraulic conductivities in x, y and z directions, $[LT^{-1}]$; h = hydraulic head, $[L]$; S_s = specific storage of the aquifer, $[L^{-1}]$, and q_s = fluid sink/source term (defined in Equation (4.1)).

The solute transport equation (Equation (4.1)) is related to the groundwater flow equation through Darcy's law

$$q_i = -K_i\frac{\partial h}{\partial x_i} \tag{4.3a}$$

and

$$v_i = \frac{q_i}{\phi}. \tag{4.3b}$$

MODFLOW (McDonald and Harbaugh, 1988; Harbaugh and McDonald, 1996) assumes that the principal components of the hydraulic conductivity tensor, K_{xx}, K_{yy}, and K_{zz} in Equations (4.2) and (4.3) are aligned with the x, y, and z coordinate axes, i.e., there are no cross terms.

4.4 GELATION MODELING

Gelation is the process of formation of networks of silica particles leading to formation of highly increased viscous material such as solid, semi-solid or gel. Gel time is the time interval between the initial mixing of the grout components *(i.e.,* since reaction is activated) and the formation of the gel. Gel time can be adjusted by varying the composition of the grout. For some grouts, like silicates, the viscosity changes gradually,

81

whereas for acrylamides and colloidal silica the viscosity remains fairly constant until the gel time is reached and then increases rapidly. Typical gel time curves may be found in Karol (1990), Finsterle *et al.* (1997) and also in Figures 3.2 and 3.3.

4.4.1 Gelation Models

The viscosity increase is a function of time and concentration. The module GROUT_GEL incorporates the option to choose any one of the gelation models for viscosity as a function of grout age presented in Chapter 2, *viz.*, Honma (1984) model (given in Table 2.2), Berkeley model (Equation (2.1)) of Finsterle *et al.* (1994) and Moridis *et al.* (1999), Equation (2.5) of Kim and Corapcioglu (2002a,b) and shear based gelation model (Equation (3.2)) proposed in the present thesis. These are:

Honma Model:
$$\mu_r = \mu_{ro}\left(1+\zeta t\right)\left[\exp\left\{\frac{\sigma * t}{geltime - t}\right\}\right] \tag{2.1}$$

Berkeley Model:
$$\mu_{gel} = a_1 + a_2 e^{(a_3 t)} \tag{2.2}$$

Kim and Corapcioglu Model:

$$\mu_{gel} = \mu_s - 0.3[\exp(0.734)]^{0.01} + 0.3\left[\exp\left\{0.734\left(1 - F_g\right)^{6.5/\ln 0.5}\right\}\right]^{0.01} \tag{2.5}$$

Present Model for Shear Gelation

$$\frac{\log(\mu_{gel}) - \log(\mu_{min})}{\log(\mu_{max}) - \log(\mu_{min})} = 1 - \frac{1}{\left(1 + [0.854 * (t/60)]^{10.419}\right)^{1.7754}} \tag{3.2}$$

μ_{min} is initial viscosity, which was observed during viscosity measurements as 5.75 x 10^{-3} Pa.s. Maximum achievable gel viscosity (μ_{max}) is expressed as a function of shear rate:

$$\mu_{max} = 22.41 \gamma^{-0.8863} \tag{3.3}$$

where γ = shear rate [T^{-1}]. Of the various expressions presented in Section 2.6.4, the expression given by Lopez *et al.* (2003) is adopted due to its simplicity.

$$\gamma = C \frac{q}{\sqrt{k\phi}} \tag{2.13}$$

The proportionality factor, C, is taken as 1.25 (Lopez *et al.*, 2003).

The gelation model of Honma was based on the sodium silicate gelation data, while the other three were based on colloidal silica gelation data. However, the gelation models reported in the grouting literature did not incorporate the shear effect. Hence the present grouting model incorporated a shear based gelation model. It is worth mentioning that any of these models could be used. The parameters should be obtained based on fitting the model for the corresponding data on gelation. Due to the modular structure of the grout model code, it is possible to incorporate any other gelation model as well.

4.4.2 Mixing

Once the grout is injected, as the front moves it mixes with water or NaCl (if the porous media is preflushed with NaCl solution). As a result, the solution gets diluted as it travels through the soil. The mixing process reduces the concentration and hence the viscosity of the solution. The viscosity of the diluted grout solution may be described by either a linear or power law mixing rule (Koval, 1963; Finsterle *et al.*, 1997; Moridis *et al.*, 1999). The linear and power law mixing rules are given by:

$$\mu_l = X_{gel}\mu_{gel} + (1 - X_{gel})\mu_w \tag{2.16}$$

$$\mu_p = \left(\frac{X_{gel}}{\mu_{gel}^{1/4}} + \frac{(1 - X_{gel})}{\mu_w^{1/4}} \right)^{-4} \tag{2.17}$$

Based on laboratory experiments of the colloidal silica composition and numerical investigations, the appropriate mixing rule may be determined.

4.4.3 Grout Medium Modification

During grout injection, the grout viscosity increases as explained above. When the viscosity increases, the flow field is altered. In order to take into account this effect, the

83

hydraulic conductivity of the grouted soil media at each of the cells is calculated based on the grout viscosity. The grout viscosity is calculated using any of the gelation equations (Equations (2.1), (2.2), (2.5) or (3.2)) in each cell, followed by mixing equation (Equation (2.16) or (2.17)). Then, the hydraulic conductivity of the grouted soil media, $K_{grouted}$, is obtained as

$$K_{grouted} = \frac{K_o}{\left(\mu_{l/}\mu_w\right)}$$

(4.4)

where K_o = initial hydraulic conductivity of the porous media and μ_w = viscosity of water.

The flow field is updated frequently using the modified hydraulic conductivity field. The process of injection continued until either the target grout mass is injected or the end of the designed injection period is reached.

4.5 GROUT AGE

Equations representing grout viscosity increase during gelation require the reaction time. Hence, the reaction time referred to as grout age needs to be tracked. The grout age was represented as one of the species and the rate of change of grout age was implemented as a reaction module, GROUT_AGE, in RT3D. Conceptually, the rate of change of grout age can be described as

$$\frac{\partial(\text{grout age})}{\partial t} = 1.$$

(4.5)

This equation indicates that the grout age (or reaction time) increases at the same rate as the simulation time. Although this equation looks logical, there is a problem of premature gelling based on this equation. Grout age is equal to reaction time in a closed system. However, it may be different in porous medium due to processes such as dispersion and mixing. In reality, when the grout concentration is too low, the reaction is stalled. The viscosity of the grout remains the same or increases very insignificantly until it gets additional grout to make the concentration enough to continue the reaction and increase the viscosity. Initially, soil was considered as saturated at time zero. For example, if we

84

inject grout at some point in space 2.0 hrs after the injection is started at the first point, grout injected at the current point has an age of zero. However, the water that was present from the beginning of the simulation had an age of 2.0 hrs. The model based on Equation (4.5) considers the age of the grout and water mixture at the current injection point as somewhere between 0.0-2.0 hrs rather than 0.0 hrs. This results in spurious premature gelling. In order to circumvent this, the concept of minimum concentration was incorporated.

Experimental studies of Persoff et al. (1999) reported that when the grout concentration was less than 7.4 % by wt, the solution did not gel. These experiments confirm the need to incorporate the minimum grout concentration effect in the gelation model representation. Under this concept, a criterion had been incorporated in the expression to check if there is a minimum amount of grout before aging of solution takes place. To incorporate minimum grout concentration, X_{min}, Equation (4.5) was modified by incorporating a smooth transition from no gelling to initiation of gelling for the rate of change of gel age as

$$\frac{\partial(grout\ age)}{\partial t} = 1 - \left[\left(X_{gel}\ \beta \right)^{\eta} + 1 \right]^{-\omega} \tag{4.6}$$

where β, η and ω are fitting parameters to decide the degree of smoothness required. In this study β, η and ω are assigned as 50, 3 and 5, respectively corresponding to X_{min} of 5 % by wt. of colloidal silica concentration.

Thus, this equation allows increase in gel age only when the concentration is higher than X_{min}. This expression yields the rate of change of grout age as 1.0, if the grout concentration is equal to or greater than X_{min}, which means the change in grout age is equal to the change in reaction time. If the grout concentration is less than the minimum concentration, X_{min}, grout does not age or cure. For concentrations around X_{min}, Equation (4.6) provides a smooth transition between 0.0 and 1.0. A schematic representation of differences in the simulation time (time since reactants are mixed) and

85

grout age is presented in Figure 4.2. This figure shows the grout aging as per Equations (4.5) and (4.6). It also shows how the grout aging stalls when the grout concentration is less than X_{min}. When the grout concentration is above the minimum grout concentration, X_{min}, required for gelation to take place, there is grout aging. On the other hand, when the grout concentration is less than X_{min}, grout age does not change. Section 4.12 presents further discussion on X_{min} and its effect on grout injection.
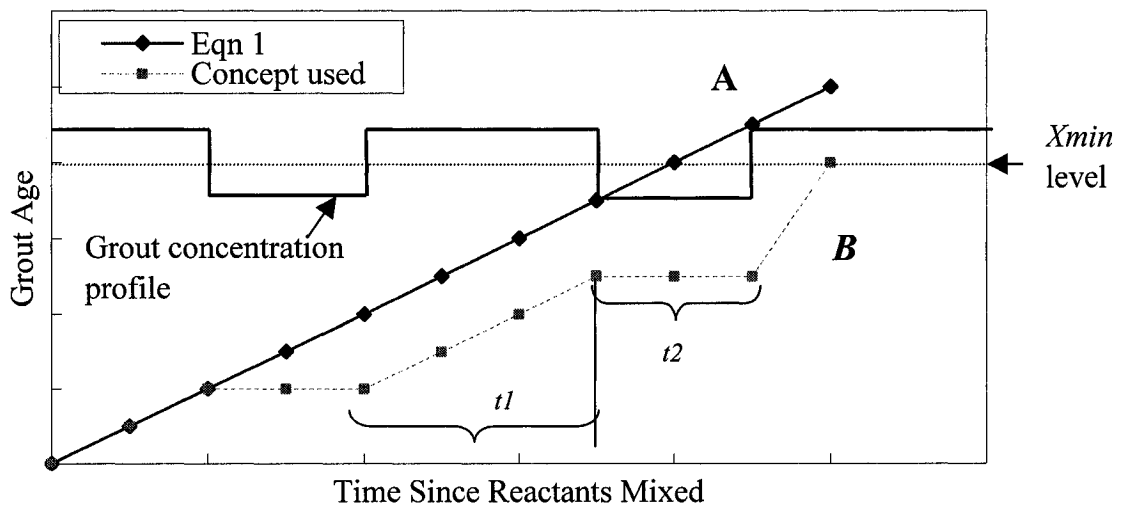
Figure 4.2: Conceptual plot of grout aging profile. During $t1$, grout ages/cures at the same rate as the simulation time. However during $t2$, grout does not age because the concentration is less than the minimum grout concentration (X_{min}) needed to gel. Right side axis represents grout concentration. Grout ages (and hence viscosity increases), only if the grout concentration is greater than X_{min}.

4.6 INITIAL AND BOUNDARY CONDITIONS

Solution of Equation (4.1) and (4.2) requires specification of boundary and initial conditions. The boundary conditions may be specified values (heads or concentrations) referred to as Dirichlet type, or specified head gradient or concentration gradient across the boundary referred to as Neumann conditions, or a combination of both referred to as Cauchy conditions. For transient problems, initial conditions *i.e.,* head and/or

86

concentration at time $t = 0$ are also required to be specified. These conditions may be expressed as

Initial conditions:

$h(x, y, z, t) = h_o(x, y, z)$	on domain Ω at time $t = 0$	(4.7)
$c(x, y, z, t) = c_o(x, y, z)$	on domain Ω at time $t = 0$	(4.8)

Boundary conditions

$h(x, y, z, t) = h_b$	along boundary Γ_1 for $t \geq 0$	(4.9)
$c(x, y, z, t) = c_b$	along boundary Γ_1 for $t \geq 0$	(4.10)

$-\dfrac{\partial h}{\partial x_j} = q_i$	along boundary Γ_2 for $t \geq 0$	(4.11)
$-\theta\, D_{ij}\, \dfrac{\partial h}{\partial x_j} = f_i\left(x, y, z, t\right)$	along boundary Γ_2 for $t \geq 0$	(4.12)

where $f_i(x, y, z, t)$ is a known function representing dispersive flux normal to the boundary Γ_2.

4.7 SOLUTION TECHNIQUES

The grout model involves solution of two sets of equations. The first set includes algebraic equations formed by finite difference discretisation of Equation (4.2) under MODFLOW. The equation set was solved using the conjugate gradient algorithm. The second set includes algebraic equations formed due to numerical implementation of Equation (4.1) under RT3D. The governing equation along with constitutive equations subjected to initial and boundary conditions in RT3D can be solved using (i) finite difference method, (ii) particle tracking methods, and (iii) Total Variation Diminishing (TVD) methods as implemented in the recent version of RT3D (Clement and Johnson, 2003). RT3D code, which is derived from a three-dimensional model for multi-species mass transport of contaminants in groundwater, MT3DMS (Zheng and Wang, 1999), was implemented with a third order TVD scheme based on the Universal Limiter for

87

Transient Interpolation Modeling of the Advective Transport Equation (ULTIMATE) algorithm. TVD methods have two advantages, *viz.,* mass conservative and minimal numerical dispersion. The reduction in numerical dispersion was achieved through the implementation of the higher order methods at the expense of spurious oscillations, which are controlled by numerical procedures referred to as flux limiters. The interface concentrations, using the ULTIMATE scheme, were determined through a third order polynomial interpolation of nodal concentrations, supplemented by a universal flux limiting procedure to minimize unphysical oscillations which may occur if sharp concentration fronts were involved (Zheng and Wang, 1999). The finite difference option may be used with either explicit mode or implicit mode. However, TVD methods were solved using the explicit mode. The TVD method was used to solve the advective part only. The dispersion, source/sink and reaction components were solved using implicit finite difference method, for which the Generalized Conjugate Gradient (GCG) solver was used. Since the ULTIMATE scheme was implemented in explicit mode, the transport time step size $(\Delta t_{transport})$ is subjected to a stability constraint, which is given as

$$\Delta t_{transport} \leq \frac{R}{\dfrac{|v_x|}{\Delta x} + \dfrac{|v_y|}{\Delta y} + \dfrac{|v_z|}{\Delta z}} \qquad (4.13)$$

where R = retardation factor, v_x v_y, v_z = velocity along x, y and z directions, and Δx, Δy and Δz are the grid sizes in the respective directions. In the present study, the retardation factor R is assigned as 1.0.

4.8 ASSUMPTIONS

The following assumptions are made during the development of the mathematical model:

- It was assumed that there was no interaction between the soil and the injected colloidal silica (Kim and Corapcioglu, 2002a,b).
- The gelation process was not affected by dilution, *i.e.,* even after dilution the grout present in the solution still behaved as a pure gel for the purpose of gelation. Its effect on the flow field, however, was governed by the diluted viscosity.

88

- Porosity was assumed to be constant and is not affected by gel macromolecules. The permeability (having L^2 units) was also assumed not to change due to the presence of macromolecules of grout. The effect of grout on profile modification was represented in terms of reduced hydraulic conductivity as explained by Equation (4.4).

- The density of the colloidal silica was not affecting the grout injection process.

- The gelation characteristics of the grout and shear rate in a rheometer were assumed to be the same as the ones encountered in the sand column.

- There were no geochemical reactions taking place between the colloidal silica grout solution and the soil.

4.9 VERIFICATION

As discussed in the literature review, verification and validation are the two steps in achieving the confidence that the model can mimic the physical system with a reasonable accuracy. Comparison of the numerical solution against an analytical solution, which is the starting point in many studies, is a critical step in code development (Oreskes *et al.,* 1994). An acceptable matching between the results obtained from analytical and numerical solutions does not guarantee an accurate solution to the problem. It only gives confidence that the governing equations thought to be representing the processes are solved with a reasonable accuracy. There were no analytical solutions available in the literature for a problem of this kind due to the complexities and non-linearities involved. Hence, a one-dimensional analytical solution was developed for this purpose in the present study. The following sub-section presented the development of an analytical solution for one-dimensional grouting and comparison of the numerical model solution against it.

89

4.9.1 Development of Analytical Solution

Testing of numerical solutions against an analytical solution is an important phase of code verification. This process ensures confidence that the numerical code approximates the set of governing differential equations subjected to given boundary conditions and initial conditions. A one-dimensional analytical solution was developed in this study to determine the required grout injection pressure with time as the grout is injected from one end at a constant rate. Due to the complex nature of the problem, for the purpose of developing the analytical solution it was assumed that dispersion and mixing do not affect the grout injection process. Thus the analytical solution considered only the advective component and the gelation. The grout injection pressures obtained from numerical simulations were compared with those obtained from the analytical solution. In order to compare the numerical solution results with those obtained from analytical solution, the dispersion and mixing modules were turned off in the numerical simulation. Thus, the comparison of the numerical solution with the analytical solution gives an idea about the numerical dispersion caused by the numerical model.

Grout was injected at a constant flux (q) through a one-dimensional column of length (L) as shown in Figure 4.3. Let h_o and h_L be initial heads on the left and right side *i.e.,* at x $=0$ and $x = L$, respectively. Assume that at time t, the grout front has reached l_1 into the column. The head at $x=l_1$ is h_1. There will be two regions, *i.e.,* grouted region from $x = 0.0$ to l_1, and ungrouted region from $x = l_1$ to L. Therefore, the head loss through the column is the sum of the head loss through grouted and ungrouted regions.

The Darcy flux is given as

$$q = -K \ \frac{dh}{dx} \tag{4.3a}$$

where K = hydraulic conductivity.

Constant flux q

$h = h_o$ $h = h_1$

| Grouted Region | Ungrouted Region |

$h_L = 0.0$

$x = l_1$

L
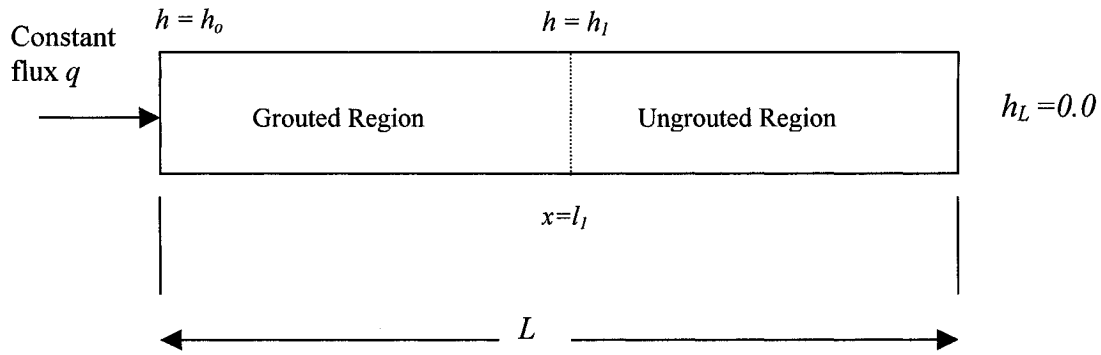
Figure 4.3: One-dimensional grouting model with constant flux on the left hand side and constant head on the right hand side

Since hydraulic conductivity (K) will vary as the grout is injected into the column, K will be a function of length. This may be rewritten as

$$-dh = \frac{q}{K(x)} dx \tag{4.14}$$

where $K(x)$ = variable hydraulic conductivity along the length.

Assume that the grout front reached a distance of l_1 from the left end at a given time. Integrating the above equation from 0 to l_1 with heads h_o and h_1 at the left and right ends of this portion of the column respectively,

$$-\int_{h_o}^{h_1} dh = q \int_{0}^{l_1} \frac{dx}{K(x)} . \tag{4.15}$$

As the grout reaction progresses, the grout viscosity increases. The viscosity of the grout results in reduction in hydraulic conductivity. The hydraulic conductivity at any location, $K(x)$, is related to original hydraulic conductivity and the viscosities at the beginning and end.

91

$$K(x) = K_o \left[\mu_w / \mu(x) \right]$$ (4.16)

where K_o = Initial hydraulic conductivity of the medium
μ_w = Viscosity of water
$\mu(x)$ = Variable viscosity along the length depending on time

Of the given different gelation models, the expression proposed by Finsterle *et al.* (1994) for $\mu(x)$ (*i.e.*, μ_{gel}), given in Equation (2.2), was considered.

$$\mu_{gel} = a_1 + a_2 \exp(a_3 t)$$ (2.2)

The distance travelled by the grout is expressed as a product of velocity (v) and time of travel (t), and is expressed as

$$x = vt.$$ (4.17)

However, velocity is determined from Darcy's flux, q, as

$$v = q/\phi$$ (4.3b)

where ϕ= porosity.

Therefore, time of travel is $t = \dfrac{x}{v} = \dfrac{x}{\left(\dfrac{q}{\phi}\right)}$. (4.18)

Assuming that there is no dispersion and no mixing, the time of travel is equal to grout reaction time and grout age. Substituting the expression for 't' from Equation (4.18) into Equation (2.2) yields

$$\mu(x) = a_1 + a_2 e^{\left(a_3 \frac{x}{q/\phi}\right)} .$$ (4.19)

92

For the purpose of analytical solution development, it was assumed that there is no time delay between the time at which the reaction is initiated and the time at which the grout injection is started. The grout age and the time since grout gelants were mixed were assumed to be the same. Hence, the time of travel is equal to the time since the grout reaction is injected. Substituting Equation (4.19) into Equation (4.16), the expression for hydraulic conductivity as a function of distance along the column may be obtained as,

$$
K(x) = K_o \mu_w \left[a_1 + a_2 e^{\left(a_3 \left(\frac{x}{q/\phi} \right) \right)} \right]^{-1} .
$$

(4.20)

Substituting the expression for $K(x)$ into Equation (4.15) gives

$$
- \int_{h_o}^{h_1} dh = \frac{q}{K_o} \int_0^{l_1} \frac{1}{\mu_w} \left[a_1 + a_2 e^{\left(a_3 \left(\frac{x}{q/\phi} \right) \right)} \right] dx .
$$

(4.21)

Integrating,

$$
- (h_1 - h_0) = \frac{q}{K_o} \frac{1}{\mu_w} \left[a_1 l_1 + \frac{q}{\phi} \frac{a_2}{a_3} \left(e^{\left(a_3 \left(\frac{l_1}{q/\phi} \right) \right)} - 1 \right) \right] .
$$

(4.22)

From Equation (4.18), $l_1 = (q/\phi)t$. Substituting $l_1 = (q/\phi)t$ into the above equation,

93

$$(h_0 - h_1) = \frac{q}{K_o} \frac{1}{\mu_w} \left[a_1 \left(\frac{q}{\phi} \right) t + \left(\frac{q}{\phi} \right) \frac{a_2}{a_3} \left(e^{a_3 t} - 1 \right) \right].$$ (4.23)

For the ungrouted region from l_1 to L

$$q = -K \frac{dh}{dx}$$ (4.24)

Since the grout solution has not reached this section, hydraulic conductivity has not changed in this section and it is held constant, $K = K_o$. Substituting $K(x)=K_o$ and integrating Equation (4.24) along the l_1 to L segment

$$- \int_{h_1}^{h_L} dh = \int_{l_1}^{L} \frac{q \, dx}{K(x)} = \frac{1}{K_o} \int_{l_1}^{L} q \, dx$$ (4.25)

That is,

$$- (h_L - h_1) = \frac{q}{K_o} [L - l_1]$$ (4.26)

$$\therefore h_1 = \frac{q}{K_o} [L - l_1] + h_L = \frac{q}{K_o} \left[L - \frac{q}{\phi} t \right] + h_L.$$ (4.27)

Substituting the above expression for h_1 into Equation (4.23) and reorganizing, the total head required at the injection end to maintain the constant flow through q the column is obtained as

$$h_o = h_L + \frac{q}{K_o} \left[L - \frac{q}{\phi} t \right] + \frac{q}{K_o \mu_w} \left[a_1 \frac{q}{\phi} t + \frac{q}{\phi} \frac{a_2}{a_3} \left(e^{a_3 t} - 1 \right) \right]$$ (4.28)

| Head at the right end $x=L$ | Head lost in the non-grouted region, $l_1 \leq x < L$ | Head lost in the grouted region $0 \leq x < l_1$ |

94

4.9.2 Verification Against Analytical Solution

Numerical grout simulation model results were compared with the analytical solution developed for the one-dimensional column test problem. A 500 mm long column with a cross-sectional area of 20 mm x 10 mm, filled with sandy soil having hydraulic conductivity 1 x 10^{-5} m/s, was selected as shown in Figure. 4.4. The domain was discretized into 1800 grids. Grout solution (colloidal silica) was injected from the left end (*i.e.*, $x = 0$) at a rate of 1 x 10^{-8} m³/s for 1500 seconds, while the head at the right end was maintained such that h_L=0.0 m. The gel time of the grout solution was set to 900 seconds. The parameters a_1, a_2 and a_3 for the gel time curve (Equation (2.2)) adopted in this experiment were 2 x 10^{-3} Pa.s, 1 x 10^{-3} Pa.s and 6.59 x 10^{-3} Pa.s, respectively. Since the effect of dispersion was not incorporated in the analytical solution, the dispersion module was turned off in the numerical model. Under these conditions, pressure heads required to maintain the constant grout solution injection were calculated at different times.
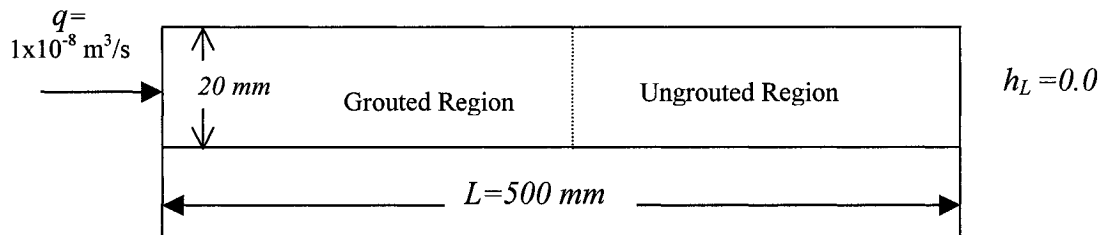
Figure 4.4: One-dimensional test case for verification of grout model against analytical solution

For the numerical simulations, two techniques, *viz.,* upstream finite difference and Total Variation Diminishing (TVD) schemes were chosen. The grout entry pressure heads at different times are plotted in Figure 4.5, one curve each for analytical solution, standard upstream finite difference solution and TVD solution schemes. The heads at the column entrance obtained by solving the governing equations using the TVD scheme are found to be closer to the analytical solution results compared to those obtained for upstream finite difference scheme. This is due to the higher dispersion in the upstream finite difference scheme. The higher dispersion in grout concentration reduced the viscosity of the grout, as a result it requires lesser injection pressure. This is also evident from the grout concentration distribution plot obtained from the two methods as shown in Figure 4.6. It

95

may be concluded from Figure 4.5 that the equations were properly solved by the numerical schemes. The plot also shows that the TVD scheme produced results that are numerically less dispersed than those of the upstream finite difference scheme. Hence, TVD scheme was chosen for the remaining part of the numerical modeling studies.
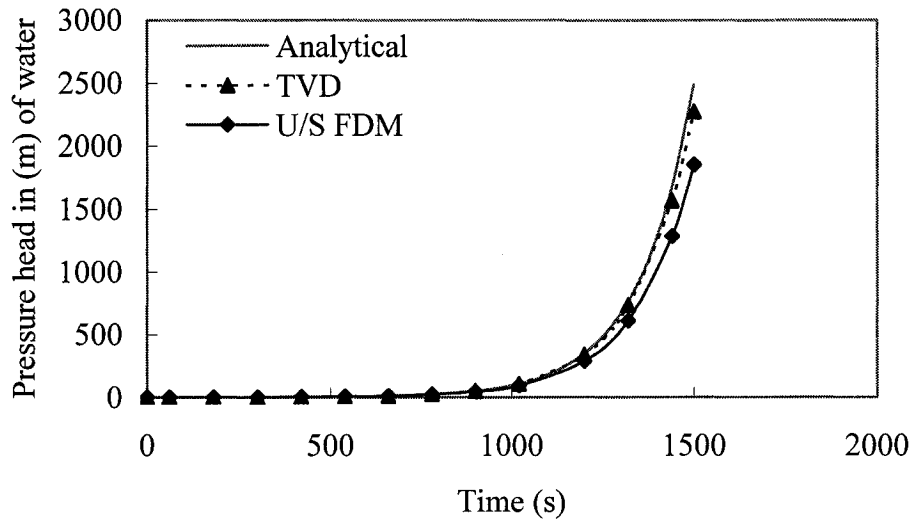
Figure 4.5: Comparison of injection pressure heads required to maintain constant grout injection rate, obtained from numerical and analytical solutions of 1-D model

Figure 4.6: Grout concentration distribution in the one-dimensional column using finite difference and Total Variation Diminishing methods

96

4.10 VALIDATION AGAINST HONMA MODEL

Mathematical models, especially numerical models, need a proof that they represent the physical problem with an acceptable accuracy. The process of validation involves representation of the physics of the processes by the appropriate equations (Roache, 1998). Usually, validation is achieved by comparing numerical simulation results with the exp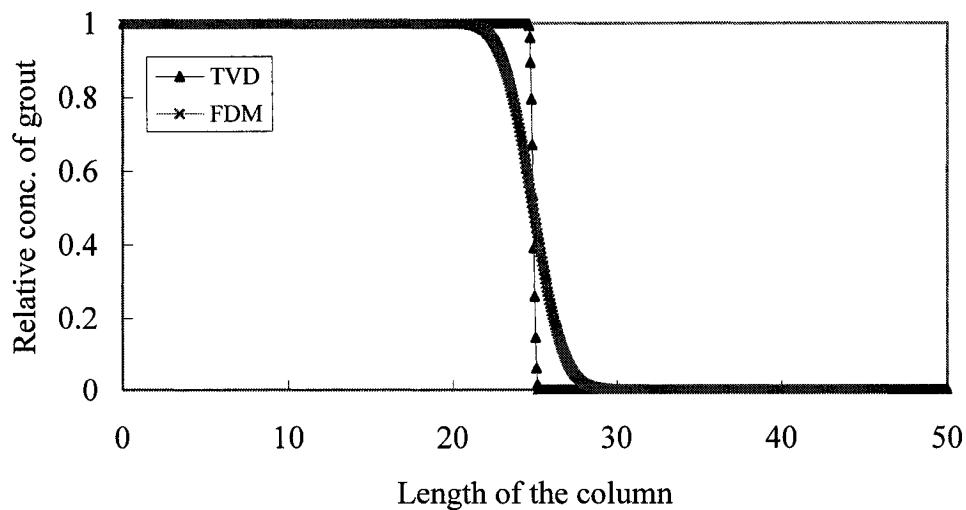erimental and/or field data. Sometimes, the model results are validated against the results obtained from other established numerical models. The present model was used to simulate the injection of sodium silicate grout solution into a vertical column as a one-dimensional problem of Honma (1984). The present model's capabilities in reproducing the modeling results obtained by Honma (1984) are demonstrated in this section.

Honma (1984) developed the grout model by solving groundwater flow and mass transport equations by employing a standard Galerkin scheme. An upstream weighted residual method was adopted to minimize the oscillations in the transport equation solution. Honma considered a 2.0 m long vertical straight pipe having a diameter of 0.1 m. This vertical pipe was discretized into grids of 0.05 m. The soil and grout properties given by Honma are presented in the Table 4.1. The grid size, soil and grout properties used in the current investigation were the same as the ones used by Honma (1984). The time step for the flow update had been set to 1.8 seconds and the transport step was determined by the criterion given by Equation (4.13). This criterion ensures the Peclet number to be less than or equal to 1.0.

The grout was injected at a pressure head of 10.34 m from the bottom and the top end was maintained at atmospheric pressure. The concentration profiles obtained from the present model and Honma's model are plotted in Figure 4.7. The sodium silicate grout concentration distributions obtained by the present model match fairly well with the ones obtained by Honma. The concentration front obtained by the present model is slightly ahead of Honma's concentration profiles for early times. The difference between the locations of the grout front obtained by Honma's model and the present model is only about 5 %. This is probably due to the effect of considering density variations in Honma's model and not considering it in the present model. The difference between the

97
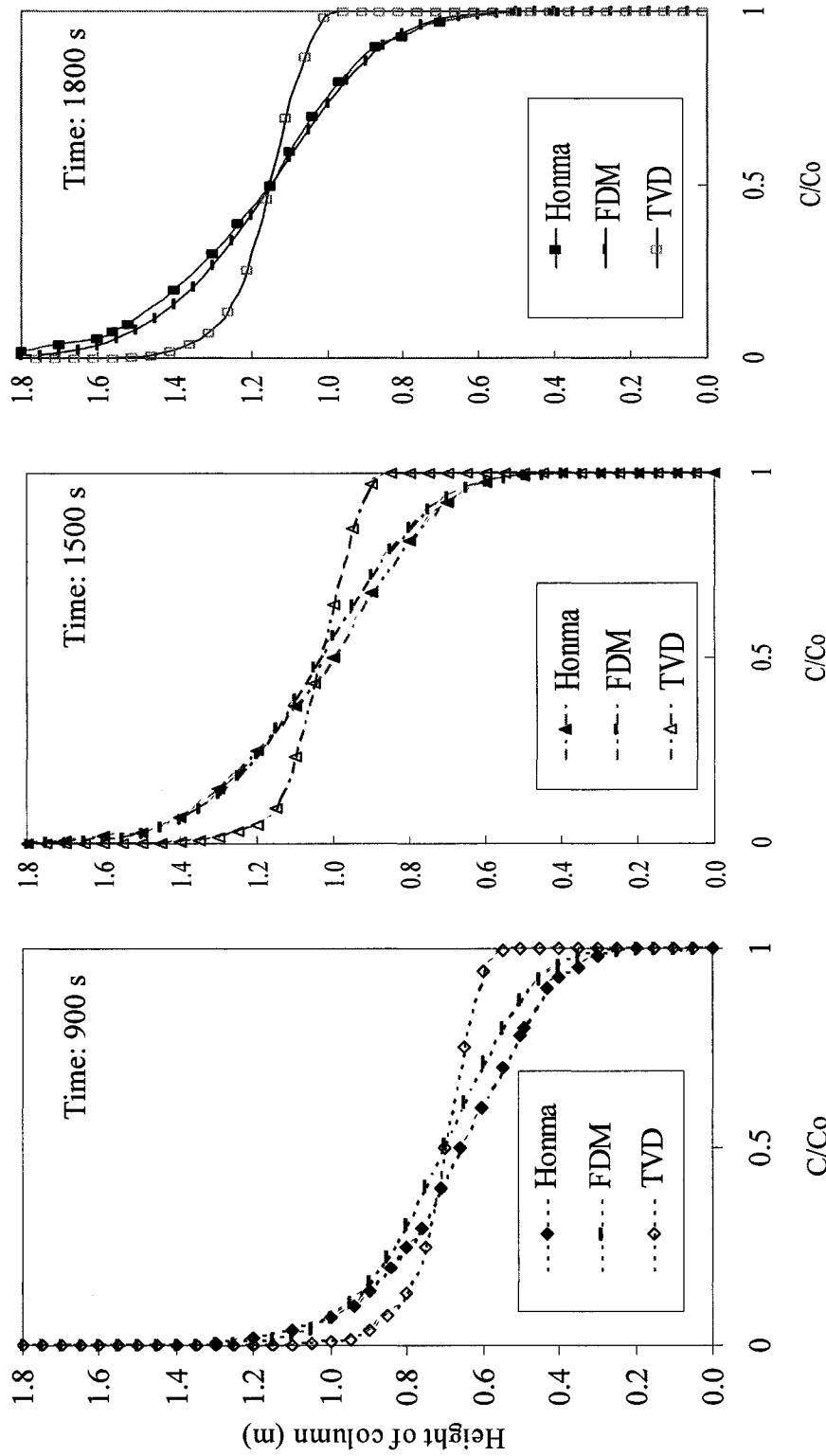
Figure 4.7: Comparison of grout concentration distributions at different times (in seconds) for one-dimensional column obtained by Honma and the present model using constant pressure head injection of sodium silicate grout

98

locations of grout front obtained from these two models vanished as the simulation time increases. This is because the viscosity plays a dominant role in the pressure head loss, as the gelation progresses. The concentration profiles obtained using upstream finite difference (FDM) option in the present model more closely match the concentration profiles obtained by Honma. However, the concentration profiles reported by Honma as well as the ones obtained using upstream finite difference option in the present model are more dispersed than the TVD solution obtained from the present model, which indicated that TVD may be used to obtain solutions having relatively low numerical dispersion. This provides a higher confidence in the ability of the present model to reproduce published results. It may be noted that the groundwater flow equations are solved using FDM method, regardless of whether FDM or TVD scheme was used for solving transport equations of RT3D.

Table 4.1: Soil and grout properties used in the analysis (Honma, 1984)

	Property	Symbol	Value	Unit
	Porosity	ϕ	$= 0.30$	---
Soil	Compressibility	α	$= 1 \times 10^{-5}$	m^2/kN
(fine sand)	Saturated Hydraulic Conductivity	K_z	$= 1 \times 10^{-5}$	m/sec
	Longitudinal Dispersivity	D_L	$= 0.001$	m
	Mass Density	ρ_s	$= 1950$	kg/m^3
	Grout Viscosity equation (ratio of grout viscosity to water viscosity)	μ_r	$= 2.27\left(1 + 2.2 \times 10^{-4} t\right)\left[exp\left\{\dfrac{0.293t}{2220 - t}\right\}\right]$	
Grout	Relative Density	ρ_r	$= 1.1$	
	Compressibility	β	$= 4.4 \times 10^{-7}$	m^2/kN
	Molecular Diffusion Coefficient	D_d	$= 2 \times 10^{-10}$	m^2/sec

99

4.11 EFFECT OF SHEAR

Shear was known to retard gelation either due to breaking of networks of particles (Carvalho and Djabourov, 1997) or due to compression of micro-gels or macromolecules of grout (Hanley *et al.*, 1999). One-dimensional column simulations were performed on the model described in section 4.10 to better understand the shear effect on apparent viscosity and the resulting pressure heads. Pressure distribution profiles inside the column at different times are plotted in Figure 4.8 for both cases, *i.e.*, (i) when the shear effect was included in the gelation model and (ii) when it was not included. From these profiles it is seen that when the shear was incorporated in the gelation model, the required injection pressure heads or pressure drops are significantly smaller than those obtained using a gelation model without shear.
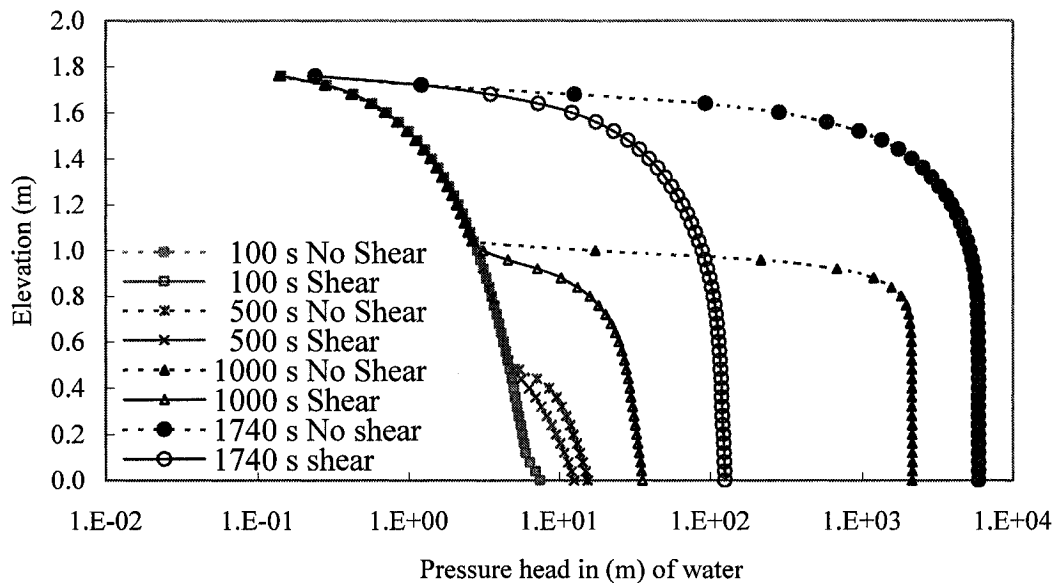
Figure 4.8: Pressure head profiles inside the column simulated as one-dimensional model

When the shear is incorporated, the viscosity of the grout is less than the viscosity obtained from a no shear gelation model. This reduction in gel viscosity resulted in lower pressure head drop. For time 100 s, the pressure profiles for both shear and no shear cases coincide because the grout gel viscosity was not yet significantly affected by shear at this time. However, for later times when the difference between shear and no shear gelation

100

viscosities were large, the difference between the shear and no shear pressure profiles increased with time. The pressure profiles in the ungrouted region, *i.e.,* downstream of the grout front or upper part of the column, fall on the same curve. Also, regardless of which gelation model was adopted, the pressure head at the grout front and beyond, at any instant of time, was the same for both the cases. These two were simple cross checks for (i) numerical performance of the model and (ii) representation of the physics on shear gelation. This does not mean that the present shear gelation model was an exact representation of the actual behaviour of grout in porous media. Assuming the shear and no shear gelation models were correct, the present model was able to simulate the grout injection into the column as expected.

Another interesting observation worth mentioning is that the maximum pressure head drop occurred near the grout front for the later times. These larger pressure drops near the grout front are reflected by the near horizontal pressure profiles near the grout front. This is because the grout at the front was the oldest and had the highest viscosity, which resulted in larger pressure head drop. This zone near the grout front with maximum viscosity determined the resulting maximum pressure drop. This is an example of how the model is behaving in an expected manner.

4.12 EFFECT OF MINIMUM GROUT CONCENTRATION

The present model implemented a grout aging function that incorporated the minimum concentration concept. As per the expression proposed in Equation (4.6), the grout cures, *i.e.,* grout ages and hence there will be increase in viscosity, only if the grout concentration is above a specified level. The need for incorporating the grout aging function, Equation (4.6) instead of Equation (4.5), is demonstrated through a test case. The test case was set up using a simulation domain having dimensions 4.2 m x 2.4 m x 1.0 m. Grout was injected in three rows. Two outer rows have three injection wells each and the centre row has two wells. Each of the injection wells on the outer row had three grout injection points. The injection wells on the centre row and the corresponding the injection points were located at the diagonal intersection of the outer row injection points. Thus there were 22 injection points in total. The injection points on the outer rows were

101

located in layers 4, 11 and 18. Grout was injected at each of the injection points for 1800 seconds. The domain was discretised into 0.05 m x 0.05 m x 0.05 m grids. The flow was updated every 2 seconds. Hydraulic conductivity of the porous media was taken as 3.01×10^{-5} m/s. Longitudinal and transverse dispersivities were assigned as 20 mm and 0.2 mm respectively. The grout composition was the same as the one considered in section 3.4. Thus, Equation (3.2) could be used to represent gelation. Two types of simulations were run. In the first case, grout aging was represented by Equation (4.5) and in the later case grout aging was represented by Equation (4.6).

The grout concentration distribution patterns in the domain at different times for both cases are plotted in Figure 4.9. The grout distribution plots obtained when Equation (4.5) was used show that the grout cannot be injected at the second and third wells. However, it was possible to inject grout at the subsequent wells when Equation (4.6) was considered. This was seen from the vertical section plot. The grout bulbs joined together. This was because, as stated in section 4.5, by the time the grout was injected at well 2, water in the porous media will have an age of 1800 seconds, *i.e.,* the time since the simulation began. When Equation (4.5) was used, the grout mixture at well 2 will have an age between 0-1800 seconds. Instead, the age should have been zero as the grout age at the time of injection was zero. In order to prevent aging of water, the minimum grout concentration concept was introduced so that the fluid in the porous media does not age unless there was enough grout for reaction to take place. The concept also helps in preventing spurious gelation of grout at the dispersed grout front.

4.13 ANALYSIS OF SODIUM SILICATE GROUTING

Sodium silicate grout injection into a sand column, used in the experiment of Honma (1984), was analysed through the use of the model to understand the processes. The results of the present grouting model were compared against the experimental observations from a column experiment of sodium silicate grouting by Honma (1984). Honma set up the column experiment as shown in Figure 4.10 using a 165.1mm diameter and 1828.8 mm (72 inches) long plexiglass tube. The tube was filled with 76.2 mm (3 inches) of thick filter gravel, over which fine sand was placed. The bottom 457 mm (18")

102

Layer 4   Layer 4

Layer 11   Layer 11

Layer 18   Layer 18

Vertical Cross-section   Vertical Cross-section
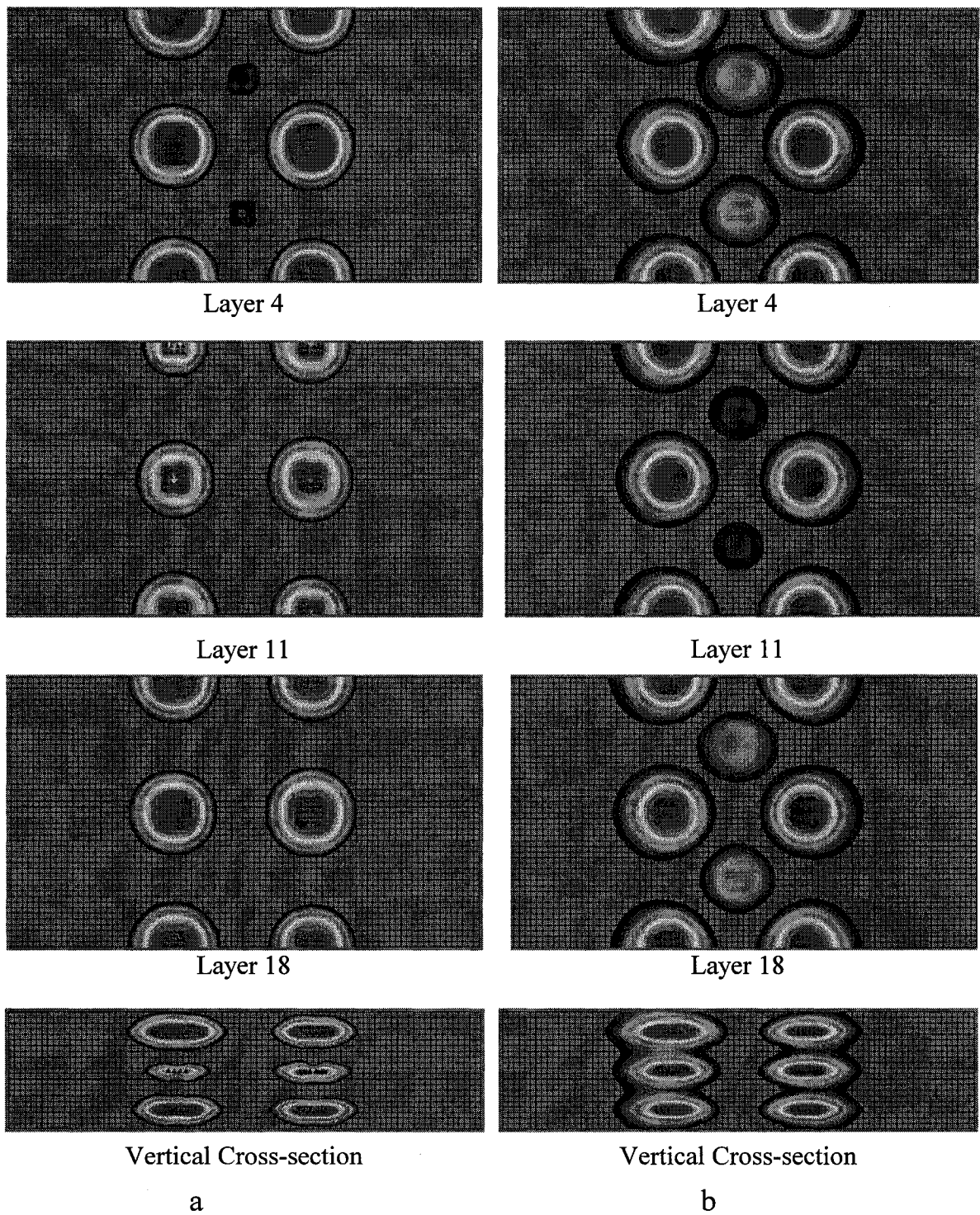
a   b

Figure 4.9: Comparison of grout concentration distribution showing differences when (a) effect of $Xmin$ is not considered and (b) $Xmin$ is considered
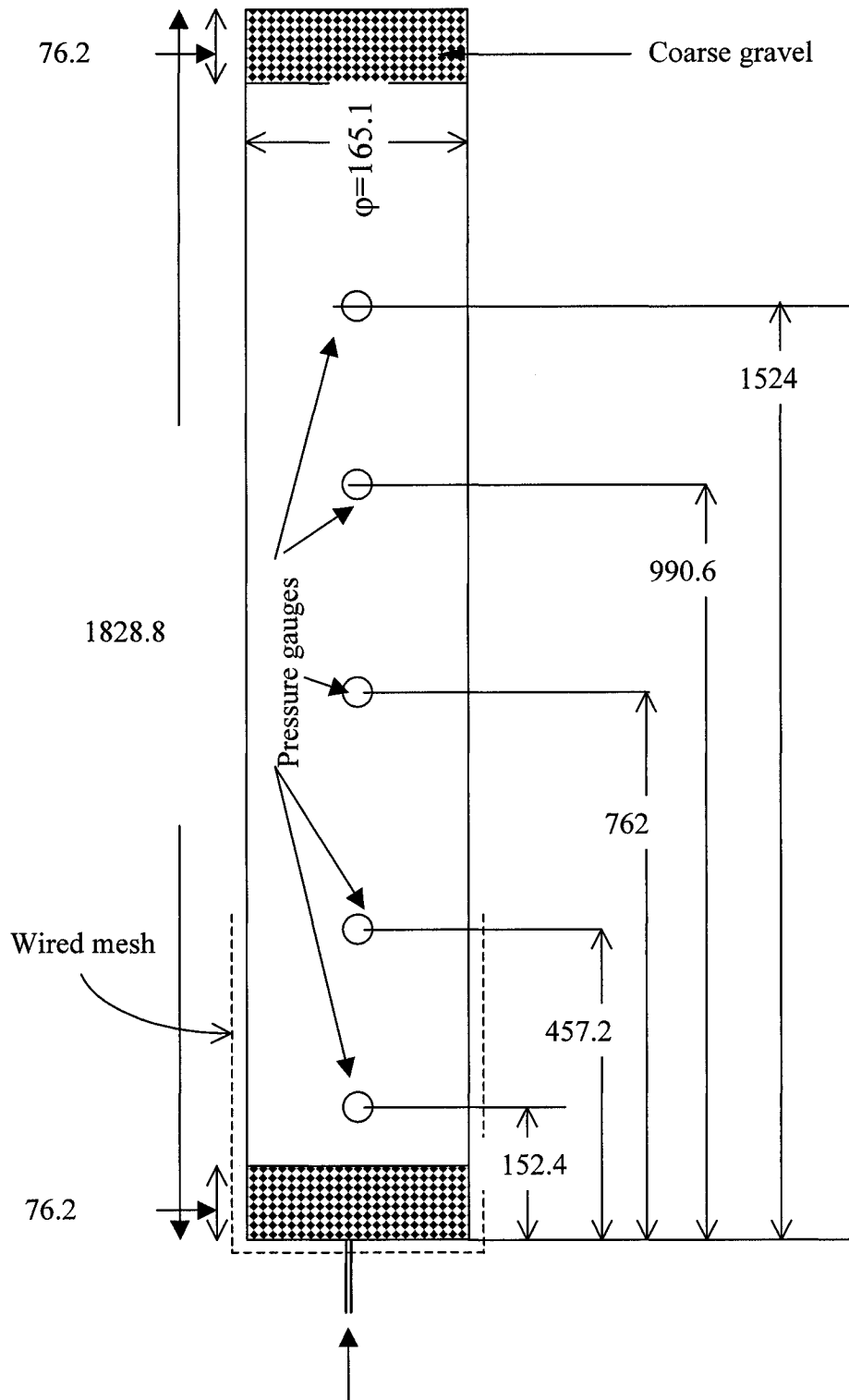
103

Figure 4.10: Schematic diagram of Honma's column experiment (dimensions are in mm)

of the column was reinforced around the circumference with aluminum mesh to withstand the high pressures expected at the injection end. The column was fitted with two pressure gages, 90° to each other, at 152.4 mm (6 inches), 457 mm (18 inches), 762 mm (30 inches), 990.6 mm (39 inches) and 1524 mm (60 inches) from the injection point at the bottom of the column. A 20-30 mesh screen was placed at the interface between the gravel and sand in order to prevent the sand particles from falling into the gravel layer.

Sodium silicate grout having initial viscosity of 15 cP and gel time of 360 seconds was injected from the bottom of the column at a rate of 7.68 x 10^{-6} m^3/s. In this experiment, even though the sodium silicate grout had a gel time of 360 seconds, it was possible to grout for 2580 seconds. Honma reported that this was an indication of delay in grout gelation due to processes such as turbulence. Since the injection pressures obtained from Honma's model, when the time dependent viscosity was used, were too large compared to the ones observed in the experiment, Honma suggested that (i) the time dependent viscosity relation was not applicable, and (ii) that concentration dependent viscosity relation be used.

The same experiment had been simulated using the present model, as a column with a square cross-section of equivalent cross-sectional area instead of circular cross-section of the experimental column. The column was discretised into 1000 grids, resulting in a grid size of 1.8 mm. Based on Honma's recommendation, the time dependent viscosity was turned off in simulating this experiment. Only concentration based viscosity was considered. The sodium silicate grout injection was simulated until 1740 seconds. The flow field was updated every 17.4 seconds. Transport step was automatically adjusted by the RT3D, based on the criteria given by Equation (4.13).

The pressures required to inject the grout at a constant flow rate of 7.68 x 10^{-6} m^3/s at different times are plotted in Figure 4.11. The experimentally observed pressures of Honma (1984) are also superimposed on the same figure. The numerical profiles matched the experimental values fairly well for times 420, 1440 and 1740seconds. The differences

105

are larger for the intermediate times. The model over-predicted the pressure heads by 8-50 % of the observed pressure heads at the bottom most pressure gage reading. Neither Honma's model nor the present model could predict the pressure profiles that match the experimental observations using concentration-only dependent viscosity relationships. This is an indication of inadequate representation of the gelation process. The processes such as shear thinning involved in the grouting were not included in the Honma model. Thus the numerical model over-predicted the pressures in the grouted region for the intermediate times. Honma (1984) considered a linear mixing rule for the grout concentration at the grout front. This could be one of the reasons for over-prediction of the viscosity and hence higher heads. One should also note that the experimental column was simulated as a one-dimensional model. As a result, viscous fingering was not observed. Hence the column experiments and slim tube experiment, performed as part of this study described in the Chapter 3, were simulated to understand the physics and to investigate the effect of variation in flow and transport parameters.
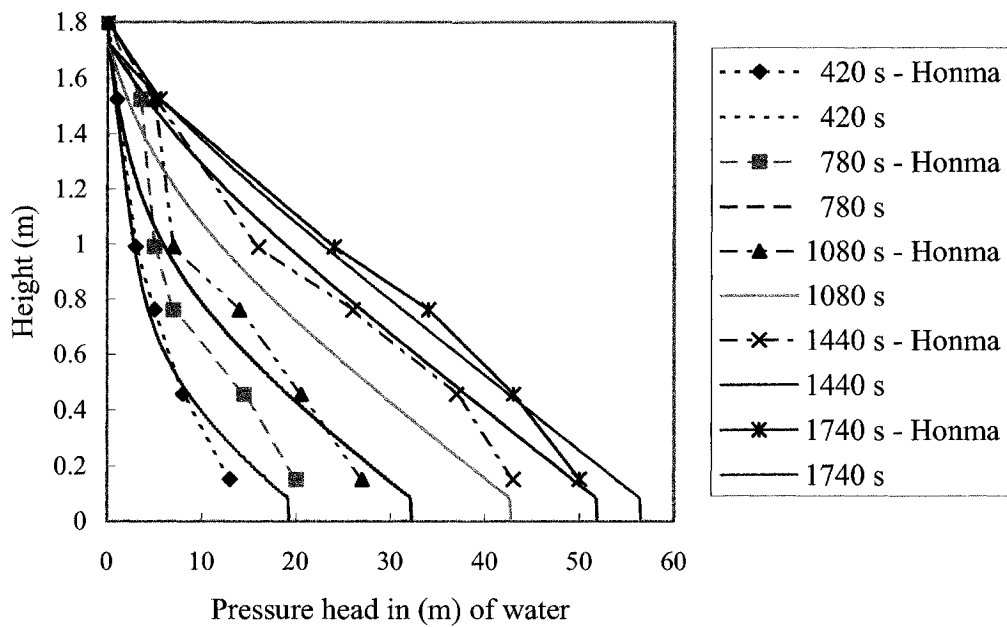

Figure 4.11: Comparison of injection pressure distribution at different times for sodium silicate grouting obtained from present model and Honma's column experiment

106

4.14 SLIM TUBE EXPERIMENT SIMULATION

The slim tube experiment described in section 3.6 was simulated as a one-dimensional square column of length 400 mm having cross-sectional area of 6.5 mm x 6.5 mm and 400 mm long. The column was discretised into a 3.25 mm grid along the length in the vertical direction. Colloidal silica grout was injected into the column from the bottom end at a rate of 0.58 ml/min (calculated to match the cross-sectional area). Grout gelation relationship incorporated in the model corresponds to gel mixture having gel time of 600 seconds. Flow field was updated every two seconds and transport step was adapted based on the lowest time step determined by the criteria given by Equation (4.13). Injection pressure heads determined from the simulation along with experimental data are plotted in Figure 4.12. The pressure heads based on no shear gelation model are at least 10 times the observed peak pressures. Whereas, the pressure profiles obtained using shear gelation model fall in the same range of pressures obtained in the experiment. From the experiment, it may be noted that it was possible to inject the grout until 1770 seconds even though the grout gelation time was 600 seconds. These two facts indicate that there was a delay in gelation. This delay in grout gelation was due to the effect of shear during its gelation. Therefore, shear needs to be incorporated.

In an effort to identify the parameters that represent the pressure profile, the effect of longitudinal dispersivity (α_L) was investigated. With increasing longitudinal dispersivity, the required grout injection pressures are found to be reducing. Various α_L's investigated include 1 mm, 20 mm, 30 mm and 40 mm. The pressure heads corresponding to $\alpha_L = 1$ mm are higher than the observed ones indicating that the viscosities are over-predicted. The pressure profiles corresponding to $\alpha_L = 20$ mm, 30 mm and 40 mm fell in the range of the experimental observations. For the case of $\alpha_L = 20$ mm, the pressure heads are over-predicted during 1000-1500 seconds and are under-predicted from then on. However, the profiles corresponding to $\alpha_L = 30$mm and 40 mm closely follow the observed pressure curve until about 1400 seconds and the pressures are under-predicted beyond 1400 seconds.

107
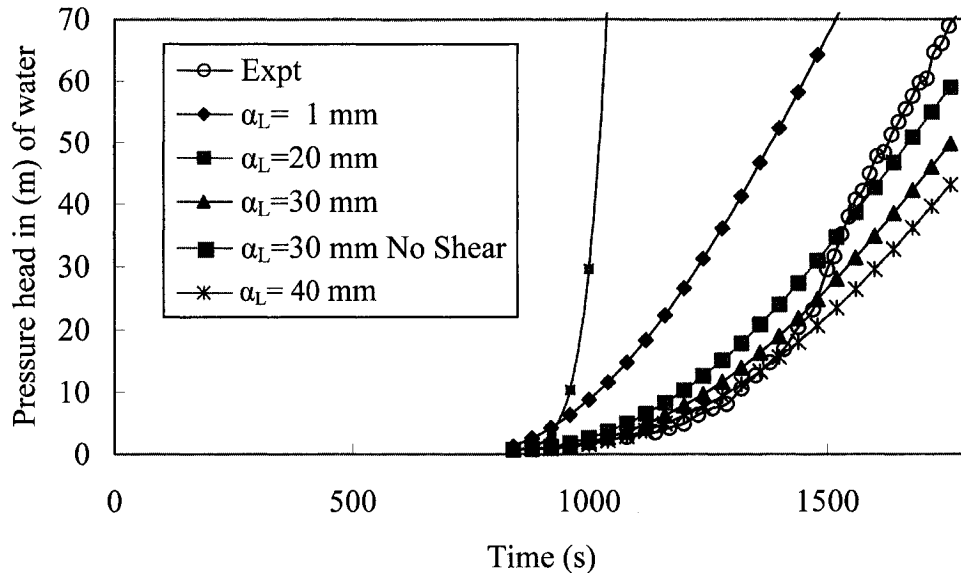
Figure 4.12: Comparison of injection pressure heads obtained from the model against slim tube experimental observations. The plot shows the pressure profiles for shear and no shear based gelation model.

4.15 ANALYSIS OF COLLOIDAL SILICA GROUTING - ONE-DIMENSIONAL MODELING

The colloidal silica grout injection into the sand column was simulated as a one-dimensional model. From the slim tube simulations, the shear and longitudinal dispersivity were found to affect the grout injection. Hence, further investigations were carried out to compare the numerical model results with the experimental observations for various longitudinal dispersivities. Though the one-dimensional simulations do not represent the physics completely, they are useful in gaining a rough idea of the relative importance of the parameters and processes. The column was simulated as a one-dimensional domain with a square cross-section having an area equal to the cross-sectional area of the 30.16 mm diameter column and length of 450 mm. The column was divided into 450 grids along the length. The colloidal silica grout was injected from the bottom end at a flow rate equal to 2 ml/min. The equivalent Darcy velocity was 4.67 x 10^{-5} m/s. The flow field was updated every second. The model outputs include injection pressure heads, grout age and grout concentration distributions.

108

The pressure heads required to inject the colloidal silica grout into the sand column for each case are plotted in Figure 4.13. The effect of shear was also investigated. The pressure head profiles in Figure 4.13 may be grouped into two categories, *viz.*, linear and power law mixing model based results. When the linear mixing rule was employed, the pressure head profiles deviate from the experimental curve beyond 1000 seconds. Variation in longitudinal dispersivity seems to make no difference to the pressure profile. The pressure head profiles corresponding to power law mixing rule fall in the range of experimentally observed pressure heads and follow the experimental pressure profiles more closely. This shows that the linear mixing rule over-predicted the viscosity of the grout mixture solution diluted in water in the pores. Since the variation in longitudinal dispersivity did not change pressure head profiles significantly, linear mixing rule was the dominating factor. Hence, it may be concluded that linear mixing rule did not represent colloidal silica grouting into the porous media, *i.e.*, the power law better represents colloidal silica grout mixing during gelation in porous media.

The effect of longitudinal dispersivity (α_L) was investigated through one-dimensional simulation for different α_L's, *i.e.*, $\alpha_L = 1$ mm, 10 mm, 20 mm and 40 mm. The pressure profiles corresponding to the $\alpha_L = 10$ mm, 20 mm and 40 mm are approximately parallel to each other. With the increase in longitudinal dispersivity, the predicted pressure heads are decreased. The pressures heads are higher and lower than the experimentally observed pressures in case of $\alpha_L = 10$ mm and 40 mm respectively. The injected pressure head profile corresponding to $\alpha_L = 20$ mm closely follows the experimental profile up to 3200 seconds and deviated from the experimental profile significantly from then on. For lower α_L's, the grout front is less dispersed resulting in higher concentrations and higher viscosities. The physics may be better described with α_L equal to 20 mm for times until 3200 seconds.

The injection pressure heads obtained by considering no shear based gelation model are compared to the heads obtained by using a shear based gelation model as shown in Figure 4.14. The effect of shear on grout injection was also investigated. The pressure heads obtained by using the gelation model without shear effect are several orders larger than

109

Figure 4.13: Grout injection pressure head profiles for different conditions in one-dimensional simulation. Grout is injected at 2.0 ml/min. (P and L refer to power-law and linear mixing rules.)
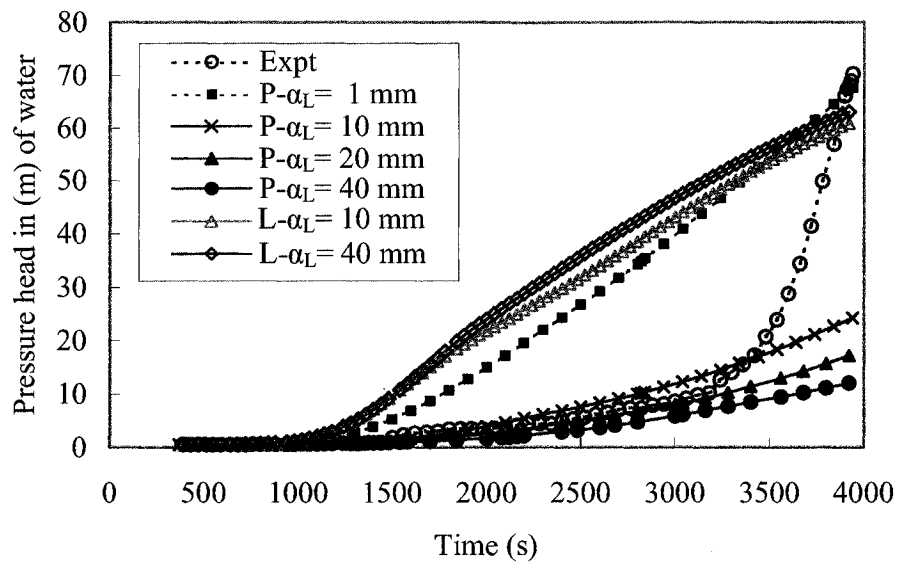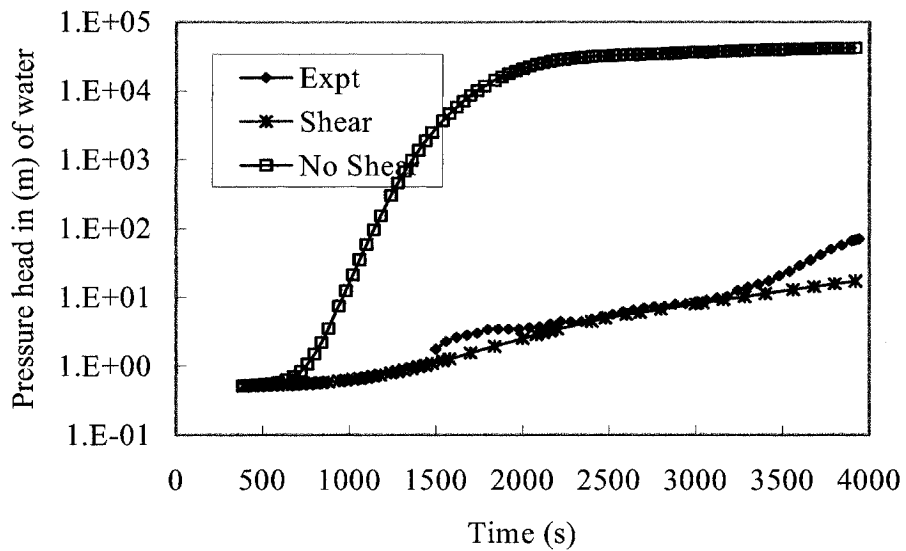

Figure 4.14: Effect of shear on grout injection pressure head from one-dimensional simulations

110

the experimental observations. The pressure heads obtained using gelation model with shear effect incorporated are in the same order of experimental observations. Hence it may be concluded that the shear effect is important. The deviations indicate that the processes included in the present grouting model are not enough to properly describe the grouting physics beyond 3200 seconds. Similar phenomenon was also observed in the slim tube experiment. To understand the reasons for the discrepancies between the observed and simulated pressure heads beyond 3200 seconds and to identify the processes that are important in the grout injection into the porous media, three-dimensional simulations were performed.

4.16   ANALYSIS OF COLLOIDAL SILICA GROUTING – THREE-DIMENSIONAL MODELING

A numerical model was set up to simulate grout injection into the fine sand column, investigated experimentally in section 3.5, by representing the column in a three dimensional domain. Since one-dimensional modeling cannot reflect the effect of fingers observed in the experimental study, it is believed that flow and transport was three-dimensional, though the predominant flow direction is one-dimensional. As noted by Smith and Zhang (2001), when the finger size is smaller than the column size, the flow and transport within the column needs to be simulated as a three-dimensional model.

From preliminary simulations it was found that a very fine grid resolution is needed to capture the physics in terms of grout distribution in the column. Due to limitations on the computer resources availability, smaller cross-sectional area is chosen in an effort to adopt the finer grid resolution. Hence, the cross-sectional area of the simulation domain was reduced to 20 mm x 20 mm as against 30.16 mm diameter of the experimental column. The length was taken as 450 mm (which is the height of sand in the experimental column). Grout injection rate was scaled according to the cross-sectional area ratio such that Darcy velocity in the numerical column model was the same as in the experimental column. It is necessary to maintain the same velocity in order to create the same shear rate, which in turn keeps the similarity in gelation characteristics. Therefore, the grout injection rate for numerical modeling is calculated as 1.12 ml/min instead of 2 ml/min

111

adopted in the experiment. Thus, the Darcy velocity is equal to 4.67×10^{-5} m/s, which is equal to the Darcy velocity corresponding to the flow rate used in the column experiment in section 3.5.

Three dimensional numerical modeling simulations were performed to identify different processes and parameters that represent the flow and transport of gelling colloidal silica grout inside the sand column. These simulations include effects of grid resolution, heterogeneity in hydraulic conductivity field, longitudinal and transverse dispersivities. The simulations were carried out using heterogeneous hydraulic conductivity fields with mean hydraulic conductivity of 3.01×10^{-5} m/s and log hydraulic conductivity variability of 0.05. However, homogeneous hydraulic conductivity fields were used for some of the grid resolution studies. The longitudinal and transverse dispersivities assigned were 1 mm and 0.01 mm respectively. These values are changed in the following sections where the effects of each of these parameters are studied.

4.16.1 Grid Resolution Studies

Numerical models simulate the continuous physical system as a discretised system. The discretisation of the domain may have a significant effect on the results (Roache, 1994). Prior to performing any further analysis, the dependence of grout injection process simulation on grid resolution is investigated in this section. Recognising the importance of grid size, Oldenburg and Pruess (1995) and Ackerer *et al.* (1999) have investigated the grid resolution effects on the solution of a density dependent problem and recommended the procedure of refining the grid until there is no difference in the results. Three grid resolutions were used in this study. The 20 mm x 450 mm x 20 mm domain was discretised into 8 x 90 x 8, 15 x 169 x 15 and 20 x 225 x 20 grids. These grids correspond to cell sizes of 2.5 mm x 5 mm x 2.5 mm, 1.33 mm x 2.67 mm x 1.33 mm and 1 mm x 2 mm x 1 mm respectively. For convenience, these grids are referred to as 8 grid, 15 grid and 20 grid, respectively. Simulations were performed on these three grid resolutions using both homogeneous and heterogeneous hydraulic conductivity fields. The details on generation of heterogeneous hydraulic conductivity fields are presented in section 4.16.2. During the first set of simulations on different grid resolutions, hydraulic conductivity

112

field was assumed to be homogeneous in order to obviate any uncertainty that might result from the use of heterogeneous hydraulic conductivity fields. The second set of simulations were performed using heterogeneous fields.

(i) Pressure heads

The simulation results for the three grid resolutions are presented in terms of pressure heads at the injection end of the column and grout age distribution in the column. The pressure heads required to inject colloidal silica grout into the column for each of the grid resolutions are plotted in Figure 4.15a. These simulations using homogeneous hydraulic conductivity fields showed instability around 1800 seconds for all the grid sizes. Even though the pressure profiles stabilized after 2000 seconds, they did not show any specific trend. These simulations using homogeneous hydraulic conductivity fields did not yield any conclusive results. However these injection pressure head profiles showed that simulation of the grout injection process using homogeneous field is not the appropriate way. Hence simulations are also performed using the same grid sizes considering the heterogeneous hydraulic conductivity fields. The pressure profiles obtained for these three grid resolution simulations, using the heterogeneous hydraulic conductivity fields, are plotted in Figure 4.15b. Contrary to our understanding about numerical simulations, the simulations that use finer grid sizes further under-predict the injection pressure heads. The pressure head profiles from all the three grid resolutions follow the experimental observations until about 1800 seconds and deviate from each other after 1800 seconds. None of the grid resolutions could yield the observed pressure heads beyond 3200 seconds. The pressure profile from 8 grid simulation falls on the experimental profile up to 3200 seconds. The difference between the observed and numerical pressure heads increases exponentially beyond 3200 seconds. Since the pressure profiles from coarse grid are close to the finer grid solutions, grout concentration and age distribution patterns corresponding to these simulations are investigated to understand the physics.
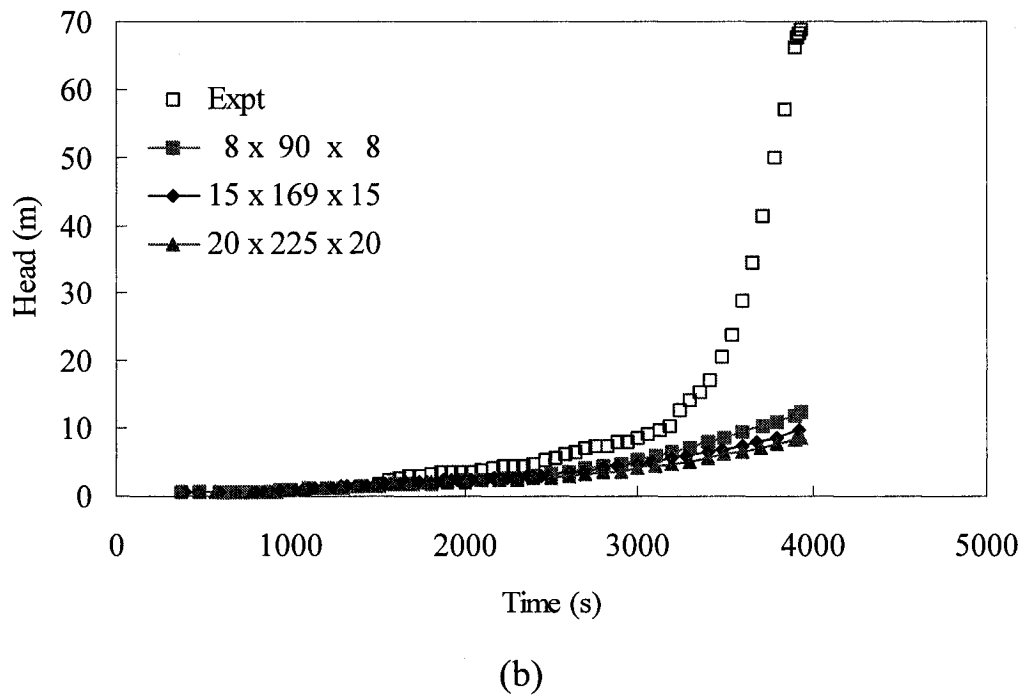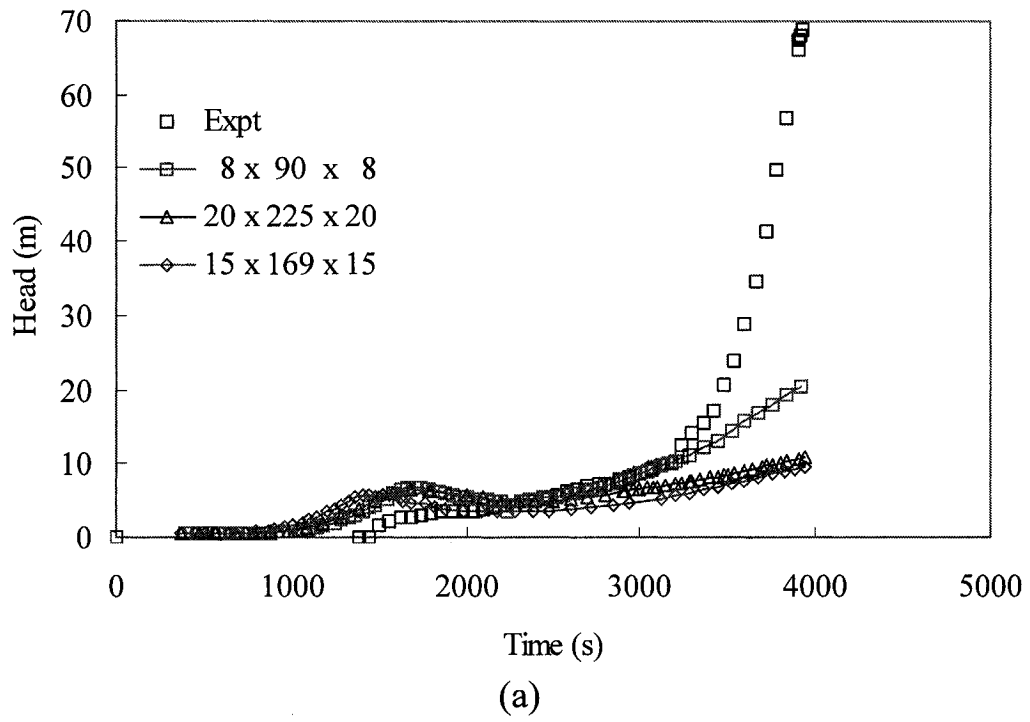
113

Figure 4.15: Effect of grid resolution on grout injection pressures using (a) homogeneous (b) heterogeneous hydraulic conductivity fields.

114

(ii) Concentration Distribution

The grout age and the concentration distributions are also investigated for the three grid sizes. Even though the grout flow is locally three-dimensional, the predominant flow direction is one-dimensional. Therefore the grout concentration is likely to be uniform. When the younger grout (having lower viscosity) displaces the older grout solution (having higher viscosity), instabilities occur. The instabilities as reflected by grout age distribution patterns are likely to reveal the physics of grouting. The grout age distribution patterns inside the column are plotted in Figure 4.16. Since the grout gelation time is 600 seconds, the grout injectivity depends on the size of the finger having grout ages less than or equal to the gel time. Hence the distribution patterns of grout with an age of 600 seconds and less are plotted in this figure. It may be noted that the finger size is reduced as the grid size increases. Increase in grid size leads to higher dispersion, which helps in forming more homogeneous grout mixture, leading to formation of thin fingers. Higher pressure heads are needed to inject the grout at the same flow rate through a constricted finger. The fingers formed in the 15 and 20 grid simulations yielded larger size fingers. These large fingers formed in the 15 and 20 grid simulations resulted in lower injection pressure heads compared to those obtained in the 8 grid simulation. If the finger formed in the 8 grid simulations had been correct, the pattern of fingers obtained from the 20 grid simulation would have been the same. Since fingers obtained from the finer grid are larger than the coarser grid, the coarse grid, *i.e.,* 8 grid discretisation, is not adequate to capture the physics of grouting. Hence, the remaining simulations are run using the 20 x 225 x 20 grid system in order to capture the fingers as accurately as possible.

4.16.2 Effect of Heterogeneity

Hydraulic conductivity (K) is a very important property in analyzing the flow and transport of contaminants through porous media. Hence, the effect of hydraulic conductivity on the grout injection process was investigated in terms of the pressure head profiles. Since it may not be possible to characterize the porous media to the detailed extent required for the modeling, recourse has been made to simulate flow and transport using simulated hydraulic conductivity fields having similar statistical characteristics.
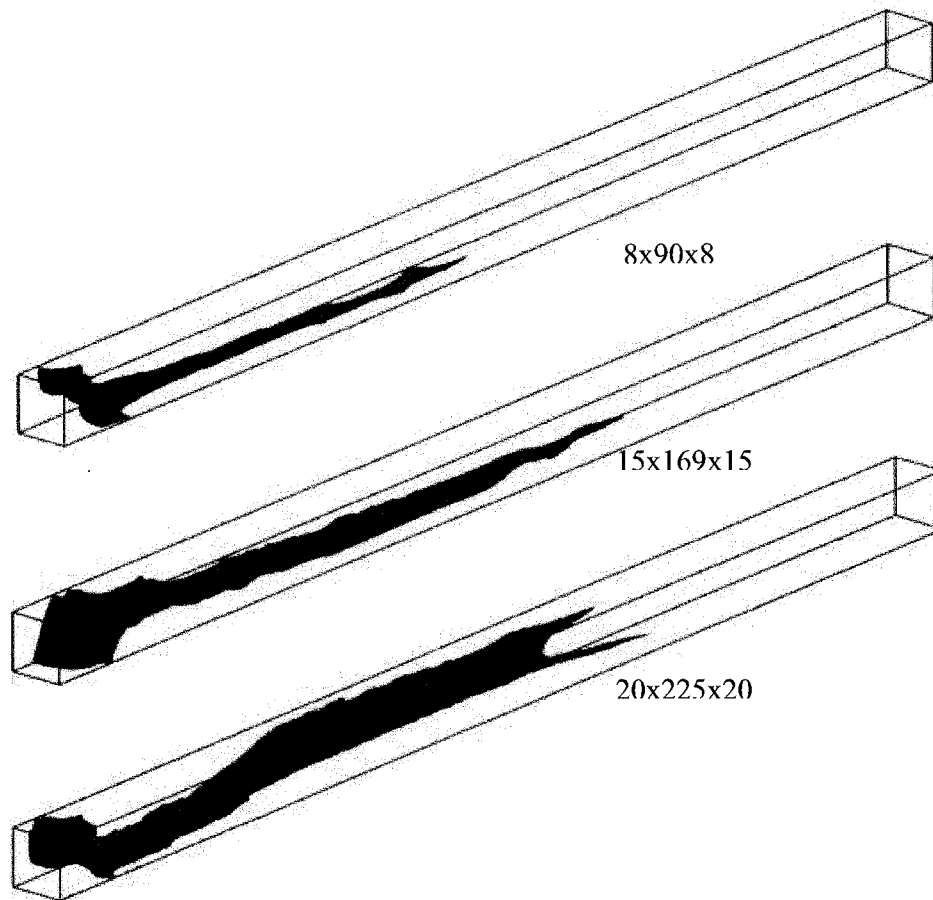
115

8x90x8

15x169x15

20x225x20

Figure 4.16: Effect of grid size on grout age distribution and finger
formation. The figure shows the finger formed by the areas
where the grout age is 600 seconds or less

116

The hydraulic conductivity field of the sand in the experimental column was assumed to be one of the several possible random scenarios, called realizations, for a given mean and variability. The hydraulic conductivity distribution in the simulation domain of sand column was generated using Sequential Gaussian Simulation (SGSim) algorithm for a given mean K and different variabilities. SGSim algorithm used in this study is part of the GSLIB suite of programs (Deutsch and Journel, 1998). SGSim generates the normal variates between 0.0 and 1.0. The range of K is specified in terms of mean hydraulic conductivity and variability. Commonly, based on field observations, K is considered to follow a log-normal distribution. The variates from SGSim are normalized values of log (K) field. These normal variates are transformed to linear scale to obtain the K distribution for a given mean and variability. A typical data set used for the present study is given in Table 4.2. The inputs specified in Table 4.2 include number of grids in each of the x, y and z directions, spatial correlation, upper and lower bounds on the numbers to be generated. Spatial correlation can be expressed in terms of exponential, spherical, Gaussian or power variograms. The spatial correlation is represented in this study in terms of exponential variogram for the K-field (Woodbury and Sudicky, 1991). The K of 3.01×10^{-5} m/s obtained from the experiments described in section 3.2 is assigned as mean K. Different variabilities considered include 0.0, 0.01, 0.05 and 0.2. A variability of zero means the medium is homogeneous. A K distribution corresponding to variability of 0.05 is shown in Figure 4.17.

The required injection pressure head profiles for different variabilities are plotted in Figure 4.18. The pressure head profiles corresponding to all the variabilities, except for the homogeneous case, follow a monotonically increasing trend. The pressure head profile obtained from the homogeneous K-field increased up to about 1700 seconds and then reduced to the levels corresponding to pressure profiles obtained from heterogeneous K-field cases. This means that the column with homogeneous K-field behaves like a 1-D column until 1700 seconds. As a result, the required injection pressure heads are governed by the highest viscosity of the grout, which is 2 to 3 times larger than the apparent viscosity as reflected from the observed pressure heads. When the differences in grout ages are large, the instabilities are triggered leading to formation of

117

viscous fingers. Thus, these formed viscous fingers make the medium behave like a heterogeneous one.

Table 4.2: Parameters used in Sequential Gaussian Simulation

```
*****************************************************
* File generated by WinGslib
* Version:      1.3.1
* Build code:   332a316/1/2_4_1381
* Date:         Wednesday, March 24, 2004
* Time:         9:38:33 PM
*****************************************************
            Parameters for SGSIM
            ***********************
START OF PARAMETERS:
c:\tempinter\20x225x20\20x225x20cluster.dat
1 2 0 3 0 0                      - columns for X,Y,Z,vr,wt,sec.var.
-100000000 100000000             -trimming limits
0                                -transform the data (0=no, 1=yes)
c:\tempinter\20x225x20\sgsim.trn
0                                - consider ref. dist (0=no, 1=yes)
c:\tempinter\20x225x20\histsmth.out
1 2                              - columns for vr and wt
0 8                              - zmin,zmax (tail extrapolation)
1 0                              -lower tail option
1 8                              -upper tail option
2                                -debug level (0-3)
c:\tempinter\20x225x20\SGS_20x225x20cluster.dbg
c:\tempinter\20x225x20\SGS_20x225x20cluster.out
1                                -number of realizations to generate
20 0 1                           -nx, xmin, xsize  ⎫
225 0 1                          -ny, ymin, ysize  ⎬ Grid Configuration
20 0 1                           -nz, zmin, zsize  ⎭
1440742                          -random number seed
0 8                              -Min and max original data for sim
12                               -number of simulated nodes to use
1                                -assign data to nodes (0=no, 1=yes)
1 3                              -multiple grid search (0=no, 1=yes), num
0                                -maximum data per octant (0=not used)
10 10 10                         -maximum search radii (hmax, hmin, vert)
0 0 0                            -angles for search ellipsoid
20 225 20                        -size of covariance lookup table
0 0 1                            -kType: 0=SK,1=OK,2=LVM,3=EXDR,4=COLC
c:\tempinter\20x225x20\ydata.dat
1                                - column
2 0.05                           -nst, nugget           ⎫
2 0.70 0 0 0                     -it, cc, ang1, ang2, ang3  ⎫
10 10 10                         -a_hmax, a_hmin, a_vert  ⎬ Spatial Correlation
2 0.25 0 0 0                     -it, cc, ang1, ang2, ang3  ⎭ Structure
2 2 2                            -a_hmax, a_hmin, a_vert  ⎭
```
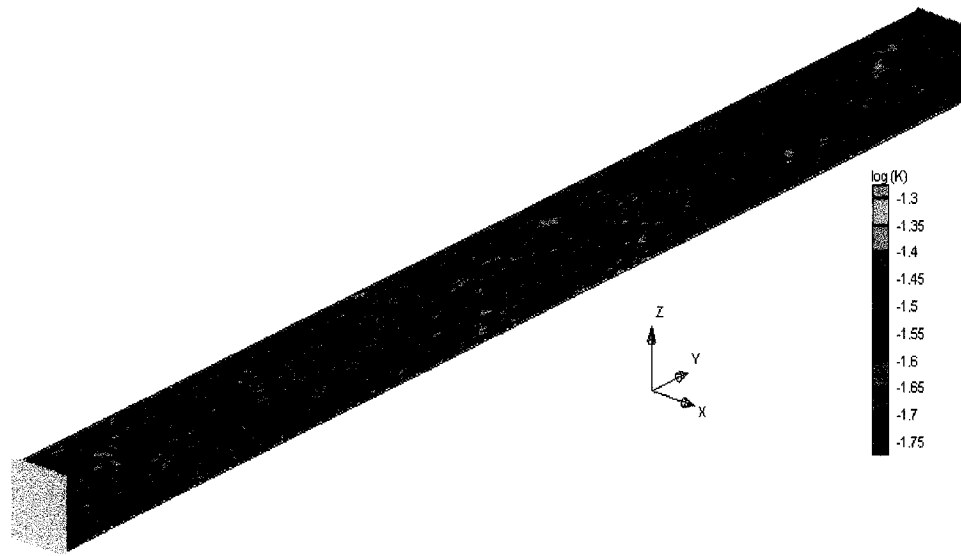
118

Figure 4.17: Hydraulic conductivity distribution generated using SGSim algorithm
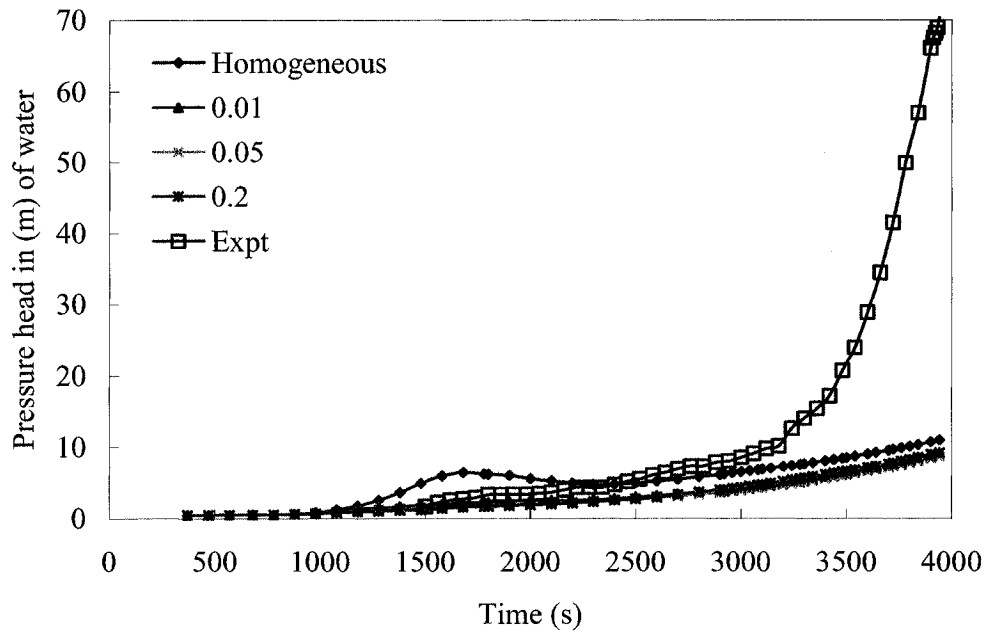(Log scale; variability = 0.05)

Figure 4.18: Effect of variability on the grout injection pressures

119

The distribution corresponding to a variability of 0.01 leads to minor oscillations in the pressure profile. Although the oscillations were not very clear in three-dimensional simulations, they were significant in the two-dimensional simulations. The smallest variability above which the pressure head profiles are stable is identified as 0.05. Hence all the simulations are performed using K-field with a variability of 0.05. Thus, one needs to be careful when deriving inferences using homogeneous K-field simulations. Increase in variability did not show any improvement in the prediction of pressure heads. Hence two conclusions are drawn based on the simulations. Simulation of the grout injection process using a homogeneous K-field lead to oscillations in pressure head profiles. The instabilities subsided after a certain level of heterogeneity is introduced. Therefore, while simulating the grout injection processes, heterogeneous K-fields may be considered even if the soil seems to be homogeneous. Secondly, the heterogeneity beyond certain minimum level did not show any effect on the predicted pressure head profiles.

Often it is necessary to perform simulations using more than one hydraulic conductivity field while working with statistically generated hydraulic conductivity fields. Therefore grout injection simulations were performed using hydraulic conductivity fields obtained from 10 different realizations. The pressure head profiles obtained from these simulations are plotted in Figure 4.19. Of the ten profiles, all of them are in the same range except one. The final pressure obtained for the simulation profile that deviated from the other grout injection profiles is about 50 % higher than the mean pressure heads obtained from the remaining nine realizations. This shows the consistency in the results obtained from different realizations having same statistics. The narrow spread of these pressure profiles reflects the reliability of the predicted profiles.

4.16.3 Effect of Longitudinal Dispersivity (α_L)

Dispersion is known to affect the way instabilities are generated and viscous fingers are formed. Effect of longitudinal dispersivity is investigated in this section to understand the grout injection process and the grout distribution inside the column. Longitudinal dispersion describes the grout mixing at the front along the mean flow direction.

Pressure head in (m) of water

70
60
50
40
30
20
10
0

—♦—R1	—■—R2
R3	R4
—✱—R5	—●—R6
+ R7	R8
—♦—R9	—+—R10

0   1000   2000   3000   4000   5000

Time (s)
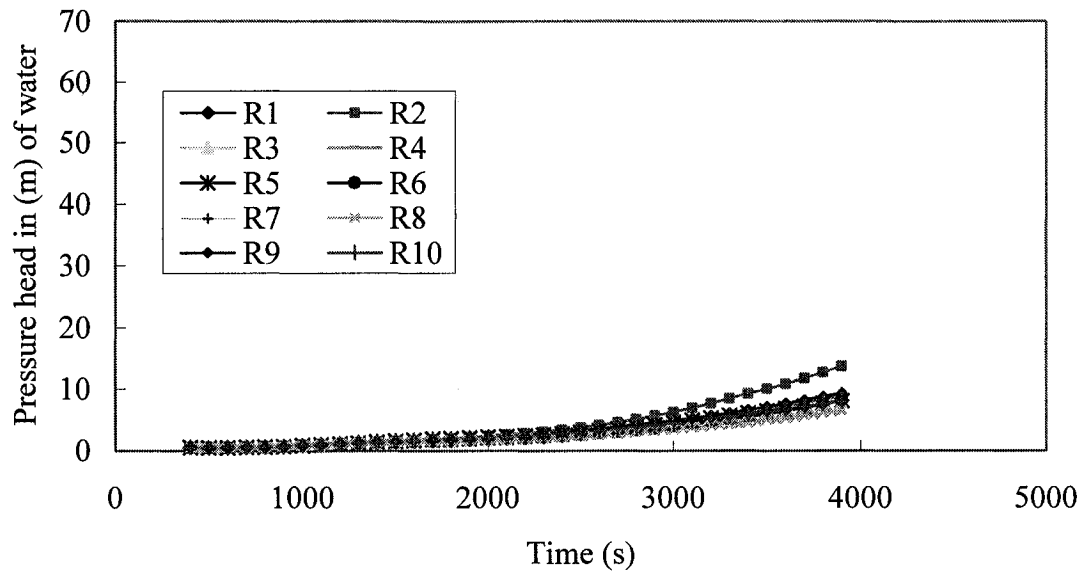
Figure 4.19: Grout injection pressure profiles obtained from different realizations for 20 x 225 x 20 grid formulation ("R" refers to realization of K-field)

Simulations were run to investigate the effect of longitudinal dispersion on grout injectivity. Three different longitudinal dispersivities were studied include α_L =1 mm, 2 mm and 10 mm. Transverse dispersivity was kept constant at 0.01 mm for all the three cases. The required injection pressure head profiles obtained for the different longitudinal dispersivities are plotted in Figure 4.20. The final pressure heads (at time 3940 seconds) required to inject the grout at 1.12 ml/min corresponding to different longitudinal dispersivities differ by about by a factor of 2/3. However, these pressures are far less than the observed injection pressure. Two inferences can be drawn from these simulations. The first one is that the longitudinal dispersion does not seem to affect the grouting process significantly enough to match the observed pressure head profiles. The second one is that there must be some other processes (such as shear) that might be so dominating that the effect of longitudinal dispersivity is not seen.

121

70

60

Pressure hea in (m) of water

50

40

30

20

10

0

—☐— Expt

—▲— αL = 1 mm

—✳— αL = 2 mm

—◆— αL = 10 mm

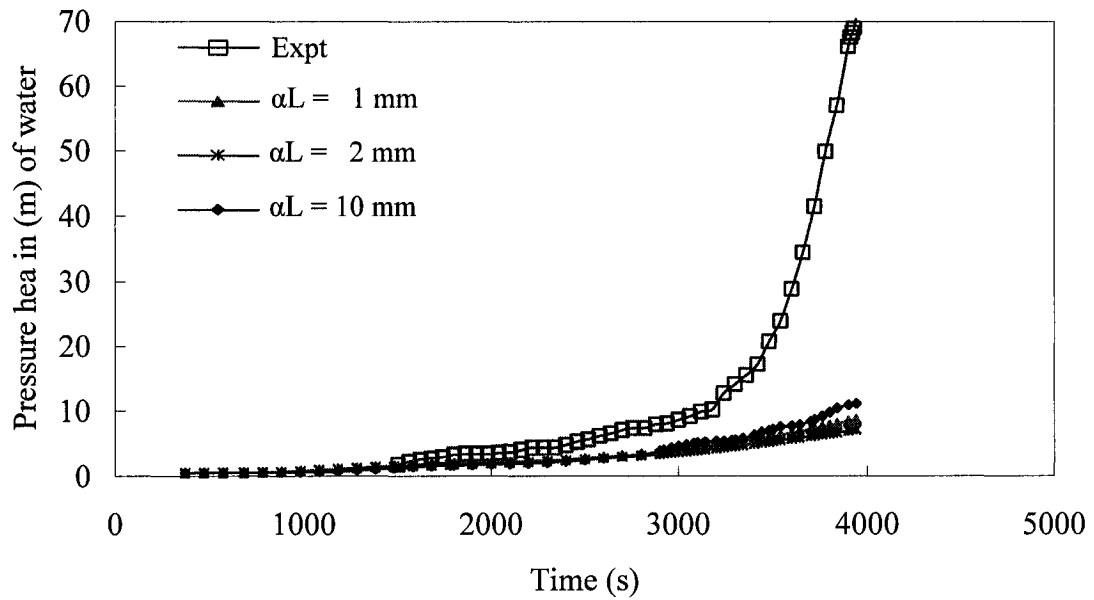0   1000   2000   3000   4000   5000

Time (s)

Figure 4.20: Effect of longitudinal dispersivity on grout injection pressures

4.16.4 Effect of Transverse Dispersivity (α_T)

Transverse dispersivity reflects the mixing process in the direction perpendicular to the mean flow direction. The effect of transverse dispersion was also investigated through simulation for different transverse dispersivities, *i.e.,* $\alpha_T = 1$ mm, 0.1 mm, 0.01 mm and 1×10^{-5} mm. In all cases α_L is set to 1 mm. It is recognized that these dispersivities are much smaller than the grid size. The smaller dispersivities are meaningful based on the profiles and grout distribution patterns. Smith and Gillham (1999) have also adopted similar smaller transverse dispersivities in comparison to their grid resolution. The smaller dispersivities may be explained by the fact that, as the grout becomes more and more viscous, its tendency to mix with either lower viscosity grout solution or water reduces.

The required injection pressure profiles for various α_T's are plotted in Figure 4.21. Unlike the injection pressure profiles corresponding to the variations in longitudinal dispersion as shown in Figure 4.20, the profiles corresponding to different α_T's are widely spread within the range of experimental observations. The pressure profile corresponding to

122

$\alpha_T = 1.0$ mm has final injection pressure much closer to the observed pressures in comparison to the pressure heads corresponding to the other α_T simulations. However, the pressure profile for the intermediate times is completely different from the observed pressure profile. The pressure heads are over-predicted for the intermediate times. On the other hand, the pressure profile of the other α_T's are closer to the observed pressure profile. In fact, the pressure profile corresponding to 0.1 mm matches the experimental pressure heads up to about 3500 seconds out of the total experimental duration of 3940 seconds, though the final injection pressure head obtained from this simulation is about half of the observed injection pressure. However, the pressure profile corresponding to $\alpha_T = 0.01$ mm deviates from the observed profile from about 1800 seconds and the pressure heads are under-predicted. Since the pressure profile corresponding to $\alpha_T = 0.1$ mm seem to match the observed profile, further investigation is made to see the grout patterns inside the column.
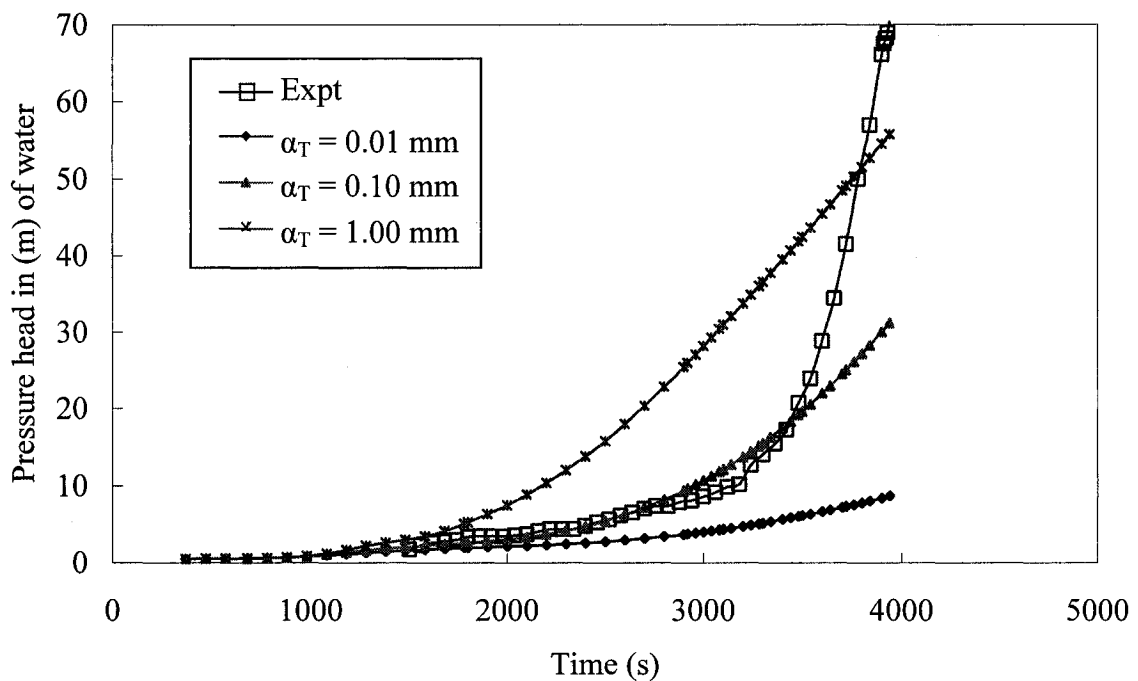

Figure 4.21: Effect of transverse dispersivity grout injection pressures

The grout patterns corresponding to the $\alpha_T = 0.1$ mm are compared with the grout patterns obtained from the simulations corresponding to $\alpha_T = 0.01$ mm to find the reasons that

123

cause the variations in the observed pressure profiles. The higher injection pressure heads are the reflection of higher grout viscosities. On the other hand, the smaller the value of α_T, the higher the scope for preserving the viscous fingers. As long as the viscous finger prevails, the grout flow can find its way through this finger with less effort and hence results in smaller pressure drops. The grout viscosity is more significantly affected by the grout age. Hence the grout age distribution patterns are studied further.

The regions of interest in grout age distribution patterns are the areas having grout age of 600 seconds or less. Hence, distributions of grout age of 600 seconds or less at different times are presented in Figure 4.22. The figure compares the fingers having grout age less than or equal to 600 seconds for the cases of $\alpha_T = 0.1$ mm and 0.01 mm. A quick glance indicates that the regions having grout age of 600 seconds are shrinking in the case of $\alpha_T = 0.1$ mm because of the higher mixing between the grout in the adjacent grids resulting in higher grout ages. When the viscous finger disappears, the grout flow in the column is a one-dimensional or plug flow. In such a situation, the pressure drop is governed by the highest viscosity grout, *i.e.,* oldest grout just behind the grout front. The grout age distribution pattern for the $\alpha_T = 0.01$ mm case preserves the finger. Even though the numerical model predicts the pressure profile that matches the experimentally observed profiles for the case of $\alpha_T = 0.1$ mm, it does not represent the grout physics in terms of age distribution. It is understood from these simulations that α_T significantly affects the formation and preservation of the viscous fingers and grout injectivity.

The results of the simulations presented in the different sub-sections of 4.16 for different cases using shear gelation model did not yield the observed trends in injection pressures. Only the simulations corresponding to different transverse dispersivities predicted the pressure heads in the ranges of observed ones. Hence the simulations are run using gelation model without incorporating the shear for the cases of $\alpha_T = 0.01$ mm and 0.1 mm. The injection pressure head profiles corresponding to these transverse dispersivities along with the experimentally observed profiles are plotted in Figure 4.23.
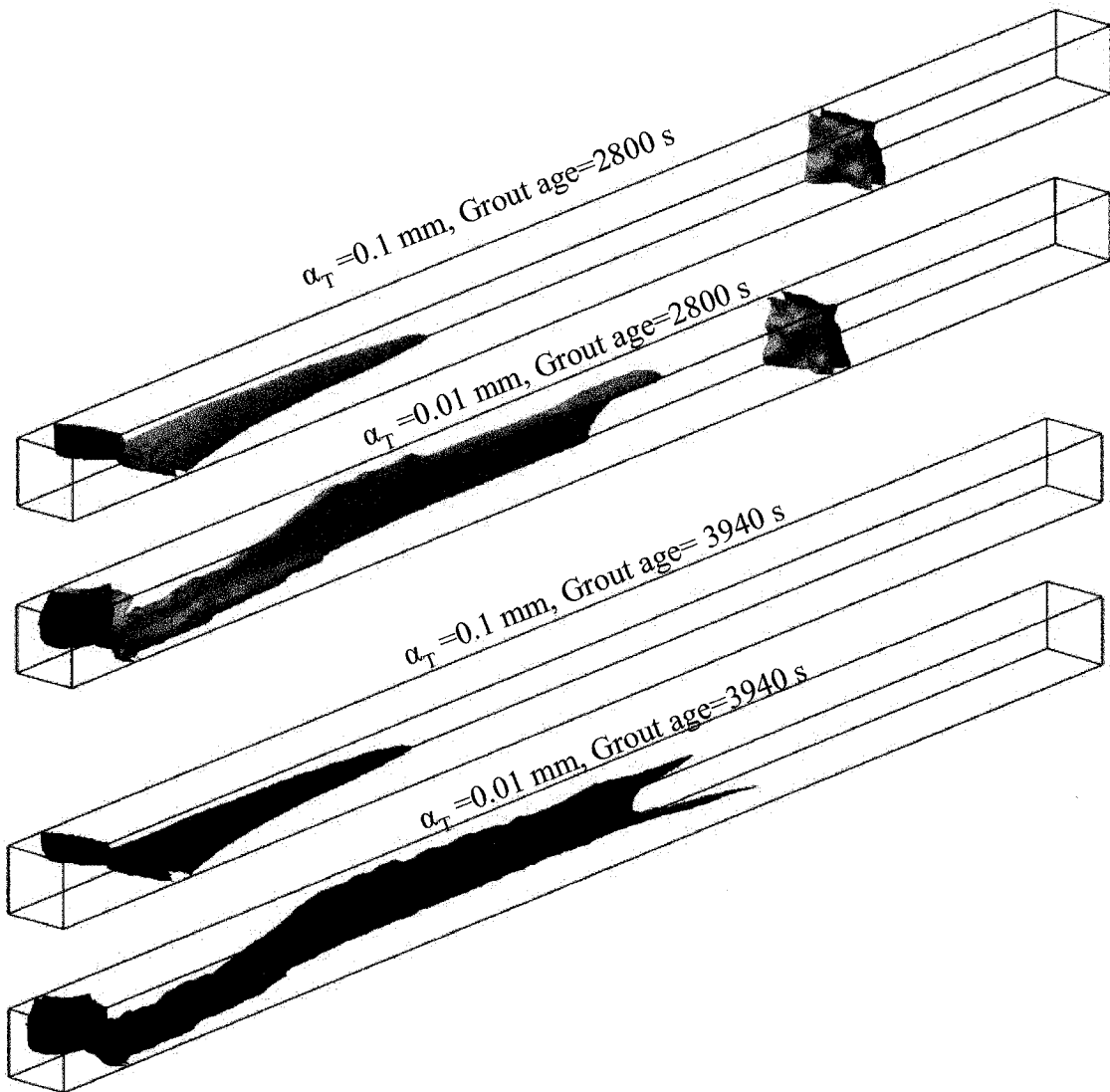
Figure 4.22: Effect of transverse dispersivity on the finger formation when the shear effect was included
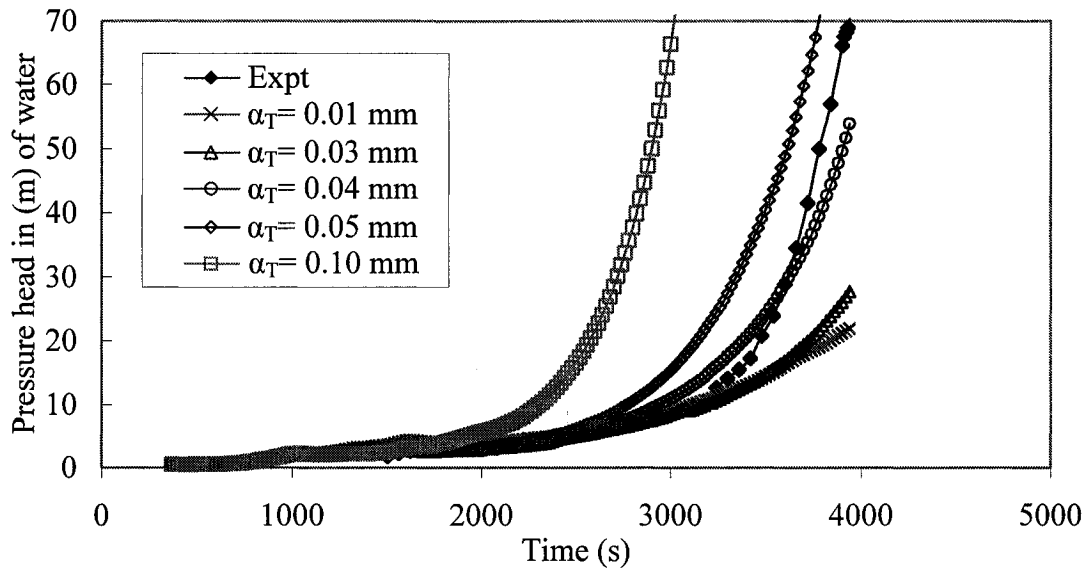
125

Figure 4.23: Effect of transverse dispersivity grout injection pressures when the gelation model is incorporated without shear

The experimental pressure profile lies between the pressure head profiles obtained for $\alpha_T = 0.01$ mm and 0.1 mm. Though the pressure profile does not match the experimental pressure heads exactly, it was clear that an intermediate transverse dispersivity might yield the pressure heads that match the experimentally observed data. Hence, simulations were run with $\alpha_T = 0.03$ mm, 0.04 mm and 0.05 mm. The pressure profile corresponding to $\alpha_T = 0.04$ mm closely matches the experimental data. Then, the grout age distribution for this case was further investigated to infer the processes occurring inside the column. The viscous finger pattern presented in Figure 4.24 shows that the fingers were slimmer than those predicted when the gelation model with shear, was used. These simulations tempt us to believe that shear is not important because gelation model without shear yielded pressure heads closer to the observed pressure heads. This is contrary to the common observation regarding non-Newtonian behavior of gelling liquids. There are neither experimental nor theoretical studies to support this argument. The differences in predicted pressures for the cases when the shear is considered and when it is not considered, may also be explained as an effect of filtration. Based on the experimental investigations, Bryant et al. (1999) reported that filtration of macromolecules occur.
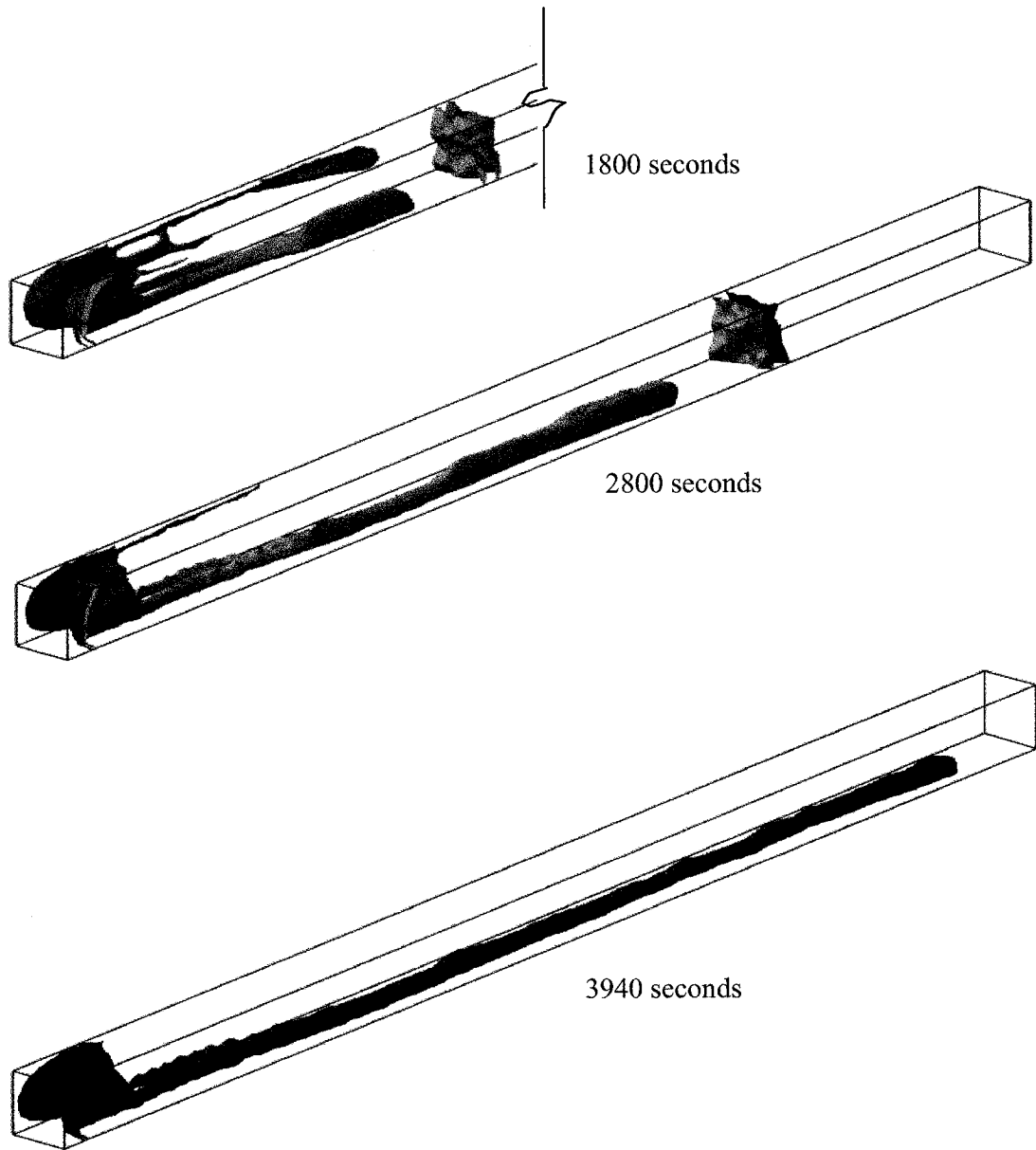
126

Figure 4.24: Grout age distribution in the viscous finger for 20x225x20 grid
when shear was not included in the gelation model

127

Filtration triggers in at an unknown stage of gelation, for which there are no studies available. Todd (1990) incorporated the filtration effect in his model to simulate injection of gelling liquids. The effect of turning off the shear effect is an indirect consideration of filtration effect. When the shear effect is turned off, the model predicts higher viscosities and consequently higher injection pressures. Experimental investigations are needed to understand the presence and absence of shear effect during grout injection into the porous media, especially during the stage of steep increase in injection pressure heads. Regardless of which of these processes is important, transverse dispersivity is found to affect the grout injection process and finger preservation.

4.17 DISCUSSION OF MODELING RESULTS

Based on the results from the slim tube experiment simulation and the one-dimensional simulation of the column experiment, it was understood that it was important to incorporate the effect of shear in the gelation model. However, the three-dimensional simulations performed on different transverse dispersivities using gelation model without shear were better able to predict the pressure heads in the ranges of experimental observations. These two observations warrant further discussion. These simulations provide an answer to the deviations between the predicted pressure heads in case of shear-based gelation model and the experimental observations beyond 3200 seconds.

The grout, during gelation, forms small networks of particles, which in turn join together to form either a single large network of particles or a few relatively smaller networks. When the grout is subjected to shear, the large networks of particles may disintegrate into smaller networks, before reaching an equilibrium state. The viscosity of the grout, subjected to shear gelation, is less than the unsheared grout gel viscosity. This lower viscosity is a reflection of the bulk fluid property. However, the viscosity of smaller networks of grout macromolecules or blobs within the bulk fluid will have the same viscosity as that of the non-sheared gel viscosity for a given reaction time. It was hypothesized that during the flow through the porous medium, when the macromolecules or blobs of grout particles grow to an extent that they are larger than the pore throat diameter, they get trapped. This phenomenon was schematically explained in Figure 4.25.

128
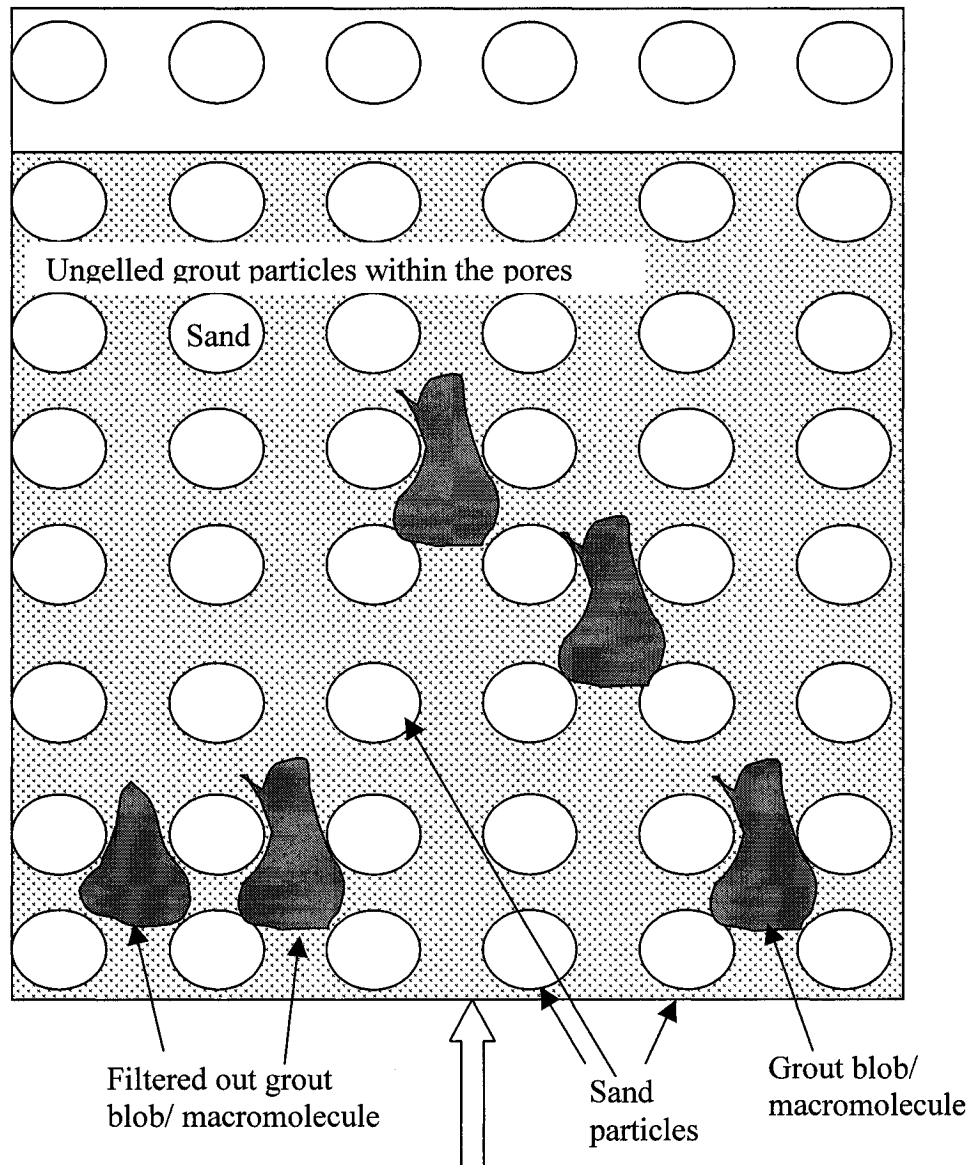
Figure 4.25: Schematic diagram of trapped macromolecules or micro-gels of the grout

The viscosity of these macromolecules trapped near the pore throat entrance contributes to the increase in pressure heads. The trapped blobs cumulatively add to the need for increasing pressure heads. Nevertheless, the bulk fluid with smaller networks or unconnected particles still travel through the porous media in the column. This explanation agrees with the observation made by Bryant *et al.* (1998) and Kim and Corapcioglu (2002a). However, Kim and Corapcioglu (2002a) did not substantiate their statement through either an experimental observation or a numerical investigation.

129

Bryant *et al.* (1998) noted that the filtration might trigger in at different stages of gelation for different polymer compositions (grouts are polymers).

The deviations between the experimental and numerical results for times prior to 3200 seconds may be due to the filtration effect. The effect of turning off shear effect is equivalent to the filtration in a smaller scale. Hence the predicted injection pressure heads match with the experimental pressure heads. The contribution of the difference between the shear and no shear based gelation models in terms of pressure heads was still not enough to predict the final pressure heads. However, this effect was good enough to predict the pressure heads that were closer to the experimental procedures when compared to the case when shear was considered. Therefore, filtration effect needs to be incorporated. Thus, the present study was successful in showing the need for incorporating the effects of shear and filtration into the gelation model.

Grout patterns were investigated further to gain confidence in the ability of the model to simulate the grout injection into porous media. The grout concentration distribution patterns, obtained from the simulations for the case when a shear-based gelation model was used, were presented in Figure 4.26. These distributions at different times show patterns that are similar to the schematic diagram presented in Figure 3.9 and the pictures taken during the experiments. The younger grout tends to puncture into the grouted regions. Initially it tries to enter as a thin finger and then it spreads into the lateral directions as it takes less effort to spread laterally compared to the longitudinal direction. When the energy required to spread laterally becomes higher than the energy required to puncture into the porous media in the longitudinal direction, the grout tries to squeeze higher into the porous media as reflected by the concentration distributions shown in Figure 4.26 for different times. The pattern at the top of the column for each time shows a bifurcation pattern of fingers, which was an indication of flow instability. First, the grout punctures into the soil as a finger. Then an additional finger enters the soil from the adjacent area and envelops the soil between the first finger and new finger. The grout concentration distribution pattern showing this phenomenon was plotted in Figure 4.27.
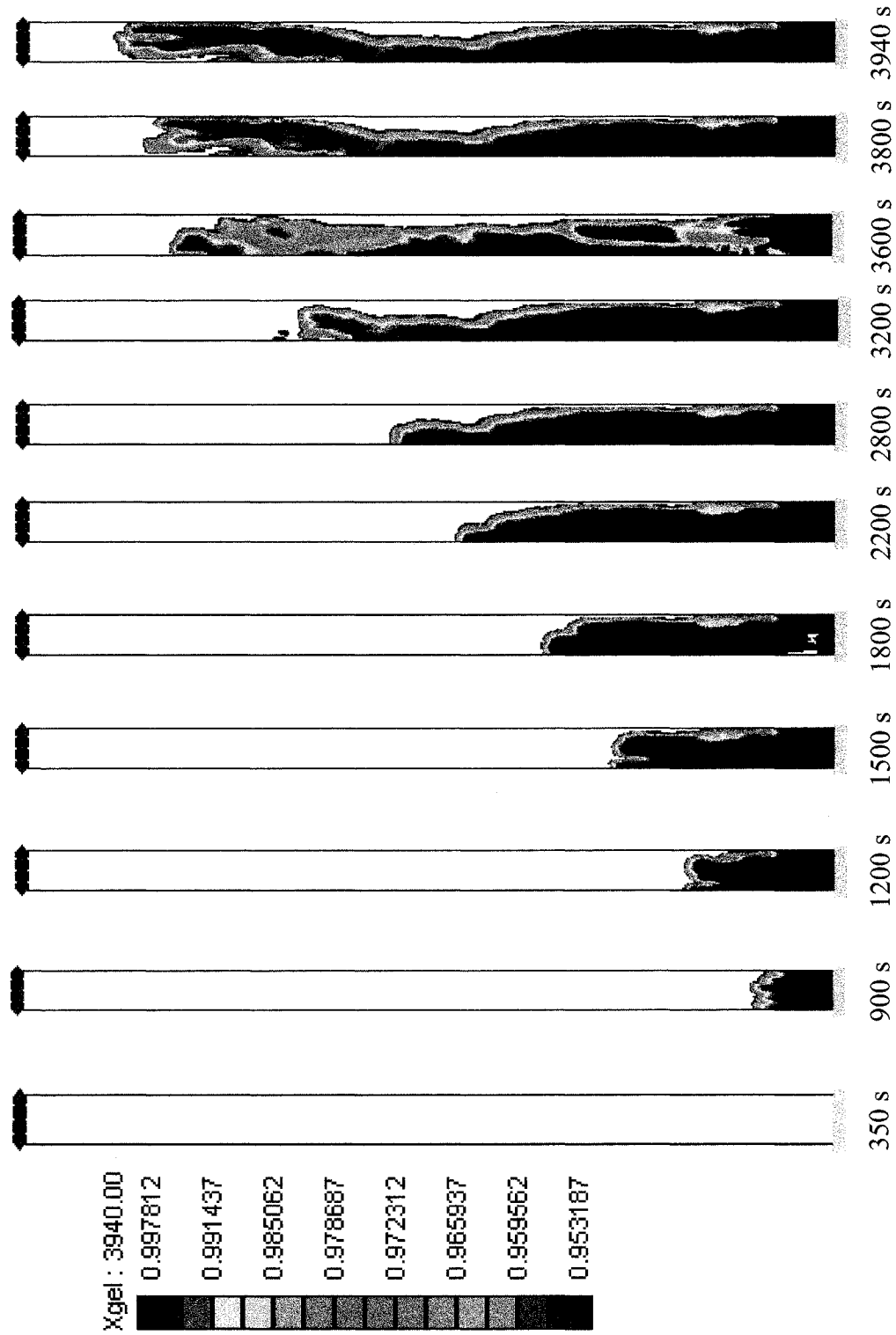
130

Figure 4.26: Simulated Grout concentration distribution in the column showing bifurcation pattern at the top as observed in experiment (shown in Figure 3.8 and 3.10)
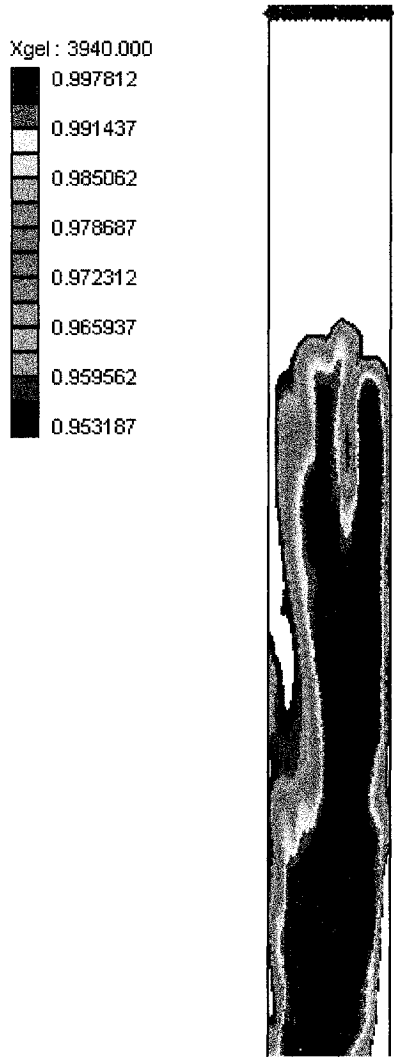
131

Figure 4.27: Numerically predicted grout concentration distribution showing flowering pattern at the front

132

The same phenomenon may be interpreted from the series of pictures (shown in Figure 3.9) taken during the experimental investigations. Another measure of confidence is demonstrated through the grout pattern obtained by the simulation model and the corresponding picture taken from the experiment is shown in Figure 4.28. Thus, the present study is able to identify the processes involved in the grout injection into the porous media and was able to incorporate the processes in the model.

4.18 CONCLUSIONS OF MODELING STUDIES

This chapter presented the chemical grout injection simulation model developed by coupling MODFLOW and RT3D and adding modules to incorporate shear and no shear based gelation process. The empirical equation developed in Chapter 3 to estimate the viscosity as a function of shear and grout age was incorporated in the model. Hydraulic conductivity is reduced by the ratio of viscosities of the grout and the water in order to reflect the effect of the grout viscosity.

The grouting simulation model was verified against an analytical solution developed as part of this study. As part of validation, the present model results were compared with (i) the model developed by Honma (1984) for sodium silicate grout injection, and (ii) the pressure profiles obtained from the present column experiments on sodium silicate grout injection. The concentration profiles obtained by the present model were found to be within 5% of those obtained by Honma. Even though the present model results matched the Honma (1984) sodium silicate experimental pressure profiles for early time periods and late time periods, the profiles did not match for the intermediate time periods. Also, the present model had over-predicted pressures. These discrepancies may be attributed to the fact that Honma's column experiment is simulated as a one-dimensional column and, as a result, the effect of the fingering process was not reflected in the modeling. The use of a linear mixing rule may also have contributed to over-predicting the grout injection pressures.

133

3200 s   3096 s
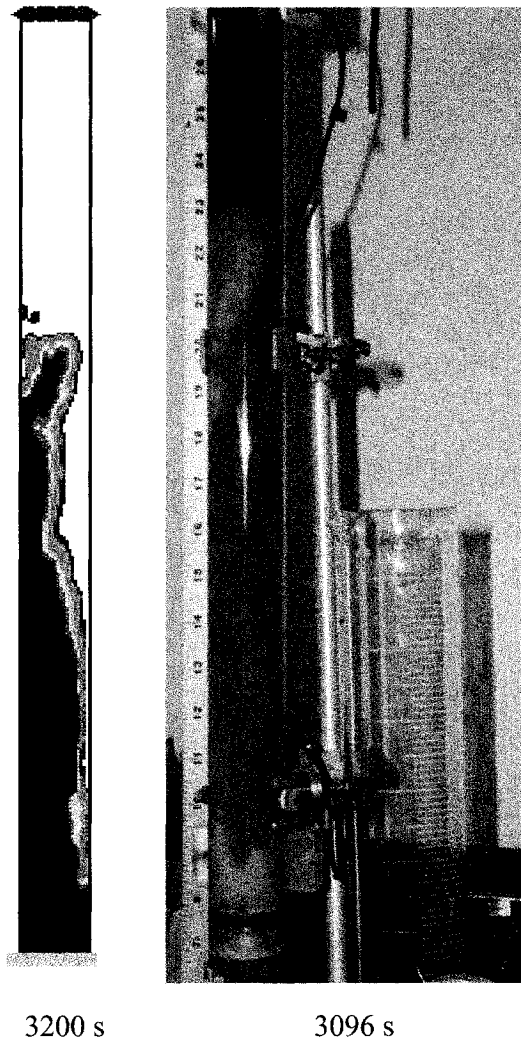
Figure 4.28: Comparison of experimentally recorded and numerically predicted grout
concentration distribution patterns

134

The present model was also used to analyse the colloidal silica grout injection into a slim tube. The model was able to produce results that matched well with the experimental observations up to about 1500 seconds out of 1770 seconds. These simulations revealed that shear was an important factor that needs to be incorporated into the model and that a major process needs to be incorporated to obtain the observed pressures for time beyond 1500 seconds.

In the next phase, the grouting model was used to analyse the observations made during colloidal silica grout injection into a 30.16 mm diameter column. These experiments were simulated by representing the column both as one-dimensional and three-dimensional models. One-dimensional simulations revealed that the power law mixing rule was appropriate to represent the colloidal silica grouting. The results obtained from the three-dimensional simulations matched the experimental data until the last few hundred seconds. Based on the findings from the previous sections and the present analysis, it is apparent that viscosification, shear and viscous fingering affect the grout injectivity. The deviation of the model results from the experimental observations at later time periods indicate that a major process, possibly filtration, needs to be incorporated in the model.

135

CHAPTER 5

SUMMARY, CONCLUSIONS AND RECOMMENDATIONS

5.1 SUMMARY AND CONCLUSIONS

Colloidal silica, an environmentally benign chemical solution, is reported as a promising alternate to sodium silicate for use as a chemical grout because of its better gel time control and the absence of syneresis problem. The present study was carried out with an aim to understand the processes occurring during chemical grouting into porous media, using colloidal silica grout. To this end, a two-pronged approach has been adopted, combining experimental investigations and numerical simulations.

The experimental work can be classified into three categories, *viz.,* viscosity measurements, grout injection into columns and grouted sand testing. The grout viscosity measurements conducted during gelation under different conditions showed that the gel viscosity is a function of reaction time, concentrations of colloidal silica and sodium chloride, and temperature. To investigate the processes that occur during the injection of colloidal silica grout into sand columns, two different sizes of columns were used. The experiments performed using a 30.16 mm diameter column were grouped into three categories based on the colloidal silica solution and the type of water used. Viscous fingering is shown to affect the grout injectivity in the 30.16 mm diameter column. This process has not been reported in any of the earlier chemical grouting studies. The smaller diameter column experiment, referred to as the slim tube experiment, was conducted to obtain the injection pressure head data in the absence of finger formation within the column. In both cases, it was possible to inject the grout until long after the gel time corresponding to no shear gelation. The dyed grout solutions aided in visualizing grout flow patterns and understanding the processes that occur during the grout injection into the sand column.

A chemical grout injection simulation model was developed by coupling MODFLOW and RT3D, and adding modules to incorporate shear and no shear based gelation

processes. In order to prevent spurious gelation, the concept of minimum grout concentration was incorporated in the grout aging function. Based on the shear viscosity measurements during gelation, an empirical equation was developed to estimate the viscosity as a function of shear and grout reaction time. The grout simulation model was verified against an analytical solution developed as part of this study. As part of the validation, the present model results were compared with results from a previously published model and experimental observations on sodium silicate grout injection into columns. The concentration profiles obtained by the present model were found to be within 5% of those obtained by Honma (1984). The simulation of Honma's sodium silicate grouting experiment resulted in pressure profiles that deviated from the experimental observations. The present model, based on Honma's approach and assumptions, over-predicted the pressures at the point of injection. These discrepancies are attributed to three different reasons. The Honma's column experiment was simulated as a one-dimensional column. As a result, the effect of the fingering process was not reflected in the modeling. The use of a linear mixing rule and the absence of shear may also have contributed to over-predicting the grout injection pressures.

The analysis of colloidal silica grout injection into sand columns through the numerical modeling revealed that four major processes occur within the column. They are: viscosification, shear, viscous fingering and filtration. The model was able to simulate the first three processes with reasonable accuracy. None of the earlier studies on chemical grouting recognized the importance of the shear effect. The present investigation has identified the importance of shear on colloidal gelation on grout injectivity. The predicted injection pressures deviated from the experimentally observed profiles in the region where the experimental pressures increased steeply. This deviation is attributed to the contribution of the filtration effect for which neither literature nor experimental data are available. It is hypothesized that when the macromolecules/micro-gels grow to a size larger than the pore throat size, they are filtered out. These trapped micro-gels contribute to the need for higher grout injection pressures.

137

Experimental investigations aided in deciphering the physics of grouting and assisted in enhancing the model. These experiments revealed that the grout injection pressures are very sensitive to salt content. A concentration difference even as low as 0.3 % slowed down the gelation process. The reduction in surface area of colloidal silica solution with time is found to affect the gelation time, which in turn affects grout injection process.

One-dimensional and three-dimensional simulation results helped in making some of the specific conclusions. Power law mixing rule is able to predict the viscosity of the colloidal silica grout at the interface between grout and water/brine. The grout flow is found to be three-dimensional even in a column of 30.16 mm diameter. The three-dimensional simulations are able to capture the fingering process, observed in the experimental investigations. Hence, simulating the grout flow through a column using a one-dimensional model will not be representative or accurate. Numerical instabilities are observed when the simulations are performed using homogeneous hydraulic conductivity fields. These instabilities are suppressed when the slightest heterogeneity is incorporated. Transverse dispersivity is found to affect the gelation process, grout distribution, and the consequent pressures required to inject the grout.

A feedback looping mechanism is needed between the numerical and experimental studies. In order to understand the behaviour of the grout system at the internal core, the numerical modeling is of paramount importance. This cannot be achieved by experiments alone.

5.2 RECOMMENDATIONS

The deviations in the injection pressure heads observed between the experimental and numerical investigations on the colloidal silica grout injection process are presumed to be due to filtration. Hence, a detailed understanding of the effects of filtration on grout injection is needed. In order to achieve this, the following tasks are identified to be necessary for further study:

- Identify the stage of grout gelation when filtration starts affecting grout injection.

138

- Quantify the effects of filtration.

- Develop equations to represent the effects of filtration.

- Incorporate the filtration equations into the grout model and simulate the grout injection process.

- Validate the grout model, incorporating the filtration effects, against the experimental data.

Experimental investigations need to be performed either in a 3-dimensional box or in the field to confirm the inferences made based on results from the present study, as well as those obtained from any model which incorporates filtration equations.

139

REFERENCES

Ackerer, P.H., A. Younes and R. Mose (1999), Modeling variable density flow and solute transport in porous medium: 1. Numerical model and verification, *Transport in Porous Media, 35(3)*, 345-373.

ACRi (1994), *PORFLOW: A Software Tool for Multiphase Fluid Flow, Heat and Mass Transport in Fractured Porous Media - Validation, Version 2.50*, Analytic & Computational Research Inc, Los Angeles, CA.

ACRi (1999), *PORFLOW Users Manual*, Analytic & Computational Research Inc, Bel Air, CA.

American Institute of Aeronautics and Astronautics (1998), *Guide for the verification and validation of computational fluid dynamics simulations*, AIAA-G-077-1998, American Institute of Aeronautics and Astronautics, Reston, VA.

American Society of Civil Engineers ASCE Task Committee on Geostatistical Techniques in Geohydrology of the Ground Water Hydrology Committee of the ASCE Hydraulics Division (1990a), Review of Geostatistics in Geohydrology: I. Basic Concepts, *Journal of Hydraulic Engineering, 116(5)*, 612-632.

American Society of Civil Engineers ASCE Task Committee on Geostatistical Techniques in Geohydrology of the Ground Water Hydrology Committee of the ASCE Hydraulics Division (1990b), Review of Geostatistics in Geohydrology: II. Applications, *Journal of Hydraulic Engineering, 116(5)*, 633-658.

American Society of Civil Engineers (1997), *Chemical Grouting*, Technical engineering and design guides as adopted from Army Corps of Engineers, No 24.

Avery, M.R., L.A. Burkholder and M.A. Gruenenfelder (1986), Use of cross-linked xanthan gels in actual profile modification field projects, *Society of Petroleum Engineers of AIME, SPE, 2*, 559-568.

Barron, R.M. and A.M. Latypov (1995), Survey of current verification and validation methodologies and resources for CFD, *Proceedings of the 3rd Annual Conference of the CFD Society of Canada*, CFD95, Banff, Alberta, June, 327-334.

Bergna, H.E. (1994), *The Colloid Chemistry of Silica*, Adv. Chem. Ser., American Chemical Society, Washington D.C., 234.

Bird, R.B., R.C. Armstrong and O. Hassager (1987), *Dynamics of Polymeric Liquids, Vol. 1, Fluid Mechanics*, J.Wiley and Sons, New York.

Bouchelghem, F. and L. Vulliet (2001a), Real-scale miscible grout injection experiment and performance of advection-dispersion-filtration model, *International Journal for Numerical and Analytical Methods in Geomechanics, 25(12)*, 1149-1173.

Bouchelghem, F. and L. Vulliet (2001b), Mathematical and numerical filtration-advection-dispersion model of miscible grout propagation in saturated porous media, *International Journal for Numerical and Analytical Methods in Geomechanics, 25(12)*, 1195-1227.

Boufadel, M., M.T. Suidan and A.D. Venosa (1997), Density-dependent flow in one-dimensional variably-saturated media, *Journal of Hydrology, 202(1-4)*, 280-301.

Bras, R.L. and I. Rodriguez-Iturbe (1985), *Random Functions and Hydrology*, Addison Wesley, Boston.

Bruce, D.A., (1994), *Permeation Grouting, Handbook on Soil Grouting*, J. Wiley and Sons, New York.

Bryant, S.L., G.P. Borghi, M. Bartosek and T.P. Lockhart (1998), Experimental investigation on the injectivity of phenol-formaldehyde/polymer gels, *SPE Journal, 3(4)*, 373-380.

Cannella, W.J., C. Huh and R.S. Seright (1988), Prediction of xanthan rheology in porous media, *Society of Petroleum Engineers of AIME, (Paper) SPE*, v GAMMA, 353-368, 18089.

Carvalho, W. D. and M. Djabourov (1997), Physical gelation under shear for gelatin gels, *Rheologica Acta, 36(6)*, 591-609.

Chauveteau, G., A. Omari, R. Tabary, M. Renard and J. Rose (2000), Controlling gelation time and microgel size for water shutoff, SPE59317, *SPE/DOE Improved Oil Recovery Symposium*, 3-5 April, Tulsa, Okla.

Chauveteau, G., A. Omari, R. Tabary, M. Renard and J. Rose (2001), Controlling gelation time and microgel size for water shutoff, *Journal of Petroleum Technology, 53(3)*, 51-52.

Clement, T.P., B.S. Hooker and R.S. Skeen (1996), Macroscopic models for predicting changes in saturated porous media properties caused by microbial growth, *Ground Water, 34(5)*, 934-942.

Clement, T.P. (1997), *RT3D, A modular computer code for simulating Reactive multi-species Transport in 3-Dimensional groundwater aquifers*, Pacific Northwest National Laboratory, Richland, WA, USA, PNNL-11720.

Clement, T.P., Y. Sun, B.S. Hooker and B.N. Petersen (1998), Modeling multi-species reactive transport in groundwater aquifers, *Groundwater Monitoring & Remediation, 18(2)*, 79-92.

Clement, T.P. and C.D. Johnson (2003), *RT3D v2.5 Update Document.* Available online at: http://bioprocess.pnl.gov/publictn/RT3Dv25_Update.pdf. >Aug 2004

Committee on Grouting (1980), Preliminary glossary of terms related to grouting, *Journal of Geotechnical Engineering, ASCE, 106(GT7)*, 803-805.

Cross, M.M. (1965), Rheology of non-Newtonian fluids: a new flow equation for pseudo-plastic systems. *Journal of Colloid Science, 20(5)*, 417-437.

Dagan, G. (1986), Statistical theory of groundwater flow and transport: pore to laboratory, laboratory to formation, and formation to regional scale, *Water Resources Research, 22*, 120S-135S.

Dagan, G. (1989), *Flow and Transport in Porous Formations*, Springer-Verlag, New York.

Delhomme, J.P. (1979), Spatial variability and uncertainty in groundwater flow parameters: a geostatistical approach, *Water Resour. Res., 15(2)*, 269-280.

Deutsch, C. and A. Journel (1998), *GSLIB: Geostatistical Software Library and Users Guide*, 2nd Edition, Oxford Press, NY.

Deverel, S.J. and R. Fujii (1988), Processes affecting the distribution of selenium in shallow groundwater of agricultural areas, western San Joaquin Valley, California, *Water Resources Research, 24(4)*, 516-524.

Diersch, H.-J.G. and O. Kolditz (2002), Variable-density flow and transport in porous media: approaches and challenges, *Advances in Water Resources, 25(8-12)*, 899-944.

Dolan, D.M. (1989), An experimental study of the effects of pH and shear on the gelation of a xanthan-chromium(III) solution, M.S. Thesis, Univ. of Kansas, Lawrence, Kansas.

Drabarek, E., J.R. Bartlett, H.J.M. Hanley, J.L. Woolfrey and C.D. Muzny (2002), Effect of processing variables on the structural evolution of silica gels, *International Journal of Thermophysics, 23(1)*, 145-160.

Durmusoglu, E. and M.Y. Corapcioglu (2000), Experimental study of horizontal barrier formation by colloidal silica, *Journal of Environmental Engineering, ASCE, 126*, 833-841.

Dwyer, B.P. (1994), *Feasibility of Permeation Grouting for Constructing Subsurface Barriers*, SAND94-0786.

Elfeki, A.M.M., G.J.M. Uffink and F.B.J. Barends (1997), *Groundwater Contaminant Transport – Impact of Heterogeneous Characterization*, A.A.Balkema Publishers, Rotterdam, 300.

Eka Chemicals AB, (2002), Selection of BINDZIL grades, http://www.colloidalsilica.com/void_a.html > Aug 2004.

Finsterle, S., G.J. Moridis and K. Pruess (1994), *A TOUGH2 equation-of-state module for the simulation of two-phase flow of air, water, and a miscible gelling liquid*, Rep. *LBL-36086*, Lawrence Berkeley Natl. Lab., Berkeley, Calif.

Finsterle, S., C.M. Oldenburg, A.L. James, K. Pruess and G.J. Moridis (1997), Mathematical modeling of permeation grouting and subsurface barrier performance, *Intl. Containment Tech. Conf. and Exhibition*, St. Petersburg, Florida, Feb 9-12, 438.

Finsterle, S. (2003), Personal communication.

Freeze, R.A. (1975), A stochastic-conceptual analysis of one-dimensional groundwater flow in nonuniform homogeneous media, *Water Resources Research, 11(5)*, 725-741.

French, T.R. and H.W. Gao (1988) *Development of Improved Mobility Control Methods*, Work performed under DoE cooperative Agreement No. DE-FC22-83FE60149, Project BE4C, published in quarterly progress review, US Dept of Energy, June 30.

Frind, E.O. (1982), Simulation of long-term transient density-dependent transport in groundwater, *Advances in Water Resources, 5*, 73-88.

Frolkovic, P. and H.D. Schepper (2001), Numerical modelling of convection dominated transport coupled with density driven flow in porous media, *Advances in Water Resources, 24(1)*, 63-72.

Galeati, G., G. Gambolati and S.P. Neuman (1992), Coupled and partially coupled Eulerian-Lagrangian model of freshwater-seawater mixing, *Water Resources Research, 28(1)*, 149-165.

Gallagher, P.M. (2000), *Passive Site Remediation for Mitigation of Liquefaction Risk*, Ph.D. Dissertation, Virginia Polytechnic Inst. and State Univ., Blacksburg, VA, 238.

Gallagher, P.M. and J.K. Mitchell (2002), Influence of colloidal silica grout on liquefaction potential and cyclic undrained behaviour of loose sand, *Soil Dynamics and Earthquake Engineering, 22(9-12)*, 1017-1026.

Gallagher, P.M. and A.J. Koch (2003), Model testing of passive site stabilization: a new grouting technique, *Grouting and Ground Treatment, Geotechnical Special Publication, 120*, 1478-1489, ASCE, Reston, VA.

Gallavresi, F. (1992), Grouting improvement of foundation soils, *Geotechnical Special Publication*, *30 (1)*, 1-38, ASCE, Reston, VA.

Gelhar, L.W. (1986), Stochastic subsurface hydrology from theory to applications, *Water Resources Research*, *22(9)*, Suppl, Aug, 135-145.

Gelhar, L.W. (1994), Stochastic subsurface hydrology, *Hydrological Sciences Journal*, *39(5)*, p 554.

Goovaerts, P. (1999), Impact of the simulation algorithm, magnitude of ergodic fluctuations and number of realizations on the spaces of uncertainty of flow properties, *Stochastic Environmental Research and Risk Assessment*, *13*, 161-182.

Grace, W.R. & Co. (2003), LUDOX-HS40 Colloidal Silica Product Information, Grace Division, W.R. Grace & Co., Conn.

Guo, W. and C.D. Langevin (2002), User's Guide to SEAWAT: A Computer Program for Simulation of Three-Dimensional Variable-Density Ground-Water Flow: Techniques of Water-Resources Investigations Book 6, Chapter A7.

Haldorsen, H.H. and E. Damsleth (1990), Stochastic Modeling, *Journal of Petroleum Technology*, *42(4)*, 404-412.

Hanley, H.J.M., C.D. Muzny, B.D. Butler, G.C. Straty, J. Bartlett and E. Drabarek (1999), Shear-induced restructuring of concentrated colloidal silica gels, *Journal of Physics Condensed Matter*, *11(2-6)*, 1369-1380.

Harbaugh, A.W. and M.G. McDonald (1996), "*User's Documentation for MODFLOW-96, an update to the USGS Modular Finite Difference Ground-water Flow Model,*" USGS Open-file Report 96-485.

Hassan, A.E., J.H. Cushman and J.W. Delleur (1998), A Monte-Carlo assessment of Eulerian flow and transport perturbation models, *Water Resources Research*, *34(5)*, 1143-1163.

Hejri, S. (1989), An experimental investigation into the flow and rheological behaviour of xanthan solutions and a xanthan/Cr(III) gel system in porous media, Ph.D. Dissertation, Univ. of Kansas, Lawrence, KS.

Hejri, S., G. P. Willhite and D.W. Green (1989), In-situ gelation of a xanthan/Cr(III) gel system in porous media, paper SPE 19634 presented at the *SPE Annual Technical Conference and Exhibition*, San Antonio, TX, Oct 8-11.

Hejri, S., F. Francois, D.W. Green, C.S. McCool and G.P. Willhite, (1993), Permeability reduction by a xanthan/chromium (III) system in porous media, *SPE Reservoir Engineering, 8(4)*, 299–302.

Herbert, A.W., C.P. Jackson and D.A. Lever (1988), Coupled groundwater flow and solute transport with fluid density strongly dependent on concentration, *Water Resources Research, 24(10)*, 1781-1795.

Hicks, P.J. (1996), Unconditional sequential Gaussian simulation for 3-D flow in a heterogeneous core, *Journal of Petroleum Sciences and Engineering, 16*, 209-219.

Honma, S. (1984), Finite element analysis of the injection and distribution of chemical grout in soils, Ph.D. Dissertation, Univ. of Wisconsin, Milwaukee, WI.

Hortes, E. (1986), *Development of Reservoir Model for Polymer/Gel Treatments*, Report 87-3, University of Texas at Austin, Texas.

Hubbard, S., L.J. Roberts and K.S. Sorbie (1988), Experimental and theoretical investigation of times-setting polymer gels in porous media, *SPERE, 3*, 1257-1267.

Iler, R.K. (1979), *The Chemistry of Silica: Solubility, Polymerization, Colloid and Surface Properties, and Biochemistry*, J. Wiley and Sons, New York.

Inyang, H.I. (1999), Balancing prescriptive and performance based design specifications for waste containment systems, *Journal of Environmental Engg., ASCE, 9(6)*, 491.

Jansson, I. (2003), Personal Communication, M/s Eka Chemicals.

Journel, A.G. and C.J. Huijbregts (1978), *Mining Geostatistics*, Academic Press, London.

Jousset, F., D.W. Green, G.P. Willhite and C.S. McCool (1990), Effect of high shear rate on in-situ gelation of a xanthan/Cr(III) system, paper SPE 20213 presented at the *SPE/DOE Symposium on Enhanced Oil Recovery*, Tulsa, OK, April 22-25.

Jurinak J. and L.E. Summers (1991), Oilfield applications of colloidal silica gel, *SPEPE, 6*, 406-412.

Karol, R.H. (1990), *Chemical Grouting*, Marcel and Dekker Inc., NY, 1990.

Kim, M. and M.Y. Corapcioglu (2002a), Gel barrier formation in unsaturated porous media, *Journal of Contaminant Hydrology, 56(1-2)*, 75-98.

Kim, M and M.Y. Corapcioglu (2002b), Modeling of gel barrier formation by using horizontal wells, *Journal of Environmental Engineering, ASCE, 128(10)*, 929-941.

145

Kitanidis, P.K. (1997), *Introduction to Geostatistics: Applications in Hydrogeology*, Cambridge University Press, New York.

Kolditz, O., R. Ratke, H. Diersch and W. Zielke (1998), Coupled groundwater flow and transport: 1. Verification of variable density flow and transport models, *Advances in Water Resources, 21(1)*, 27-46.

Koval, E.J. (1963), A method for predicting the performance of unstable miscible displacement in heterogeneous media, *Society of Petroleum Engineers Journal, 3(2)*, 145-154.

Krieger I.M. and T.J. Dougherty (1959), A mechanism of non-Newtonian flow in suspensions of rigid spheres, *Trans. Soc Rheol. III 137*.

Law, J. (1944), Statistical approach to the interstitial heterogeneity of sand reservoirs, *Trans., AIME, 160(34)*.

Liao, H.J., C.C. Huang and B.S. Chao (2003), Liquefaction resistance of a colloidal silica grouted sand, *Grouting and Ground Treatment, Geotechnical Special Publication,120*, 1305-1313, ASCE, Reston, VA.

Liang, J., H. Sun and R.S. Seright (1992), Reduction of oil and water permeabilities using gels. Paper SPE/DOE 24195 presented at the *SPE/DOE 8th Symp. on Enhanced Oil Recovery*, Tulsa, OK, 22–24 April.

Lin, Y.P, C.C. Lee and Y.C. Tan (2000), Geostatistical approach for identification of transmissivity structure at Dulliu area in Taiwan, *Environmental Geology, 40(1-2)*, 111-120.

Littlejohn, S. (2003), The development and practice of permeation and compensation grouting: A historical perspective 1802-2002 Part 1: Permeation grouting, *Grouting and Ground Treatment, Geotechnical Special Publication, 120*, 50-99, ASCE, Reston, VA.

Lopez, X., P.H. Valvatne and M.J. Blunt (2003), Predictive network modeling of single-phase non-Newtonian flow in porous media, *Journal of Colloid and Interface Science, 264(1)*, 256-265.

Marty, L., D.W. Green and G.P. Willhite (1991), Effect of flow rate on the in situ gelation a chrome/redox/polyacrylamide system, *SPERE, 6(2)*, 219-224.

May, J.H., R.H. Larson, P.G. Malone, J.A. Boa and D.L. Ben (1986), *Grouting Techniques in Bottom Sealing of Hazardous Waste Sites*, USEPA Hazardous Waste Engineering Research Laboratory, Cincinnati, OH.

McCool, C.S., D.W. Green and G.P. Willhite (1988), Permeability reduction mechanism involved in situ gelation of a polyacrylamide/chromium (VI) /Thiourea system,

146

SPE/DOE 17333 presented at the *Sixth SPE/DOE Enhanced Oil Recovery Symposium*, Tulsa, OK, 17-20 April.

McCool, C.S., D.W. Green and G.P. Willhite (1991), Permeability reduction mechanism involved in situ gelation of a polyacrylamide/chromium (VI) /Thiourea system, *SPERE*, *77(2)*, Trans., AIME, 291.

McDonald, M.D. and A.W. Harbaugh (1988), *A modular three-dimensional finite difference flow model, Techniques in Water Resources Investigations of the U.S. Geological Survey*, Book 6, 586.

Mitchell, J.A. and R. Rumer (1997), Waste containment barriers: Evaluation of the technology, *In Situ Remediation of the Geoenvironment, Geotechnical Special Publication, 71*, ASCE, Reston, VA.

Mitchell, J.A. and W.A. van Court (1997), The role of soil modification in environmental engineering applications, *Geotechnical Special Publication, 30(1)*, 1992, 136-137, ASCE, Reston, VA.

Montoglou, A. and J.L.Wilson (1982), Turning bands method for simulation of random fields using line generation by a spectral method, *Water Resources Research, 18(5)*, 1379-1394.

Moridis, G.J., P. Persoff, H.-Y. Holman, S.J. Muller, K. Pruess, P. Witherspoon and C.J. Radke (1994), *Containment of Contaminants Through Physical Barriers Formed from Viscous Liquids Emplaced under Controlled Conditions*, Rep LBL-29400, Lawrence Berkeley National Laboratory, Berkeley, Calif.

Moridis, G.J., L. Myer, P. Persoff, S. Finsterle, J. Apps, D. Vasco, P. Williams, S. Flexser, S. Muller, B. Freifeld, and K. Pruess (1995), *First Level Field Demonstration of Subsurface Barrier Technology Using Viscous Liquids*, Rep LBL-37520, Lawrence Berkeley National Laboratory, Berkeley, Calif.

Moridis, G.J., S. Finsterle and J. Heiser (1999), Evaluation of alternate designs for an injectable subsurface barrier at the Brookhaven National Laboratory site, Long Island, New York, *Water Resources Research, 35(10)*, 2937-2953.

MSE Technology Applications Inc. (2001), *Final Completion Report: Viscous Liquid Barrier Deployment at Brookhaven National Laboratory*, Butte, MT.

Naff, R., D.F. Haley and E.A. Sudicky (1998a), High resolution Monte-Carlo simulation of flow and conservative transport in heterogeneous porous media 1. Methodology and flow results, *Water Resources Research, 34(4)*, 663-677.

147

Naff, R., D.F. Haley and E.A. Sudicky (1998b), High resolution Monte-Carlo simulation of flow and conservative transport in heterogeneous porous media 2. Transport results, *Water Resources Research, 34(4)*, 679-698.

Noll, M.R., C. Bartlett and T.M. Dochat (1992), In situ permeability reduction and chemical fixation using colloidal silica, *Presented at the 6th Natl. Outdoor Action Conference on Aquifer Restoration*, Las Vegas, NV, 11–13 May.

Oberkampf, W.L. and R.G. Trucano (2002), Verification and validation in computational fluid dynamics, *Progress in Aerospace Sciences, 38*, 209-272.

Oostrom, M., J.S. Hayworth, J.H. Dane and O. Guven (1992), Behaviour of dense aqueous phase leachate plumes in homogeneous porous media, *Water Resources Research, 28(10)*, 2123-2134.

Oldenburg, C.M. and K. Pruess (1995), Dispersive transport dynamics in a strongly coupled groundwater-brined flow system, *Water Resources Research, 31(2)*, 289-302.

Oreskes, N., K. Shrader-Frechette and K. Belitz (1994), Verification, validation and confirmation of numerical models in earth sciences, *Science, 263(4)*, 641-646.

Pearlman, L. (1999), *Subsurface containment and monitoring systems: Barriers and beyond,* OSWER, Technology Innovation of Office, USEPA, Washington, DC. *http://www.epa.gov/tio/download/remed/pearlman.pdf* > Aug 20, 2004.

Persoff, P., G.J. Moridis, J.A. Apps, K. Pruess and S.J. Muller (1994), Designing injectable colloidal silica barriers for waste isolation at the Hanford site, *33rd Hanford Symposium on Health and the Environment – In-situ Remediation: Scientific Basis for Current and Future Technologies*, G.W. Gee and N.R. Wing, Eds., pp. 87-100 Battelle Press, Richmond, WA, 7-11 Nov. (Lawrence Berkeley Laboratory Report LBL-35447, Berkeley, CA).

Persoff, P., S. Finsterle, G.J. Moridis, J.A. Apps, K. Pruess, and S.J. Muller (1995), Injectable barriers for waste isolation, *Proceedings of ASME/AIChE National Heat Transfer Conference*, Porland, Oregon, 5-9 Aug, (AIChE Symposium Series 91 (306) 58-67. Lawrence Berkeley Laboratory Report LBL-36884, Berkeley, CA).

Persoff, P., J.A. Apps, G.J. Moridis and J.M. Whang (1999), Effect of dilution and contaminants on sand grouted with colloidal silica, *Journal of Geotechnical and Geoenvironmental Engineering, ASCE, 125(6)*, 461-469.

Pinder, G.F. and H.H. Cooper Jr. (1970), A numerical technique for calculating the transient position of the saltwater front, *Water Resources Research, 6(3)*, 875-882.

Pruess, K. (1991), TOUGH2 - *A General Purpose Numerical Simulator for Multiphase Fluid and Heat Flow*, Rep LBL-29400 Lawrence Berkeley Natl. Lab., Berkeley, Calif.

148

Raghavan, S.R. and S.A. Khan (1995), Shear-induced microstructural changes in flocculated suspensions of fumed silica, *Journal of Rheology*, *39*, 1311-1318.

Ranganathan, R., R. Lewis, C.S. McCool, D.W. Green and G.P. Willhite (1997), Experimental study of the in situ gelation behavior of a polyacrylamide/aluminum citrate 'colloidal dispersion' gel in a porous medium and its aggregate growth during gelation reaction, SPE37220, *Proceedings - SPE International Symposium on Oilfield Chemistry*, 103-116.

Roache, P.J. (1994), Perspective: A method for uniform reporting of grid refinement studies, *Journal of Fluids Engineering, 116*, 405-413.

Roache, P.J. (1998), *Verification and Validation in Computational Science and Engineering*, Hermosa Publishers, Sorroco, NM.

Rumer, R. and M.E. Ryan (1995), *Barrier Containment Technologies for Environmental Remediation Applications*, J. Wiley and Sons, NY, 170.

Schlesinger, S. (1979), Terminology for model credibility, *Simulation, 32 (3)*, 103-104.

Seright, R.S. (1992), Impact of permeability and lithology on gel performance, SPE/DOE 24190, Paper presented at the *SPE/DOE Eighth Symp. on Enhanced Oil Recovery*, Tulsa, OK, 22-24 April, 347-357.

Seright, R.S. (1993), Reduction of gas and water permeabilities using gels. Paper SPE 25855 presented at the *SPE Rocky Mountain/Low Permeability Reservoir Symp.*, Denver CO, 12–14 April.

Seright, R.S. (1994), *Propagation of an Aluminum Citrate-HPAM Colloidal Dispersion Gel Through Berea Sandstone*, Report No. PRRC 94-29, New Mexico Inst of Mining and Tech.

Seright, R.S. (1995), Reduction of gas and water permeabilities using gels, *SPE Production and Facilities, 10(4)*, 103-108.

Smith, J. E. and R. W. Gillham (1999), Effects of solute concentration-dependent surface tension on unsaturated flow: Laboratory sand column experiments, *Water Resources Research*, 35(4), 973-982.

Smith, J.E. and F.Z. Zhang (2001), Determining effective interfacial tension and predicting finger spacing for DNAPL penetration into water-saturated porous media, *Journal of Contaminant Hydrology, 48(1-2)*, 167-183.

Sorbie, K.S., L.J. Roberts and P.J. Clifford (1985), Calculations on the behaviour of time-setting polymer in porous media, *American Institute of Chemical Engineers, National Spring Meeting*, Houston, TX, March, 62A, 95p.

Spooner, P.A., G.E. Hurt, V.E. Hodge, P.M. Wagner and I.R. Melnyk (1984), *Compatibility of Grouts with Hazardous Wastes*, USEPA Municipal Environmental Research Laboratory, Cincinnati, OH.

Sugita, F. and R.W. Gillham (1995), Pore scale variation in retardation factor as a cause of nonideal reactive breakthrough curves 3. Column investigations, *Water Resources Research, 31(1)*, 121-128.

Sullivan, T.M., J. Heiser, A. Gard and G. Senum (1998), Monitoring subsurface barrier integrity using perfluorocarbon tracer, *Journal of Environtal Engineering, ASCE, 124(6)*, 490-497.

Swartz, C.H. and F.W. Schwartz (1998), Experimental study of mixing and instability development in variable-density systems, *Journal of Contaminant Hydrology, 34(3)*, 169-189.

Todd, B.J. (1990), Numerical modeling of in situ gelation in porous media, Ph.D. Dissertation U. of Kansas, Lawrence, Kansas.

Todd, B.J., G.P. Willhite and D.W. Green (1991), Radial modeling of in-situ gelation in porous media, *Proc. SPE Prod. Oper. Symp.*, 183-195.

U.S. Army Corps of Engineers (1995), *Chemical Grouting*, EM 1110-1-3500. USACE, Washington.

van Genuchten, M.Th. (1980), Closed-form equation for predicting the hydraulic conductivity of unsaturated soils, *Soil Science Society of America Journal, 44(5)*, 892-898

Voss, C.I. and A.M. Provost (2002), *SUTRA, a Model for Saturated-Unsaturated Variable Density Ground-Water Flow with Energy or Solute Transport*: U.S. Geological Survey Open-File Report 02-4231, 250 p.

Warren, J.E. and H.S. Price (1961), Flow in heterogeneous porous media, *Society of Petroleum Engineering, 1(3)*, 153-169.

Welsh, J.P. (1997), State of the art of grouting in North America, *Grouting and Deep Mixing*, eds. R.Yonekura, M.Terashi and M.Shibazaki, 825-831, A.A.Balkema, Rotterdam.

150

Wreath, D., G.A. Pope and K. Sepehrnoori (1990), Dependence of polymer apparent viscosity on the permeable media and flow conditions, *In Situ: Oil-Coal-Shale-Minerals, 14(3)*, 263-284.

Woodbury, A.D. and E.A. Sudicky (1991), The geostatistical characteristics of Borden aquifer, *Water Resources Research, 27(4)*, 533-546.

Yonekura, R. and M. Kaga (1992), Current chemical grout engineering in Japan, *Grouting, Soil Improvement, and Geosynthetics, Geotechnical Special Publication, 30*, 725-736, ASCE, Reston, VA.

Yonekura, R. (1997), The developing process and the new concepts of chemical grout in Japan, *Grouting and Deep Mixing*, eds R.Yonekura, M.Terashi and M.Shibazaki, 889-901, A.A.Balkema, Rotterdam.

Younes, A., P.H. Ackerer and R. Mose (1999), Modeling variable density flow and solute transport in porous medium: 2. Re-evaluation of the salt dome flow problem, *Transport in Porous Media, 35(3)*, 375-394

Zhao, A., R.M. Barron and G.W. Rankin (2000), Systematic grid convergence studies and error estimations of numerical solutions of the exit region of submerged laminar jets, *Proceedings of the Southeastern Conference on Theoretical and Applied Mechanics - XX, (SECTAM XX)*, Pine Mountain, Georgia, USA, April 2000.

Zheng, C. (1991), *MT3-D User's Manual*, S.S.Papadapulos & Associates, Rockville, MD.

Zheng, C. and P.P. Wang (1999), *MT3DMS, A Modular Three-Dimensional Multi-Species Transport Model for Simulation of Advection, Dispersion and Chemical Reactions of Contaminants in Groundwater Systems; Documentation and User's Guide*, U.S. Army Engineer Research and Development Center Contract Report SERDP-99-1, Vicksburg, MS, 202.

VITA AUCTORIS

NAME: Tirupati Bolisetti

PLACE OF BIRTH: Korasavada, Srikakulam Dist, Andhra Pradesh, India

YEAR OF BIRTH: 1965

EDUCATION:

>   Andhra University, Visakhapatnam, India
>   1983-87   Bachelors in Engieering (Civil Engineering)
>
>
>   Indian Institute of Technology, Kanpur, India
>   1987-1989   Master of Technology (Civil Engineering)

PAPERS PUBLISHED/PRESENTED DURING Ph.D.

Bolisetti T. and S. Reitsma (2003) " Flow and Transport Simulation of Chemical Grouts in Porous Media: Shear Effects on Gelation," *Eos Trans. AGU, 84*(46), Fall Meet. Suppl., 2003.

Bolisetti T. and S. Reitsma (2003) "Numerical simulation of chemical grouting in heterogeneous porous media," *Grouting and ground treatment, Geotechnical Special Publication No. 120*, ASCE, Reston, VA, pp1454-1465.

Bolisetti T. and S.Reitsma, (2002) "Effect of heterogeneity scale on chemical grouting in porous media," Intl. Conf. on Computational Methods in Water Resources XIII June 2002, pp891-898.

da Silva, A.M.A.F. and **T. Bolisetti**, (2000) " A method for formulation of Reynolds Number Functions," Can. J. of Civil Engineering, 27(4), p.829-833.

Reitsma, S. and **T. Bolisetti**, (2000) "Comparison of finite analytic scheme with conventional solution schemes for the advection-dispersion equation," Proc. Intl. Conf. on Computational Methods in Water Resources XII June 2000, Calgary, Vol.1, p 411-416.